Master Project
TVVR 09/5007

Hydrological Modeling to Assess Climate Change Impact at Gilgel Abay River, Lake Tana Basin – Ethiopia

Yihun Dile Taddele

Water Resources Engineering
Department of Building and Environmental Technology
Lund University

Department of Water Resources Engineering
TVVR- 09/5007
ISSN-1101-9824

Hydrological Modeling to Assess Climate Change Impact at Gilgel Abay River, Lake Tana Basin – Ethiopia

Lund 2009
Author: Yihun Dile Taddele
Supervisor: Professor Ronny Berndtsson
Co-Supervisor: Mr. Shimelis G. Setegn

Division of Water Resources Engineering
Department of Building and Environmental Technology
Lund University
P.O.Box 118, SE-221 00 Lund
http://www.tvrl.lth.se/

ISSN-1101-9824

Printed in Sweden

Abstract

Climate changes have had marked impacts on the natural systems. However its impact will be significant with the hydrological cycle. It is agreed that climate change have adverse impacts on socio-economic development of all nations. But, it is expected that its impact will hit developing countries the worst. The objective of this thesis is to assess the impact of climate change on Gilgel Abay River. Gilgel Abay River is the largest tributary to Lake Tana basin. Lake Tana basin is located in the north-western Ethiopia. It lies between latitude 10.95^{o} and 12.78^{0}N, and longitude 36.89^{o} and 38.25^{o}E. Lake Tana is the key socio-economic focal point in the area. However, due to climate variability and change, the water level in the lake fluctuates. GCM derived scenarios of climate change were used for predicting the plausible future climate of the study area. The HaDCM3 A2a and B2a scenario experiments were used for the climate projection. As the GCM data are too coarse for impact assessment at regional level, SDSM was used to downscale the GCM data into finer scale. A physically based hydrological model, SWAT, was developed, calibrated and validated. SDSM downscaled climate outputs were used as an input to the SWAT model and used to assess the impact of climate change on the Gilgel Abay River and Lake Tana basin. The climate projection analysis was done dividing the coming 90 years into three time periods. The 1990-2001 was taken as baseline period against which comparison was made. The mean annual precipitation may decrease in the 2020s and increase in the 2050s and 2080s. However, the mean monthly precipitation may both increase and decrease. The decrease in mean monthly precipitation may be up to 30% in 2020s and the increase may reach up to 34% in 2080s. The maximum and minimum temperature indicated an increasing trend. The change in monthly mean maximum temperature ranges between -2.5 ^{0}c in the 2020s and +5 ^{0}c in the 2080s. The change in monthly mean minimum temperature ranges between -1.4 ^{0}c in the 2020s and +4.2 ^{0}c in the 2080s. The impact of climate change may cause a decrease in monthly flow volume up to 46% in the 2020s and increase up to 135% in the 2080s. It is observed that climate change has negligible effect on the low flow condition of the river. Seasonal flow volume may show increase up to 136% and 36% for Belg and Kiremit respectively. The increase in Belg season flow will have a paramount importance for small scale irrigation activities practiced by local farmers. It is observed that there may be a net annual increase in flow volume in Gilgel Abay River due to climate change. As Gilgel Abay is the largest tributary river feeding into Lake Tana, any effect on this river is reflected in the Lake water level. The increase in flow will help to harness a significant amount of water for the ongoing dam projects in the Gilgel Abay river basin. However, it may also aggravate the recurrent flooding problems in the Lake Tana surrounding area.

Key Words: Climate Change, Gilgel Abay, Lake Tana, GCM, SDSM, SWAT

Acknowledgement

First of all I would like to thank the almighty God for giving me the audacity and wisdom to reach this point in life.

I am very grateful to Lund University, Department of Water Resources Engineering for allowing me to take part in the International Master Program for Water Resources and the Swedish Institute for granting me MKP scholarship. Thank you SI, you made my dream come true.

I would like to express my sincere gratitude to my supervisor, Professor Ronny Berndtsson, for giving me valuable guidance and support throughout my research. I am also indebted to my co-supervisor, Mr. Shimeles Gebriye, who helped me in the hydrological modeling part. I will also like to extend my appreciation to Nancy Sammons, member of the SWAT model developers, who solved my problems when I got stuck at some critical points. I am very grateful to all my teachers who taught me from grass root to this level.

I will also like to thank the Ethiopian Ministry of Water Resources, National Meteorological Services Agency and Amhara Region Water Resources Office members for the data and keen assistance they gave me during field work. I like to thank Getnet Baynesagne for the data and priceless comments he gave me at each point of my modeling work. I will also like to thank Lijalem Zeray and Yared Ashenafi for the data and helpful documents they gave me.

Thanks to God, I have lots of exciting friends whom I met in my walk of life. Letters and words limit me to list your names. You all were great. I learnt a lot from you. Those of you I met you in Sweden, thank you for those beautiful days we spent together and for the cultures and views we shared. For those in which our friendship extends to Europe, thank you. Our chats and discussions made my stay in Europe very easy. Friends back home, thank you. You were my courage to go forward.

At last but not least, I would like to extend my deepest gratitude to my family, without your encouragement and care this would not have happened.

Acronyms

AGCM – Atmospheric General Circulation Model
ArcSWAT – SWAT Integrated with ArcGIS
AOGCM – Coupled Atmospheric-Ocean General Circulation Model
CGIAR – Consultantive Group on Agricultrural Research
CICS – Canadian Institute for Climate Studies
CN – Moisture condition Curve Number
DDC – Data Distribution Ceneter
DEM – Degital Elevation Model
ESCO – Soil Evaporation Compensation Factor
FAO – Food and Agricultural Organization of the United Nation
FDRE – Frederal Democratic Republic of Ethiopia
GCM – General Circulation Model
GHG – Green House Gas
GIS – Geographic Information Systems
GW_Delay – Groundwater Delay time
GW_Revap – Groundwater Revap Coefficient
GWQMN – Threshold Water Depth in the shallow aquifer for flow
HaDCM3 – Hadly Center Coupled Model, version 3
HRU – Hydrological Response Unit
IPCC – International Panel on Climate Change
ITCZ – Inter-tropical Convergence Zone
masl – meters above sea level
MoWR – Ministry of Water Resources, Ethiopian
NASA – National Aeuronautics and Space Administration
NCEP – National Center for Environmental Prediction
NMSA – National Metrological Services Agency, Ethiopian
OGCM – Ocean General Circulation Model
RCM – Regional Climate Models
ROTO – Routing Outputs to Outlet
SCS – Soil Conservation System
SDSM – Statistical DownScaling Model
SRES – Special Report on Emission Scenarios
SRTM – Shuttle Radar Topographic Mission
SWAT – Soil and Water Assessment Tool
SWRRB – Simulator for Water Resources in Rural Basins
TGCIA – Task Group on Scenarios for Climate and Impact Assessment
USBR – United States Beuro of Reclamation
UNFCCC – United Nations Framework Convention on Climate Change
USDA – United States Department of Agriculture
WHAT – Web Based Hydrograph Analysis Tool
WMO – World Metrological Organization

List of Tables

List of Figures

1. Introduction

1.1 Background

Weather is the state of the atmosphere at a given time whilst climate is the average weather over a period of time (Thorpe, 2005). Despite the annual periodicity in weather patterns, the Earth's climate has changed many times during the planet's history, with events ranging from ice ages to long periods of warmth. Climate changes have had visible impacts on the natural systems. However its impact will be significant with the hydrological cycle. Climate change is expected to aggravate current stresses on water resources availability from population growth, urbanization and land-use change. Wide spread mass losses from glaciers and reductions in snow cover over recent decades are projected to accelerate throughout the 21st century, reducing water availability, hydropower potential, and changing seasonality of flows in regions supplied by melt water from mountain ranges (IPCC, 2008).

Scientists agreed that climate change have adverse impacts on socio-economic development of all nations. But the degree of the impact will vary across nations. It is expected that changes in the earth's climate will hit developing countries like Ethiopia first and hardest because their economies are strongly dependent on crude forms of natural resources and their economic structure is less flexible to adjust to such drastic changes (NMSA, 2001).

Ethiopia has twelve major river basins. Most of them are untapped for modern irrigation and energy development. According to NMSA (2001), only 4% of the potential irrigable land are developed and the water supply coverage is 76% for urban and 18.8% for rural areas. Besides financial constraints, the transboundary nature of the rivers is a problem for the development in the sector. Currently, there are flash spot development in some river basins for energy generation and large scale irrigation projects to sell power to neighbouring countries and attain food self sufficiency respectively. However, the impact of climate change is behind the set objectives.

1.2 Problem Statement

Water is one of several current and future critical issues facing Africa. About 25% of the contemporary African population experience water stress, while 69% live under conditions of relative water abundance (Vörösmarty et al., 2005). Water supplies from rivers, lakes and rainfall are characterized by their unequal natural geographical distribution and accessibility, and unsustainable water use. By 2025, water availability in eastern Africa is limited to 1000-1700 m^3/person/yr. These estimates are based on population growth rates only and climate change has the potential to impose additional pressures on water availability and accessibility (IPCC, 2008).

As Ethiopia is following agricultural based industrialization which is strongly tied with climate and being a large part of the country is arid and semi-arid, climate change should be a concern. Studies done by many researchers indicated that the water resources are sensitive to climate change. The studies done in Awash and Abay (Blue Nile) can be taken as an example. However, most of the studies made so far are mainly at the catchment level. As a catchment encompasses different climatic zones, it might be difficult to identify the exact impact of the climate change so as to take adaptive measures. Therefore it is advisable to study the impact of climate change in sub-basin level. Hence, this study was targeted to address the impact of climate change on sub-basin level.

This study focused on Gilgel Abay sub-basin which is among the tributeries of Abay (Blue Nile). Gilgel Abay is used for various purposes like, water supply and irrigation. Recently, the Federal Democratic Republic of Ethiopia (FDRE) is giving greater attention for the development of irrigation projects in the basin. Gilgel Abay is the largest river feeding Lake Tana, the biggest lake in Ethiopia. Lake Tana is the key socio-economic focal point in the area. It is used for hydropower generation, irrigation, recreation, fishing and navigation. However, due to climate variability and change, the water level in the lake fluctuates. Inundation of the flood plains bordering Lake Tana is a yearly recurrent phenomenon. On the other hand, water level drop is also observed in some periods of the year and navigation of the boats is hampered to different islands in the lake. Hence, this study will have a paramount importance in giving an insight on the vulnerability of Gilgel Abay and Lake Tana to climate change.

1.3 Objective

The objective of this thesis is to assess the impact of climate change in the time scale up to 2100 on Gilgel Abay river in particular and on Lake Tana in general. The specific objectives include:

- Downscaling climate model outputs and developing physically based distributed hydrological model for lake Tana basin
- Calibration and validation of the hydrological model for Gilgel Abay sub-basin, and
- Assessing the impact of climate change on Gilgel Abay river and giving an overall insight on Lake Tana effects

1.4 Delimitation

World Meteorological Organization recommends a baseline period of at least 30 years against which future climate projection to be done. Owing to data availability this study considered 1990 to 2001 as a baseline period, which ought to be from 1961 to 2001.

In this study the impact of climate change was assessed assuming the land cover will remain the same. However, in real world the land cover is dynamic due to natural and human influences. It is also assumed that the socio-economic condition in the area will remain the same.

2. Description of the Watershed

2.1 Location

Lake Tana basin is located in the north western Ethiopia. It lies between latitude 10.95^{o} and 12.78^{0}N, and longitude 36.89^{o} and 38.25^{o}E. It has a drainage area of approximately 15,000 km^{2} (USBR, 1964). Figure 1 shows the location of the 12 major Ethiopian drainage basins. Lake Tana basin is the beginning of Abay (Blue Nile) basin. The Abay Basin is the most important drainage basin in Ethiopia. It accounts for almost 20 percent of Ethiopia's land area and 50 percent of its total average annual runoff (BCEOM, 1999).

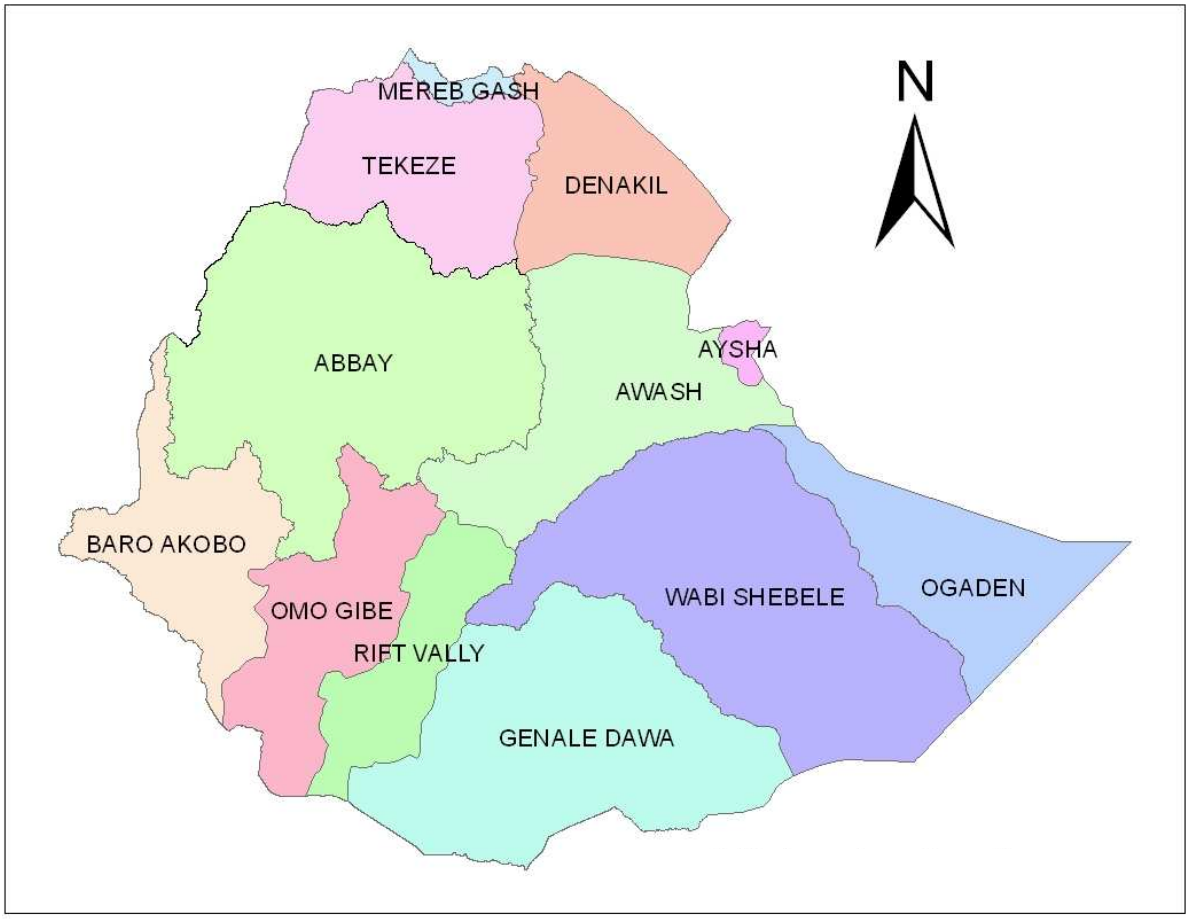

Figure 1: Major Ethiopian river basins (shape file from MoWR)

2.2 Topography

The Lake Tana basin is characterized by a large, flat to very gently sloping plain bordering the lake on the north and east and an extensive area of rolling to hilly uplands on the south. The elevation ranges from 1786 to 2991 masl for Megech river basin, 3050 masl for Gumera river basin, 3524 masl for Gilgel Abay river basin, and 4100 masl for Ribb river basin.

2.3 Climate

The climate of Ethiopia is mainly controlled by the seasonal migration of the Inter-tropical Convergence Zone (ITCZ) and associated atmospheric circulation as well as by the complex topography of the country. It has a diversified climate ranging from semi-arid desert type in the low lands to humid and temperate type in the southwest.

The climate of the Lake Tana sub-basin is dominated by tropical highland monsoon. There are three recognized seasons. The main rainy season (kiremt) lasts generally from June to September during which south-west winds bring rains from the Atlantic Ocean. About 70-90 percent of total rainfall occurs during this season which is also typified by minimum levels of sunshine, low variation in daily temperatures and high relative humidity. A dry season (Bega) lasts from October to January during which clear skies are associated with maximum sunshine, high daily temperature variation, and low relative humidity. Minor rainy season (Belg) lasts from February to May during which south-east winds bring the small rains from the Indian Ocean and temperatures are at their highest.

There is a climatic variability in time and space in the basin. According to analysis of the climatic data from 1995-2004, the annual rainfall is within the range of 1118 to 1658 mm or an average of 1438 mm at Bahir Dar station, and 991 to 1904 mm or an average of 1365 mm at Gondar, indicating that the south region of the lake has a tendency for more rain than the north region. There is a diurnal difference in temperature, but the temperature is comparatively uniform throughout the year. The annual average daily maximum and minimum temprateure at Bahir Dar station are 27.7^0c and 13.12^0c respectively, and those at Gondar are 22.1^0c and 9.7^0c respectively.

2.4 Hydrology

2.4.1 Rivers

The major rivers feeding Lake Tana are the GilgelAbay, Ribb, Gumara, and Megech. These rivers contribute more than 93% of the flow (Setegn, 2008). The outflow from the lake is the

main source of the Blue Nile river. The Blue Nile flows through the eastern outskirts of the city of Bahir Dar at the southern end of the lake and, flows down approximately 35 km in a southeast direction where it forms the famous Tis Isat Falls to drop into a gorge having a depth of about 45 m. According to a study done by the Japan International Cooperation Agency, the river flows down this deep canyon for approximately 800 km to reach the Ethiopian-Sudanese border approximately 650 km beyond which it joins with the White Nile.

The Megech River catchment is situated in the northern portion of the sub-basin and has a catchment area of about 700 km^2. The river flows generally in the southerly direction, emptying into Lake Tana. The main tributeries of the Megech River are the West Fork and the Angereb. The Ribb River is one of the two rivers on the east side flowing in to the Lake Tana with a watershed 1800 km^2. The second river flowing on the east side of the lake is Gumara River which has a drainage area of 1500 km^2. The main tributeries of the Gumera River are the North Fork, the South Fork, and the Little Gumara. The fourth and largest river draining to Lake Tana is the Gilgel Abay River. It has a catchement area of 5004 km^2. Though the initial target of the study was to assess the impact of climate change on the entire Lake Tana basin, due to time limitation the study concentrates on this river.

2.4.2 Lake and Lake Level

Lake Tana is the largest lake in Ethiopia and the third largest in the Nile Basin. Lake Tana is 73 km long by 68 km wide and has a surface area of 3042 km^2 at 1786 masl. The lake is shallow and has a mean depth of 9.53 m, while the deepest part of the lake is 14 m (Abay river basin integrated development master plan project, 1999). The lake has an extensive shore length fringed by shallow wetlands and cliffs. The lake was created by a basalt outflow in the Pleistocene, cutting off the basin at the southern extremity of the lake at Chara-Chara which is near to a city called Bahir Dar. There are about 37 islands in the lake, some with several historical monasteries and churches having religious and cultural importance.

Due to the restriction at its outlet and its large storage capacity, the lake rises slowly to reach its maximum level in September at the end of heavy rains and recedes slowly to its minimum water level in June. According to the ministry of water resources Abay River Basin integrated master plan project, Lake Tana stores $29.175*10^9$ m^3 of water at an altitude of 1786 masl and when the water level is at an altitude of 1785 masl, the lake may have a volume of about $26*10^9$ m^3.

According to information from the Zonal Water Offices, flooding and water level drop are frequent phenomenon happening in the Lake. The water level of the lake was more or less steady however it has shown great fluctuation of its level since 1995. Figure 2 shows the annual mean water level variation at Bahir Dar station between 1.9 and 3.2 m.

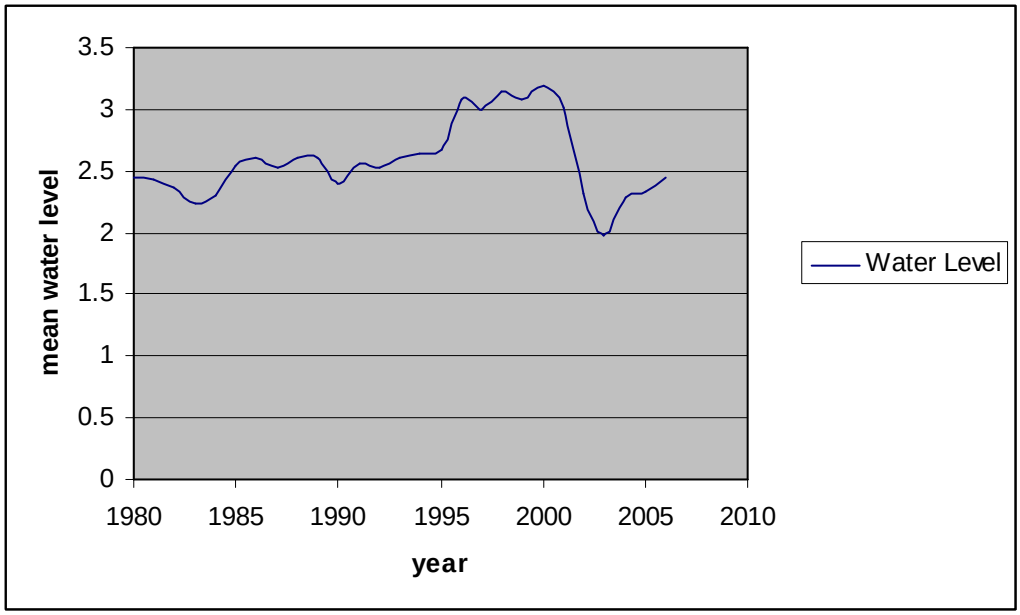

Figure 2: Annual mean lake Tana water level variation at Bahirdar station

According to the analysis done on the measured water level data from 1981 to 2006 at Bahir Dar gauging station, the maximum recorded gauge level was 4.2 m in September and the minimum was 0.88 m in June.

2.5 Land Cover and Land Use

Aerial photographs and SPOT imagery surveys taken at different time showed that the land cover of the area is bushland, cultivated, Eucalyptus, glassland, lake, shrubland, settlement, swamp, water surface, wetland and wood. Cultivated area is understood as an area devoted to crops but including fallow land, private grazing land and scattered homesteads. Cultivated area surrounded by Eucalyptus plantation is noticeable, as Eucalyptus has become an important source of income from the sale of poles. Wetland and swamp are used as grazing land during the dry season in the same way as cultivated land is used for aftermath grazing. The farming system of the area is a mixed farming system with more emphasis on crop production. The main crops grown in the area are: teff, sorghum, maize, finger millet and chick peas.

2.6 Geology and Soil

Lake Tana lies in a large structural basin surrounded by volcanic mountains composed mostly of basaltic lava. The lakebeds northwest of Lake Tana are the only sedimentary rock formations in the vicinity of the lake and consist mostly of siliceous shales, sand-stones, lignite beds, and cherty marl (USBR, 1964). The rocks with in the basin are all extrusive volcanic rocks representing three or more phases of volcanic activity.

The soils in the Lake Tana sub-basin are a mixture of delatic and recent river alluvial deposits and are not homogeneous. The major soil types in the area includes chromic luvisols, eutric cambisols, eutric fluvisols, eutric leptosols, eutric regosols,, eutric vertisols, haplic luvisols, haplic alisols, haplic nitisols, and lithic leptosols.

3. Literature Review

3.1 Climate Change

3.1.1 Definition of Climate Change

Climate change refers to a change in the state of the climate that can be identified by changes in the mean and/or the variability of its properties and that persists for an extended period, typically decades or longer (IPCC, 2007).

3.1.2 Global Climate Change

Warming of the climate system in recent decades is obvious, as is now evident from observations of increases in global average air and ocean temperatures, widespread melting of snow and ice, and rising global sea level (IPCC, 2008). The global average temperature showed a 100 year linear trend of 0.74 ^{0}c from 1996-2005 (IPCC, 2007). Trends in precipitation amount have been observed in many large regions. Globally, the area affected by draught has likely increased since the 1970's (IPCC, 2007). The ocean circulation is also predicted to change and sea level is expected to rise at a rate of about 1.7 mm/year as the ocean expands as heat is gradually diffused downwards in the ocean (Thorpe, 2005). There are also numerous long term changes in other aspects of climate. Some extreme weather events have changed in frequency and/or intensity. Hot days, hot nights, heat waves, and heavy precipitation events have become more frequent over most land areas.

3.1.3 Climate Change and Variability in Ethiopia

According to the Ethiopian National Meteorological Services Agency (NMSA, 2001) study for 42 meteorological stations, the country has experienced both dry and wet years over the last 50 years. Trend analysis of the annual rainfall showed there was a declining trend in the northern half of the country and southern Ethiopia while there is an increasing trend in the central part of the country. However, the overall trend in the entire country is more or less constant. Figure 3 shows the year to year variation of rainfall over the country expressed in terms of normalized rainfall anomaly averaged over 42 stations.

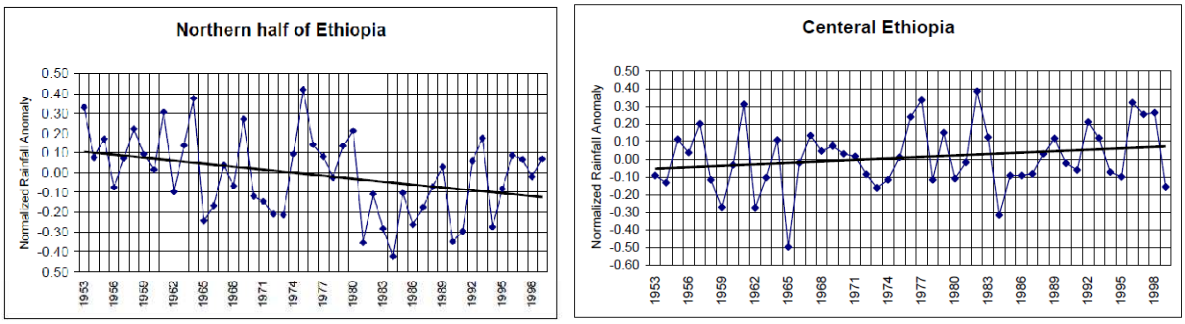

Figure 3: Annual variability of rainfall over Northern half (left side) and Central (right) Ethiopia expressed in normalized devation (NMSA,2001)

The study of NMSA at the same year for 40 stations showed that there have been very warm and very cold years. However the general trend showed there was an increase in temperature over the last 50 years. The average annual minimum temperature over the country has been increasing by about 0.25 ^{0}c every ten years while average annual maximum temperature has been increasing by about 0.1 ^{0}c. The study also noted that the minimum temperature is increasing at a higher rate than the maximum temperature. Figure 4 shows the year to year variation of annual maximum and minimum temperatures expressed in terms of normalized temperature anomalies averaged over 40 stations.

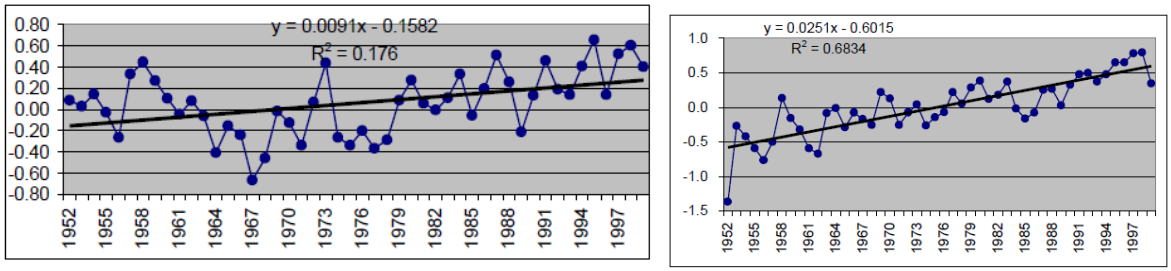

Figure 4: Annual mean maximum (left side) and minimum (right side) temprature variability and trend over Ethiopia (NMSA, 2001)

Associated with rainfall and temperature change and variability, there was a recurrent draught and flood events in the country. There was also observation of water level rise and dry up of lakes in some parts of the region depending on the general trend of the temperature and rainfall pattern of the regions.

3.1.4 Causes of Climate Change

Climate change may be due to both natural (i.e. internal or external processes of the climate system) as well as anthropogenic forcing (ex. increase in concentrations of greenhouse gases). Historically, natural factors such as volcanic eruptions, changes in the Earth's orbit, and the amount of energy released from the Sun have affected the Earth's climate. Beginning late in the 18th century, human activities associated with the Industrial Revolution have also changed the composition of the atmosphere and therefore very likely are influencing the Earth's climate (http://www.epa.gov/climatechange/basicinfo.html). The IPCC (2007) report, concluded that most of the observed warming over the last 50 years was likely due to the increase in greenhouse gas concentrations.

The radiative forcing[1] of the climate system is dominated by the long lived green house gases (GHG). The green house gases include Carbon dioxide (CO_2), methane (CH_4), nitrous oxide (N_2O), and halocarbons. Carbon dioxide (CO_2) is the most important anthropogenic GHG. Global GHG emissions due to human activities have grown since pre-industrial times, with an increase of 70% between 1970 and 2004 (IPCC, 2007). Global increase in CO_2 concentrations is primarily due to fossil fuel use, with land-use change providing another significant contribution. The increase in CH_4 concentration is predominantly due to agriculture and fossil fuel use. The increase in N_2O concentration is primarily due to agriculture. Changes in the atmospheric concentrations of GHGs and aerosols, land cover and solar radiation alter the energy balance of the climate system and are drivers of climate change. They affect the absorption, scattering and emission of radiation within the atmosphere and at the Earth's surface. The resulting positive or negative changes in energy balance due to these factors are expressed as radiative forcing, which is used to compare warming or cooling influences on global climate (IPCC, 2007).

3.1.5 Climate Change and Water

Water is involved in all components of the climate system. Therefore, climate change affects water through a number of mechanisms. Although climate change is expected to affect many sectors of the natural and man-made sectors of the environment, water is considered to be the most critical factor associated with climate change impacts. Therefore, it is very important to

[1] In an equilibrium climate state the average net radiation at the top of the atmosphere is zero. A change in either the solar radiation or the infrared radiation changes the net radiation. The corresponding imbalance is called radiative forcing.

make evaluations of the expected impact on the hydrology and water resources due to expected climate changes regardless of the direction of the change (Ringius et al. 1996).

3.1.6 Developing Climate Change Scenarios

A climate scenario is a plausible representation of future climate that has been constructed for explicit use in investigating the potential impacts of anthropogenic climate change (IPCC, 2001). Climate change scenarios are developed to give coherent, internally consistent and plausible descriptions of future state of the world (IPCC, 1999). The climate change scenarios should be assessed according to consistency with global projections, physical plausibility, applicability in impact assessments and representativity (Smith and Hulme, 1998). Figure 5 shows the alternative data sources and procedures for constructing climate scenarios.

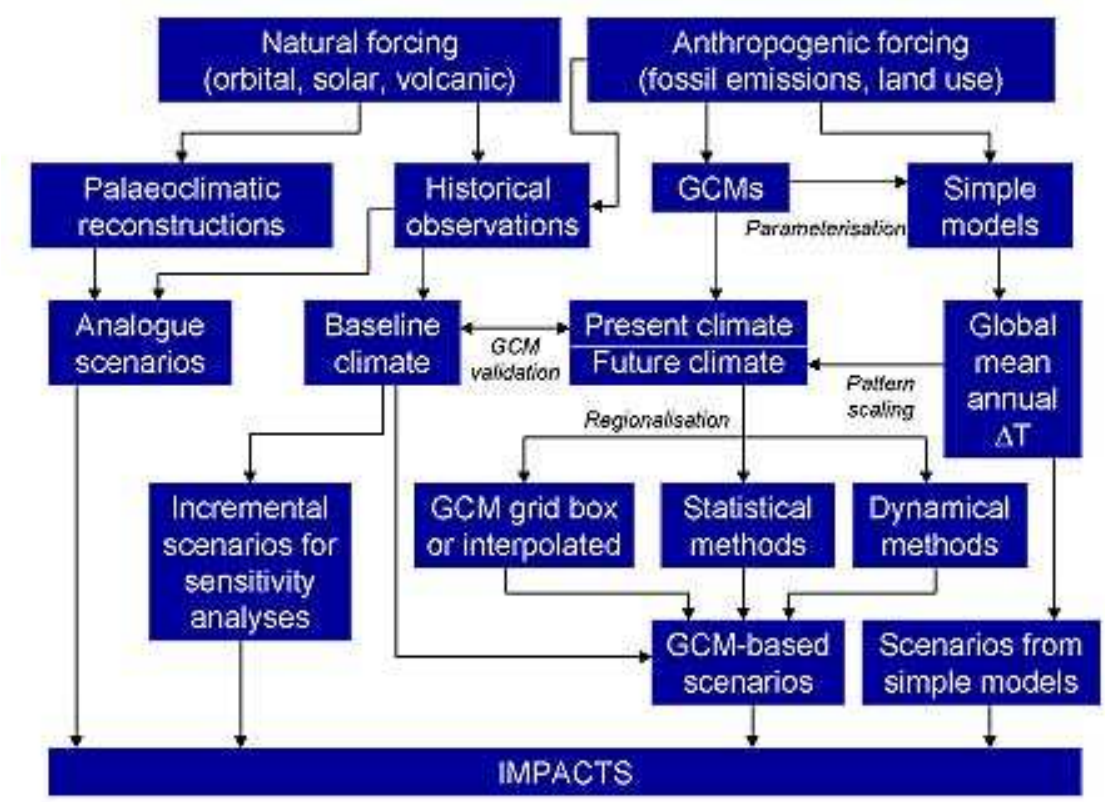

Figure 5: Some alternative data sources and procedures for constructing climate scenarios for use and impact assessments (IPCC, 2001)

Climate change scenarios for impact assessment can be developed in three major techniques; analogue, synthetic and GCM-based climate change scenarios. These scenario construction techniques were dealt as below.

a. **Analogue Scenarios**: Analogue scenarios are constructed by identifying a recorded climate regime which may resemble the future climate anticipated for a particular site

or region. These recorded climates may be identified in the long observational record at a site *(*temporal analogues*)* or from other geographical locations (spatial analogues*).* Temporal analogues can be either palaeoclimatic analogues or instrumental analogues. In palaeoclimatic analogues the past climate may be reconstructed by using information from the geological record and used to construct scenarios used to represent future climate conditions. While the instrumental analogues uses the past periods of instrumental records to provide analogue for the future climate. Spatial analogues are regions which today have a climate analogous to that anticipated for the study region in the future. In essence, the climate record from one location is assumed to represent the future climate at a different location. Such scenarios have the advantage of representing conditions that have actually been observed and experienced. However, since the causes of the analogue climate are most likely due to changes in atmospheric circulation, rather than due to greenhouse gas-induced climate change, these types of scenarios are not recommended to represent the future climate in quantitative impact assessments (Smith and Hulme, 1998).

b. **Synthetic Climate Change Scenario:** it is also called arbitrary scenario, which is the simplest scenario available. In this scenario type, a historical record for a particular climate variable is simply perturbed by an arbitrary amount. For example the station temperature may increase by $+2^0$c. It is mainly important to identify the sensitivity of an exposure unit to a plausible range of climatic variations. In this scenario it is impossible to describe a realistic set of changes for all climate variables that are physically plausible and internally consistent.

c. **Scenario from Global Circulation Models**: global climate models are the only credible tools currently available for simulating the response of the global climate system to increasing green house gas concentrations (IPCC-TGCIA, 1999). Although the output from GCMs is not generally of a sufficient resolution or reliability to be applied directly to represent present day climate or consequently future climate conditions, it is standard practice to use observed data in the form of daily or monthly time series representing the current baseline period (e.g. 1961-1990) and to apply changes derived from GCM information (i.e. the scenarios) to these observed data.

The climate models simulate the present climate for extended simulation periods under present climate conditions without any change in external climate forcing. Then the quality of the simulation is evaluated with observations of the current climate. After the model is evaluated, two different strategies have been applied to make projections of future climate change. The first, so-called equilibrium method is to change, e.g. double, the carbon dioxide concentration and to run the model again to a new equilibrium. The differences between the climate statistics of the two simulations provide an estimate of the climate change corresponding to the doubling of carbon dioxide, and of the sensitivity of the climate to a change in the radiative forcing. This method does not provide insight into the time dependence of climate change. The second, so-called transient method is to force the model with a greenhouse gas and aerosol scenario. The difference between such simulation and the original baseline simulation provides a time-dependent projection of climate change. This transient method requires a time-dependent profile of greenhouse gas and aerosol concentrations. These may be derived from so-called emission scenarios (IPCC, 2001).

The IPCC Data Distribution Center[2] (DDC) archives climate change scenarios constructed from GCM experiments undertaken at several international modeling centers. The IPCC DDC also provides access to baseline and scenario data for a range of non-climatic data like land use and land cover, sea level, and water availability and water quality which need to be considered in conducting climate change impact and vulnerability assessments. Below are some of the agencies whose data is archived in the IPCC DDC.

- BCCR:BCM2: Bjerknes Centre for Climate Research (BCCR), University of Bergen, Norway
- CCCMA:CGCM3_1-T47: Canadian Centre for Climate Modeling and Analysis (CCCma)
- CONS:ECHO-G: Meteorological Institute of the University of Bonn (Germany), Institute of KMA (Korea), and Model and Data Group.
- GFDL:CM2: Geophysical Fluid Dynamics Laboratory, NOAA

[2] http://www.ipcc-data.org/

- INM:CM3: Institute of Numerical Mathematics, Russian Academy of Science, Russia.
- MPIM:ECHAM5: Max Planck Institute for Meteorology, Germany
- MRI:CGCM2_3_2: Meteorological Research Institute, Japan Meteorological Agency, Japan
- NASA:GISS-EH: NASA Goddard Institute for Space Studies (NASA/GISS), USA
- NCAR:CCSM3: National Center for Atmospheric Research (NCAR)
- UKMO:HADCM3: Hadley Centre for Climate Prediction and Research, Met Office, United Kingdom
- UKMO:HADGEM1: Hadley Centre for Climate Prediction and Research, Met Office United Kingdom

3.1.7 Defining the Baseline Climate

Baseline climate information is important to characterize the prevailing conditions and its thorough analysis is valuable to examine the possible impacts of climate change on a particular exposure unit[3]. It can also be used as a reference with which the results of any climate change studies can be compared. The choice of baseline period has often been governed by availability of the required climate data. According to World Meteorological Organization (WMO), the baseline period also called reference period generally corresponds to the current 30 years normal period. A 30-year period is used by WMO[4] to define the average climate of a site or region, and scenarios of climate change are also generally based on 30-year means. Most impact assessments seek to determine the effect of climate change with respect to the present, and therefore recent baseline periods such as 1961 to 1990 are usually in favor. A further attraction of using 1961 to 1990 is that observational climate data coverage and availability are generally better for this period compared to earlier ones (IPCC, 2001).

2.1.8 Emission Scenarios

To determine how the composition of the atmosphere, and consequently how climate may change in the future, it is necessary to construct scenarios of greenhouse gas and sulphat aerosol emissions for the next 100 years and beyond. This requires assumptions to be made

[3] 'Exposure unit' is the term used by the IPCC to describe an activity, group, region or resource that may be exposed to significant climate variations (IPCC, 1994)
[4] http://www.wmo.int/pages/index_en.html

about how society will evolve in the future. Four different narrative storylines were developed to describe the relationship between emission driving forces and their evolution. Each storyline represents different demographic, socio-economic, technological and environmental developments. The four qualitative storylines yield four sets of scenarios called families (A1, A2, B1, B2). The four scenario families give 40 SRES scenarios which are all equally valid with no assigned probabilities of occurrence. According to the special report on emission scenarios (SRES, IPCC 2000) the associated storylines are summarized below.

- *The A1 storyline and scenario family describes a future world of very rapid economic growth, global population that peaks in mid-century and declines thereafter, and the rapid introduction of new and more efficient technologies. Major underlying themes are convergence among regions, capacity building, and increased cultural and social interactions, with a substantial reduction in regional differences in per capita income. The A1 scenario family develops into three groups that describe alternative directions of technological change in the energy system. The three A1 groups are distinguished by their technological emphasis: fossil intensive (A1FI), non-fossil energy sources (A1T), or a balance across all sources (A1B).*
- *The A2 storyline and scenario family describes a very heterogeneous world. The underlying theme is self-reliance and preservation of local identities. Fertility patterns across regions converge very slowly, which results in continuously increasing global population. Economic development is primarily regionally oriented and per capita economic growth and technological changes are more fragmented and slower than in other storylines.*
- *The B1 storyline and scenario family describes a convergent world with the same global population that peaks in midcentury and declines thereafter, as in the A1 storyline, but with rapid changes in economic structures toward a service and information economy, with reductions in material intensity, and the introduction of clean and resource-efficient technologies. The emphasis is on global solutions to economic, social, and environmental sustainability, including improved equity, but without additional climate initiatives.*
- *The B2 storyline and scenario family describes a world in which the emphasis is on local solutions to economic, social, and environmental sustainability. It is a world with continuously increasing global population at a rate lower than A2, intermediate levels of economic development, and less rapid and more diverse technological change than in the B1 and A1 storylines. While the scenario is also oriented toward environmental protection and social equity, it focuses on local and regional levels.*

All of these scenarios do not include climate initiatives of the United Nations Framework Convention on Climate Change (UNFCCC) or the emission targets of the Kyoto Protocol[5]. However, non-climatic change policies designed for a wide range of other purposes influence the GHG emission divers such as demographic change, social and economic development, technological change and pollution management. This influence is reflected in the storylines and resultant scenarios.

3.2 Climate Models

‘’The major components of the climate system that are important for climatic change and its consequences, such as sea level rise, during the next century are: the atmosphere, oceans, terrestrial biosphere, glaciers and ice sheets and land surface. In order to project the impact of human perturbations on the climate system, it is necessary to calculate the effects of all the key processes operating in these climate system components and the interactions between them. These climate processes can be represented in mathematical terms based on physical laws such as the conservation of mass, momentum, and energy. However, the complexity of the system means that the calculations from these mathematical equations can be performed in practice only by using a computer. The mathematical formulation is therefore implemented in a computer program, which is referred to as a model. If the model includes enough of the components of the climate system to be useful for simulating the climate, it is commonly called a climate model’’ (IPCC, 1997). Modern climate models are composed of a system of interacting model components, each of which simulates a different part of the climate system (Bader et al., 2008). The atmospheric and ocean components are known as General Circulation Models (GCMs) because they explicitly simulate the large scale global circulation of the atmosphere and ocean (Bader et al.2008).

Atmospheric general circulation models (AGCMs) are computer programs that evolve the atmosphere’s three dimensional state forward in time. This atmospheric state is described by such variables as temperature, pressure, humidity, winds, water and ice condensate in clouds. These variables are defined on a spatial grid, with grid spacing determined in large part by available computational resources (Bader et al., 2008). The model’s grid-scale evolution is determined by equations describing the thermodynamics and fluid dynamics of an ideal gas (Bader et al., 2008). Ocean general circulation models (OGCMs) solve the primitive equations for global incompressible fluid flow analogous to the ideal-gas primitive equations solved by

[5] http://unfccc.int/kyoto_protocol/items/2830.php

atmospheric GCMs (Bader et al. 2008). AGCM and OGCM can be coupled together to form an atmosphere-ocean coupled general circulation model (AOGCM). With the addition of other components (such as a sea ice model or a model for evapotranspiration over land), the AOGCM becomes a full climate model.

Most GCMs have a horizontal resolution of between 250 and 600 km, and 10 to 20 vertical layers in the atmosphere. A typical ocean model has a horizontal resolution of 125 to 250 km and a resolution of 200 to 400 m in the vertical (IPCC, 2001). Their resolution is thus quit coarser relative to the scale needed by impact assessors.

3.3 Regionalization Techniques

The horizontal resolution of coupled AOGCMs is relatively coarse to explicitly capture the fine scale structure that characterizes climatic variables in many regions of the world that is needed for impact assessments studies. Many important aspects of the climate of a region (e.g., climatic means in areas of complex topography or extreme weather systems such as tropical cyclones) can only be directly simulated at much finer resolution than that of current AOGCMs (IPCC, 2001). Therefore, a number of techniques have been developed to enhance the regional information provided by the AOGCMs and to get a finer scale regional information. These approaches are called regionalization techniques and are classified into three categories:

- High resolution and variable resolution AGCM experiments
- Nested limited area (regional) climate models (RCMs)
- Statistical methods

RCMs and statistical models are often referred to as downscaling tools of AOGCM information. It might be important to define resolution levels when we deal about regionalization techniques. According to IPCC (2001), range of 10^4 to 10^7 km^2 is defined as regional scale, scales smaller than 10^4 km^2 are referred to as local scale and scales greater than 10^7 km^2 are referred to as planetary scales. Circulations occurring between 10^4 and 10^7 km^2 are resolved using the regional circulation models.

3.3.1 High Resolution and Variable Resolution AGCM Experiments

The concept behind the use of high or variable resolution AGCM simulations is that, given the sea surface temperature, sea ice, trace gas and aerosol forcing, relatively high-resolution information can be obtained globally or regionally without having to perform the whole

transient simulation with high resolution models. The main theoretical advantage of this approach is that the resulting simulations are globally consistent, capturing remote responses to the impact of higher resolution. The use of higher resolution can lead to improved simulation of the general circulation in addition to providing regional detail (e.g., HIRETYCS, 1998; Stratton, 1999a cited from IPCC, 2001).

Use of high resolution and variable resolution global models is computationally very demanding, which poses limits to the increase in resolution obtainable with this method. However, it has been suggested that high-resolution AGCMs could be used to obtain forcing fields for higher resolution RCMs or statistical downscaling, thus effectively providing an intermediate step between AOGCMs and regional and empirical models (IPCC, 2001).

3.3.2 Regional Climate Models

The nested regional climate modeling technique consists of using initial conditions, time-dependent lateral meteorological conditions and surface boundary conditions to drive high-resolution RCMs. The driving data is derived from GCMs (or analyses of observations) and can include GHG and aerosol forcing (IPCC, 2001). They can provide high resolution (up to 10 to 20 km or less) and multi-decadal simulations and are capable of describing climate feedback mechanisms acting at the regional scale. An important advantage of dynamical models is that they account for local conditions, which may include changes in land-surface vegetation or atmospheric chemistry in physically consistent ways.

Two main limitations of this technique are the effects of systematic errors in the driving fields provided by global models and lack of two-way interactions between regional and global climate (IPCC, 2007). This technique has been used only in one-way mode, i.e., with no feedback from the RCM simulation to the driving GCM.

3.3.3 Statistical Methods

Statistical downscaling is based on the view that regional climate is being conditioned by two factors: the large scale climatic state and regional/local physiographic features (e.g., topography, land-sea distribution and land use). From this viewpoint, regional or local climate information is derived by first determining a statistical model which relates large-scale climate variables (predictors) to regional and local variables (predictands). Then the predictors from an AOGCM simulation are fed into this statistical model to estimate the corresponding local and regional climate characteristics.

One of the primary advantages of these techniques is that they are computationally inexpensive, and thus can easily be applied to output from different GCM experiments. Another advantage is that they can be used to provide local information, which can be most needed in many climate change impact applications. The applications of downscaling techniques vary widely with respect to regions, spatial and temporal scales, type of predictors and predictands, and climate statistics (IPCC, 2001).

The major theoretical weakness of statistical downscaling methods is that their basic assumption is not verifiable, i.e., that the statistical relationships developed for present day climate also hold under the different forcing conditions of possible future climates. In addition, data with which to develop relationships may not be readily available in remote regions or regions with complex topography.

3.4 Uncertainties in Climate Change Studies

There are several sources of uncertainty in the generation of climate change information. There is uncertainty associated with alternative scenarios of future emissions and their radiative effects. Uncertainties in the climatic effects of manmade aerosols (liquid and solid particles suspended in the atmosphere) constitute a major hesitation in quantitative studies. Bader et al., 2008 stated that we do not know how much warming due to greenhouse gases has been cancelled by cooling due to aerosols. Uncertainties related to clouds increase the difficulty in simulating the climatic effects of aerosols, since these aerosols are known to interact with clouds and potentially can change cloud radiative properties and cloud cover **(**Bader et al., 2008**).** The numerical models introduce uncertainties because of the finite approximation to the continuous equations. This approximation has two related aspects: one that there is a truncation error because of the numerical method and the other because of the effects of scales of motion smaller than the grid resolution on the resolved scale flow must be included (Thorpe, 2005).

3.5 Hydrological Models

There are many different reasons why modeling of the rainfall-runoff processes of hydrology is needed. The main reasons behind are a limited range of hydrological measurement techniques and a limited range of measurements in space and time (Beven, 2000). Therefore, it is necessary to develop a means of extrapolating from those available measurements in

space and time to ungauged catchments and into the future to assess the likely impact of future hydrological change. Hydrological models are characterizations of the real world system. A wide range of hydrological models are used by the researchers, however the applications of those models are highly dependent on the purposes for which the modeling is made. Beven (2000) stated that many rainfall-runoff models are carried out purely for research purposes as a means of enhancing knowledge about hydrological systems. He also added that other types of models are developed and employed as tools for simulation and prediction aiming ultimately to allow decision makers to improve decision making about hydrological problems.

Before developing the hydrological models it is vital to understand how the catchment responds to rainfall under different conditions.

3.5.1 Classification of Hydrological Models

There are a number of ways of classifying models. Classifications are generally based on the method of representation of the hydrological cycle or a component of the hydrologic cycle. Owing to the complex nature of rainfall-runoff processes, different hydrologists have different modeling approaches even to the same hydrological system. This process is called perceptual modeling (Beven, 2000).

Beven (2000) categorized rainfall-runoff models into lumped or distributed and deterministic or stochastic. In lumped models the hydrologic parameters do not vary spatially with in the basin and thus, basin response is evaluated only at the outlet, without explicitly accounting for the response of individual sub-basins (Cunderlik, 2003). Cunderlik added that the representation of hydrologic processes in lumped hydrologic models is usually very simplified; however they can often lead to satisfactory results, especially if the interest is in the discharge prediction only. The distributed models make predictions that are distributed in space by discretizing the catchment into a large number of elements or grid squares and solving the equations for the state variables associated with every element or grid square (Beven, 2000). Distributed models generally require large amounts of data parameterization in each grid cell. Cunderlik (2003) stated that if governing physical processes are modeled in detail and properly applied, distributed models can provide the highest degree of accuracy. There is a third type of model in this category called semi-distributed model. In semi-distributed model, the parameters of the model are allowed to vary partially in space by dividing the basin into a number of smaller sub-basins. The main advantage of semi-

distributed models is that their structure is more physically based than the structure of lumped models, and that they are less demanding an input data than fully distributed models (Cunderlik, 2003). Deterministic models permit only one outcome from a simulation with one set of inputs and parameter values while stochastic models allow for some randomness or uncertainty in the possible outcomes due to uncertainty in input variables, boundary conditions or model parameters (Beven, 2000).

Conceptual and physically based models are the other forms of model classification. Conceptual models are based on limited representation of the physical processes acting to produce the hydrological outputs, for instance the representation of a drainage basin by a cascade of stores, while physically based models are based more solidly on understanding of the relevant physical processes (Ward & Robinson, 2000). Ward & Robinson added that models may also be linear or non-linear in either the systems theory or statistical regression sense.

3.5.2 Hydrologic Model Selection

There are a range of possible model structures within each class of models. Hence, choosing a particular model structure for a particular application is one of the challenges of the model user community. Beven (2000) suggested four criterions for selecting model structures as below.

1. Consider models which are readily available and whose investment of time and money appeared worthwhile.
2. Decide whether the model under consideration will produce the outputs needed to meet the aims of a particular project.
3. Prepare a list of assumptions made by the model and check the assumptions likely to be limiting in terms of what is known about the response of the catchment. This assessment will generally be a relative one, or at best a screen to reject those models that are obviously based on incorrect representations of the catchment processes.
4. Make a list of the inputs required by the model and decide whether all the information required by the model can be provided within the time and cost constraints of the project.

4. Methodology

4.1 Climate Projection

4.1.1 Climate Scenario

GCM derived scenarios of climate change were used for predicting the plausible future climate of the study area as they conform to most of the criteria proposed by the IPCC task group on data and scenario support for impact and climate assessment (IPCC-TGICA). IPCC recommends using multiple scenarios; at minimum scenarios constructed from two different GCMs in impacts assessments. However, in this study due to availability of limited public domain GCM data and time constraint, only the GCM data from UK Hadley Center (HadCM3) was used. Besides, it was also for this GCM data a freely available downscaling tool was obtained. The GCMs data obtained were so coarse in resolution that it was less certain to apply them directly into impact assessment. Despite the advances in computing technology that have enabled large increases in the resolution of GCMs over the last few years, climate model results are still not sufficiently accurate at regional scales to be used directly in impacts studies (Mearns et al., 1997). Hence, downscaling techniques were used to bridge the spatial and temporal resolution gaps between what climate modelers are currently able to provide and what impact assessors require (Wilby & Dawson, 2007). In this study Statistical DownScaling Model was used for this task.

4.1.2 Statistical DownScaling Model

Statistical DownScaling Model (SDSM) is a decision support tool for assessing local climate change impacts using a robust statistical downscaling technique. SDSM facilitates the rapid development of multiple, low cost, single site scenarios of daily surface weather variables under present and future climate forcing. SDSM calculates statistical relationships, based on multiple linear regression techniques, between large-scale (the predictors) and local (the predictand) climate. These relationships were developed using observed weather data and, it was assumed that these relationships remain valid in the future. SDSM used to obtain downscaled local information for future time period by driving the relationships with GCM-derived predictors.

4.1.3 Statistical DownScaling Model Input

The predictor variables provide daily information concerning the large-scale state of the atmosphere, while the predictand describes conditions at the site scale (i.e. temperature or precipitation observed at a station).

Large-scale predictor variable information obtained from the National Center for Environmental Prediction (NCEP) reanalysis data set (for the calibration and validation) and HadCM3 GCM data for the baseline and climate scenario periods. The HadCM3 predictor variables are available for the A2a and B2a experiments and are downloaded from the Environment Canada[6] website. The predictor variables are supplied on a grid by grid box basis on entering the location of the site. For the study area (latitude: $10^0 56^{'}$-$11^0 51$'N and Longitude: $36^0 44^{'}$-$37^0 23^{'}$E) the correct grid box calculated and a zipped file was downloaded. The downloaded data consists of three data files as listed below and represents a resolution of 2.5^0 latitude by 3.75^0 longitude.

- NCEP_1961-2001: This directory contains 41 years of daily observed predictor data, derived from the NCEP reanalyses, normalized over the complete 1961-1990 period
- H3A2a_1961-2099: This directory contains 139 years of daily GCM predictor data, derived from the HadCM3 A2(a) experiment, normalized over the 1961-1990 period
- H3B2a_1961-2099: This directory contains 139 years of daily GCM predictor data, derived from the HadCM3 B2(a) experiment, normalized over the 1961-1990 period

The predictors of the NCEP and HadCM3 GCM experiment were listed in the **Table 1** with their descriptions.

[6] http://www.cccsn.ca/Download_Data/HadCM3_Predictors-e.html

Table 1: Daily predictor variable held in the grid box data archive

Variable	**Description**	**Variable**	**Description**
Temp	Mean temperature at 2m	s850	Specific humidity at 850 hpa height
Mslp	Mean sea level pressure	Derived variables	The following variables have been derived using the geostrophic approximation
p500	500hpa geopotential height	**_f	Geostrophic air flow velocity
p850	850 hpa geopotentail height	**_z	Vorticity
Rhum	Near surface relative humidity	**_u	Zonal velocity component
r500	Reative humidity at 500 hpa height	**_v	Meridional velocity component
r850	Relative humidity at 850 hpa height	**zh	Divergence
Shum	Near surface specific humidity	**th	Wind direction
s500	Specific humidity at 500 hpa height		

** refers to different atmpspheric levels: the surface (p_), 850hpa height (p8) and 500 hpa height (p5)

The predictand variables used in this study were precipitation, maximum and minimum temperature. Among the stations in the study area, Dangila station was considered for downscaling as it had a relatively better data quality. All of the stations in the drainage basin lay in the same grid box in the African window and it was assumed that the results obtained at Dangila station will also represent other stations in the drainage basin as well.

4.1.4 SDSM Modeling Approach

The downscaling of the GCMs data using SDSM was done following the procedures in the flow chart (Figure 6). Before starting the main SDSM downscaling operation, quality control of the data was undertaken to check an input data file for missing and unreasonable values. Scatter plot analysis was performed and it was checked that all the predictands were normally

distributed; hence transformation operation was found unimportant. The other operations performed for downscaling are dealt in detail in the following sections.

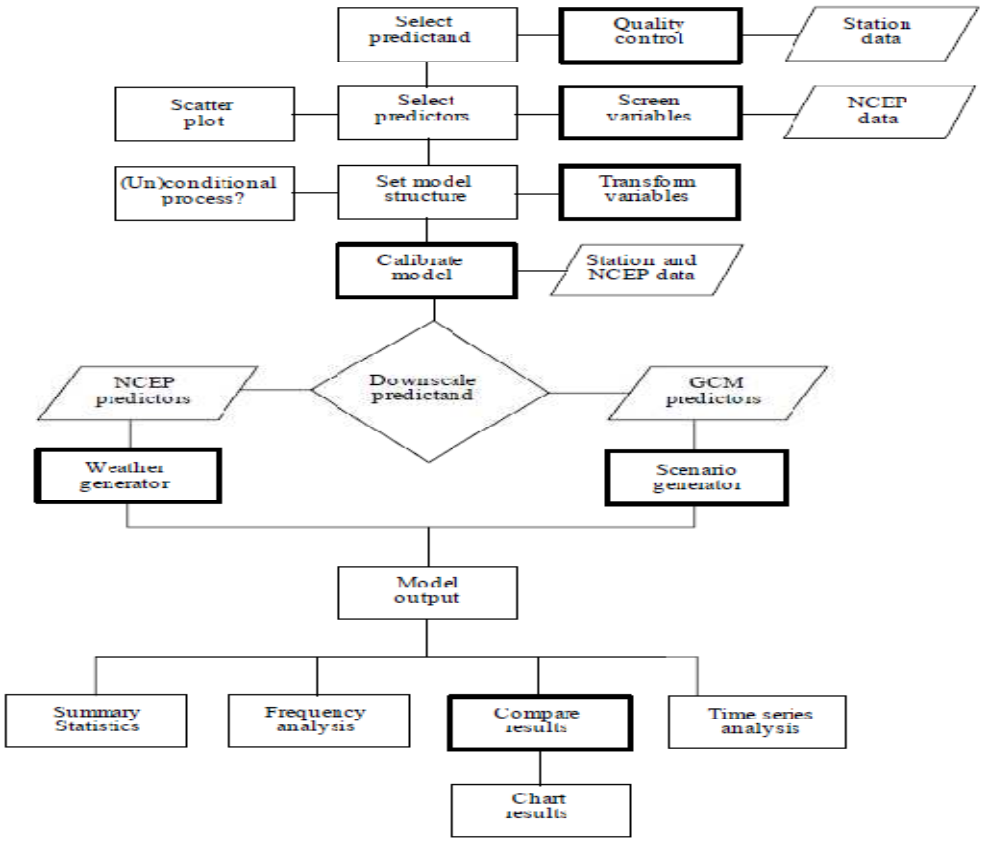

Figure 6: SDSM 4.1 climate scenario generation flow chart (Wilby & Dawson, 2008)

4.1.4.1 Screening of downscaling predictor variables

The screen variables option used to select the appropriate downscaling predictors for model calibration. The screening of variables was done by trial and error procedure and it was the most time consuming activity in the downscaling process. For maximum and minimum temperature downscaling an unconditional process was selected as the predictor-predictand process is not regulated by an intermediate process where as for the precipitation as the amount depends on wet-dry day occurrence, a conditional process was selected. The significance level which tests the significance of predictor-predictand correlation was set to the default ($P<0.05$). The correlation analysis was used to investigate inter-variable correlations for specified periods (monthly, seasonal, or annual). The correlation matrix gives a report for the partial correlations between the selected predictors and predictand which helped to identify the amount of explanatory power that is unique to each predictor. Using the partial correlations statistics, predictors which showed the strongest association with the

predictand were selected. The scatter plot operation was also performed for visual inspection of inter-variable behavior for specified sub-periods (monthly, seasonal, or annual). The scatter plots were used to see the nature of association (linear, non-linear, etc) between the predictor and predictand which was important to decide whether or not data transformation was necessary.

4.1.4.2 Model Calibration

The NCEP reanalysis data which was used to calibrate and validate the model has a range of data from 1960-2001 and the observed data collected from the Ethiopian National Metrological Services Agency (NMSA) was from 1990-2001. Hence, the data from 1990-1997 was used for model calibration and from 1998-2001 was used for model validation.

The calibrate model process constructs downscaling models based on multiple regression equations, given daily weather data (predictand) and regional scale, atmospheric (predictor) variables. The ordinary least squares optimization technique was preferred against the dual simplex to calibrate the SDSM because the modeling process was slowed down when chow test was performed with the dual simplex optimization. An unconditional process was selected for the maximum and minimum temperature and conditional for the precipitation owing to the presence of intermediate processes. A monthly temporal resolution of the downscaling model was chosen to derive different model parameters for each month. Upon completion of the appropriate selections, the model was calibrated. The resultant model calibration parameter (*.par) file generated was attached in appendix-2 for the precipitation, maximum and minimum temperature.

4.1.4.3 Weather Generation

A synthetic ensembles of daily weather series were produced giving the observed (NCEP reanalysis) atmospheric predictor variables and regression model weights produced by the calibrate model operation. The generated weather was used for the verification of the calibrated model for an independent data set (1998-2001) withheld from the calibration process. An ensemble size of 20 (default) values was generated. Despite individual ensemble members are considered equally plausible, the mean of the 20 ensembles was used for the model validation process.

4.1.4.4 Scenario Generation

The calibrated and validated model was used for the generation of ensembles of synthetic daily weather series giving daily atmospheric predictor variables from the HadCM3 A2a and

B2a experiment. The scenario generation produced 20 ensembles of synthetic weather data for 139 years (1961-2099), and the mean of the ensembles was calculated and used for impact assessment. It was adequate to consider the mean of the ensembles as the aim of such type of study is to see the general trend of climate change in the future, and to preserve inter-variable relationships (Lijalem, 2007).

4.2 Hydrological Modeling

A physically based hydrological model was developed for the Lake Tana basin to assess the impact of climate change on tributary rivers and on the lake. Soil and Water Assessment tool (SWAT) was selected as the best modeling tool owing to many reasons. First and for most it is a public domain model and it is used for free. Secondly in countries like Ethiopia, there is a shortage of long term observational data series to use sophisticated models; however, SWAT is computationally efficient and requires minimum data. Besides SWAT was checked in the highlands of Ethiopia and gave satisfactory results (Setegne, 2007). SWAT model was developed to predict the impact of land management practices on water, sediment, and agricultural chemical yields. However, this study concentrated on the hydrological aspect of the sub-basin. The description of the model, model inputs and model setup are discussed in detail in the subsequent sections.

4.2.1 Soil and Water Assessment Tool (SWAT) Background

SWAT is a physically based river basin scale model developed by Dr. Jeff Arnold to predict the impact of land management practices on water, sediment and agricultural chemical yields in large complex watersheds with varying soils, land use and management conditions over long periods of time (Neitsch et al., 2005). SWAT model is a continuation of several non-point sources modeling but a direct outgrowth of SWRRB model (Simulator for Water Resources in Rural Basins). SWRRB is a continuous time step model that was developed to simulate nonpoint source loadings from watersheds (Neitsch et al., 2005). The number of sub-basins in SWRRB was limited to ten and the model routed water and sediment transported out of the sub-basins directly to the watershed outlet which were the difficulty to use the model for large watersheds. These limitations led to the development of a model called ROTO (Routing Outputs to Outlet) (Arnold et al., 1995), which took output from multiple SWRRB runs and routed the flows through channels and reservoirs. The input and outputs of multiple SWRRB files were cumbersome and required considerable computer storage. Besides, all SWRRB runs had to be made independently and then input to ROTO for channel and reservoir routing. To overcome the awkwardness of this arrangement, SWRRB and ROTO

were merged into a single model, SWAT in the early 1990s (Neitsch et al., 2005). SWAT has undergone continued review and expansion of capabilities since its development. The interfaces for the model have been developed in Windows (visual basic), GRASS, and ArcView. The ArcSwat2005 ArcGIS extension was used for this study.

For all types of problems dealt in SWAT, water balance is the driving force behind everything that happens in the watershed. Simulation of the hydrology of a watershed in SWAT is separated into two major divisions. The first division is the land phase of the hydrological cycle as depicted in Figure 7 which controls the amount of water, sediment, nutrient and pesticide loadings to the main channel in each sub-basin. The land phase of the hydrological cycle is simulated by SWAT based on the water balance equation:

$$\mathbf{SW_t = SW_0 + \sum_{i=1}^{t}\left(R_{day} - Q_{surf} - E_a - w_{seep} - Q_{gw}\right)}\ldots\ldots\ldots\ldots\ldots\ldots\text{Eqn 1}$$

where: SW_t is the final soil water content (mm H_2O)

SW_o is the initial soil water content on day i (mm H_2O)

t is the time in days

R_{day} is the amount of precipitation on day i (mmH_2O)

Q_{surf} is the amount of runoff on day i (mmH_2O)

E_a is the amount of evapotranspiration on day i (mmH_2O)

W_{seep} is the amount of water entering the vadose zone from the soil profile on day i (mmH_2O)

Q_{gw} is the amount of return flow on day i (mmH_2O)

The second division is the water or routing phase of the hydrological cycle which is the movement of water, nutrients, sediment and pesticides through the channel network of the watershed into the outlet.

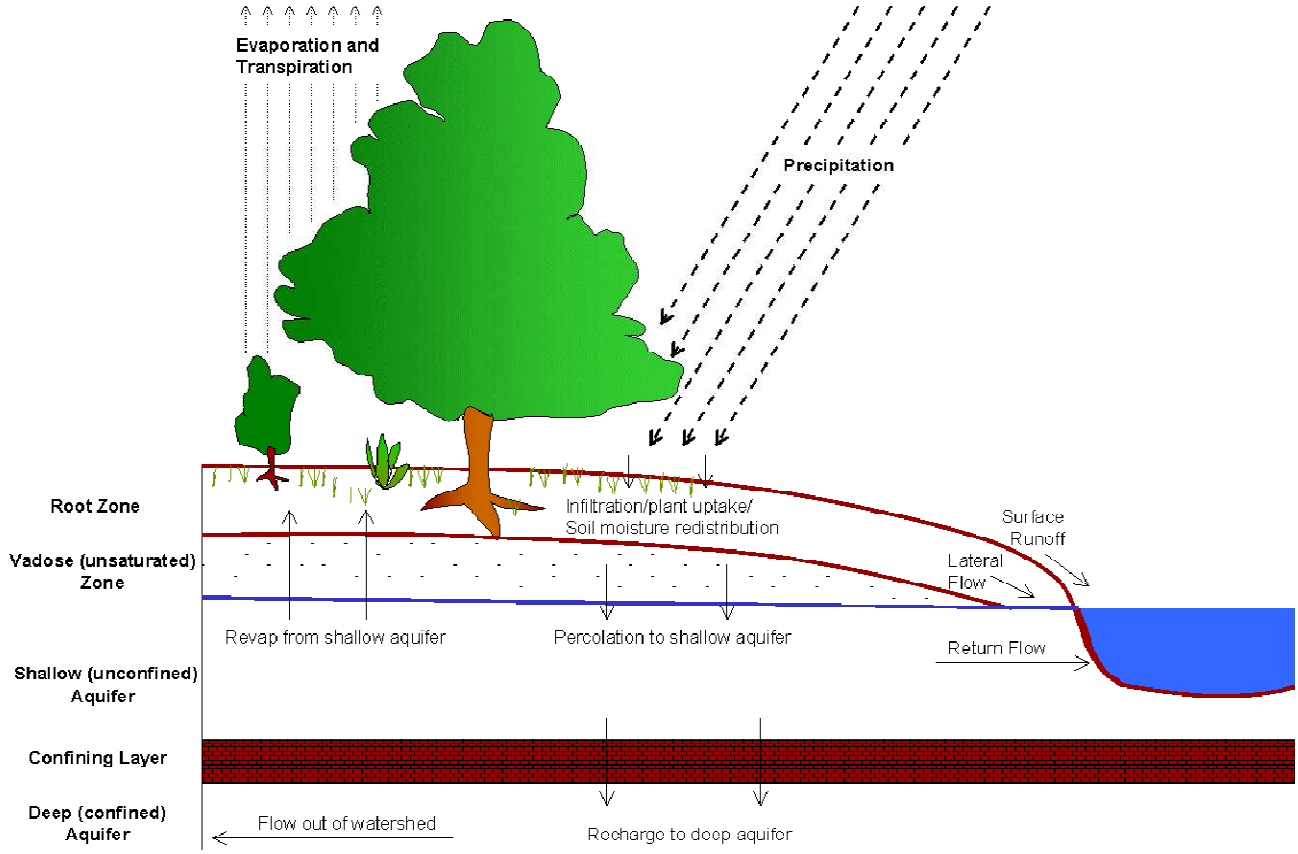

Figure 7: Schematic representation of the hydrological cycle (Neitsch et al., 2005)

SWAT requires daily values of precipitation, maximum and minimum temperature, solar radiation, relative humidity and wind speed. These files may be given as an input to the model or can be generated from the monthly average data summarized over a number of years using WXGEN (an in-built weather generator model). These climatic variables are central in the determination of hydrological cycle of the drainage basin besides land use, soil and management practices inputs.

It might be vital to discuss the most important hydrological cycle components and their estimation by SWAT model for this study; for further detailed explanation the author recommends referring the SWAT2005 theoretical documentation.

Most of the water in the earth's surface is removed by evapotranspiration. Roughly 62% of the precipitation that falls on the continents is evapotranspired (Neitsch et al., 2005). Hence accurate estimation of Evapotranspiration is vital in the assessment of water resources and the impact of climate and land use on these resources. SWAT uses the Penman-Monteith method, the Priestley-Taylor method, and the Hargreaves method for the estimation of potential

evapotranspiration. Three of the methods have different input data requirements. The Penman-Monteith method requires solar radiation, air temperature, relative humidity and wind speed. The Priestley-Taylor method requires solar radiation, air temperature, and relative humidity. The Hargreaves method requires only air temperature. For this study due to availability of only temperature data, the Hargreaves method was used for the determination of the potential Evapotranspiration.

The Hargreaves method was developed in 1975 but several improvements were made to the original equation. The form used in SWAT (Eqn 2) was published in 1985 (Neitsch et al., 2005).

$$\boldsymbol{\lambda E_0 = 0.0023 * H_0 * (T_{mx} - T_{mn})^{0.5}(\overline{T}_{av} + 17.8)} \text{ … … … … … … … … … … …..Eqn 2}$$

where: λ is the latent heat of vaporzation (MJ kg^{-1})

E_0 is the potential evapotranspiration (mm d^{-1})

H_0 is the extraterrestrial radiation ($MJm^{-2}d^{-1}$)

T_{mx} is the maximum air temprature for a given day (^0C)

T_{mn} is the minimum air temprature for a given day(^0C)

$\overline{T}_{av}$ is the mean air temprature for a given day (^0C)

SWAT provides the SCS curve number procedure and the Green & Ampt infiltration method for estimating surface runoff. For this study the SCS curve number procedure was preferred over the Green & Ampt infiltration method. The Green & Ampt infiltration method assumes that there will be excess water at the surface at all times which was invalid assumption in the study area. Besides, the Green and Ampt infiltration method requires sub-daily precipitation data which was other limitation to use this method.

The SCS curve number method is simple, widely used and efficient for determining the approximate amount of runoff from a rainfall event under a varying land use and soil types. The 1972 SCS curve number equation (Eqn 3) is used in SWAT model.

$$\mathbf{Q_{surf}} = \frac{(\mathbf{R_{day} - I_a})^2}{(\mathbf{R_{day} - I_a + S})} \text{ … … … … … … … … … … … … … … … ….Eqn 3}$$

where Q_{surf} is the accumulated rainfall excess (mm H_2O)

R_{day} is the rainfall depth for the day (mm H_2O)

$I_a$is the initial abstraction which includes surface storage, infilitration

and infiltration prior to runoff (mm H_2O)

S is the the retention parameter (mm H_2O)

The retention parameter varies spatially due to changes in soils, land use, management and slope and temporarily due to changes in the soil water content. The retention parameter is defined as in Eqn 4.

$$\mathbf{S = 25.4\left(\frac{1000}{CN} - 10\right)} \text{ … … … … … … … … … … … … … … … … …..Eqn 4}$$

where, CN is the curve number for the day. The curve number is based on the area's hydrologic soil group, land use and hydrologic condition. The initial abstractions,I_a, is commonly approximated as 0.2S and Eqn 3 becomes:

$$\mathbf{Q_{surf} = \frac{(R_{day} - 0.2S)^2}{(R_{day} + 0.8S)}} \text{ … … … … … … … … … … … … … … … … …..Eqn 5}$$

The other component of the hydrological cycle which contributes to the stream flow is the groundwater. SWAT simulates two aquifers in each sub-basin: shallow and deep. The shallow aquifer is an unconfined aquifer and deep aquifer is the confined aquifer.

The water balance for the shallow aquifer is described in Eq 6.

$$\mathbf{aq_{sh,i} = aq_{sh,i-1} + w_{rchrg,sh} - Q_{gw} - w_{revap} - w_{pump,sh}} \text{ … … … … … …..Eqn 6}$$

where $aq_{sh,i}$ is the amount of water stored in the shallow aquifer on day i (mm H_2O)

$Aq_{sh,i-1}$ is the amount of water stored in the shallow aquifer on day i − 1 (mm H_2O)

w_{rchrg} is the amount of recharge entering the shallow aquifer on day i (mm H_2O)

Q_{gw} is the groundwater flow, or base flow, into main channel on day i (mm H_2O)

$w_{revap}$is the amount of water moving into the soil zone in response to water difficiencie on day i (mm H_2O)

$w_{pump,sh}$ is the amount of water removed from shallow aquifer by pumping on day i (mm H_2O)

Water that moves past the lowest depth of the soil profile by percolation or bypass flow enters and flows through the vadose zone before becoming shallow and/or deep aquifer recharge. The lag between the time that water exits the soil profile and enters the shallow aquifer will

depend on the depth to the water table and the hydraulic properties of the geologic formations in the vadose zone and groundwater zones.

SWAT utilizes an exponential decay weighing function proposed by Venetis (1969) and used by Sangrey et al. (1984) in a precipitation/groundwater response model to estimate the time delay in aquifer recharge once the water exits the soil profile (Neitsch et al., 2005). The recharge to both aquifers on a given day is calculated using Eqn 7.

$$\mathbf{w_{rchrg,i}} = \left(\mathbf{1} - \mathbf{exp}\left[-\mathbf{1}/\boldsymbol{\delta}_{\mathbf{gw}}\right]\right) * \mathbf{w_{seep}} + \mathbf{exp}\left[-\mathbf{1}/\boldsymbol{\delta}_{\mathbf{gw}}\right] * \mathbf{w_{rchrg,i-1}} \quad \text{... ... ...Eqn 7}$$

where: $w_{rchrg,i}$ is the amount or recharge enetering the aquifers on day i ((mm H_2O)

δ_{gw} is the delay time of the overlaying geologic formations (days)

W_{seep} is the total amount of water exiting the bottom of the soil profile on day i (mm H_2O)

$w_{rchrg,i-1}$ is the amount or recharge entering the aquifers on day i $-$ 1 ((mm H_2O)

The total amount of water exiting the bottom of the soil profile on a day i is calculated using Eqn 8.

$$\mathbf{w_{seep}} = \mathbf{w_{perc,ly=n}} + \mathbf{w_{crk,btm}} \quad \text{... ... ...Eqn 8}$$

where: $w_{crk,btm}$ is the amount of water percolating out of the lowest layer, n, in the soil profile on day i (mm H_2O)

$w_{crk,btm}$ is the amount of water flow past the lower boundary of the soil profile due to pass flow on day i (mm H_2O)

The shallow aquifer contributes base flow to the main channel or reaches within the sub-basin. Base flow is allowed to enter the reach only if the amount of water stored in the shallow aquifer exceeds a threshold value specified by the user, $aq_{shthr,q}$.

SWAT uses the Hooghoudt's (1940) equation (Eqn 9) to determine the steady-state response of groundwater flow recharge.

$$\mathbf{Q_{gw}} = \frac{\mathbf{8000} * \mathbf{k_{sat}}}{\mathbf{L_{gw}^2}} * \mathbf{h_{wtbl}} \quad \text{... ... ...Eqn 9}$$

where: K_{sat} is the hydraulic conductivity of the aquifer $\left(\frac{\text{mm}}{\text{day}}\right)$

L_{gw} is the distance from the ridge or sub $-$ basin divide for the groundwater

system to the main channel (m)

h_{wtbl} is the water table height

SWAT calculates the water level fluctuations due to non-steady-state response of groundwater flow to periodic recharge using Eqn 10 (Smedema and Rycroft, 1983).

$$\frac{\mathbf{dh_{wtbl}}}{\mathbf{dt}} = \frac{\mathbf{w_{rchrg,sh} - Q_w}}{\mathbf{800 * \mu}} \ldots\ldots\ldots\ldots\ldots\ldots\ldots\ldots\ldots\ldots\ldots\ldots\ldots\ldots\ldots. \ldots\text{Eqn 10}$$

where: $\frac{dh_{wtbl}}{dt}$ is the change in water table height with time (mm/day)

μ is the specific yield of the shallow aquifer $\left(\frac{m}{m}\right)$

assuming that variation in groundwater flow is linearly related to the rate of recharge in water table height, Eqn 9 & 10 can be combined to obtain Eqn 11.

$$\frac{\mathbf{dQ_{gw}}}{\mathbf{dt}} = \mathbf{10} * \frac{\mathbf{K_{sat}}}{\mathbf{\mu * L_{gw}^2}} * \left(\mathbf{w_{rchrg,sh}} - \mathbf{Q_{gw}}\right) = \boldsymbol{\alpha}_{\mathbf{gw}} * \left(\mathbf{w_{rchrg,sh}} - \mathbf{Q_{gw}}\right) \ldots\ldots\ldots\ldots\ldots\ldots\ldots\text{Eqn 11}$$

where:

α_{gw} is the baseflow recission constant and all the other terms are as defined before

Integration and rearranging of Eqn 11 yields Eqns 12 & 13 which is used to calculate the groundwater flow.

$$Q_{gw,i} = Q_{gw,i-1} * \exp[-\alpha_{gw} * \Delta t] + w_{rchrg,sh} * \left(1 - \exp[-\alpha_{gw} * \Delta t]\right)$$

$$\textbf{if } \mathbf{aq_{sh}} > \mathbf{aq_{shthr,q}} \ldots\ldots\ldots\text{Eqn 12}$$

$$\mathbf{Q_{gw,i}} = \mathbf{0} \qquad \textbf{if } \mathbf{aq_{sh}} < \mathbf{aq_{shthr,q}} \ldots\ldots\ldots\ldots\ldots\ldots\ldots\ldots\text{Eqn 13}$$

where: $Q_{gw,i}$ is the groundwater flow in to the main channel on day i (mm H_2O)

$Q_{gw,i-1}$ is the ground water flow into the main channel on day $i - 1$ (mm H_{2O})

Δt is the time step (1day)

$aq_{shthr,q}$ is the threshold water level in the shallow aquifer for groundwater contribution to the main channel to occur (mm H_20) and all the other terms are as defined above

Water may move from the shallow aquifer into the overlaying unsaturated zone. SWAT models the movement of water into the underlying unsaturated layers as a function of water

demand for evapotranspiration. When the material overlying the aquifer is dry, water in the capillary fringe evaporate and diffused upward. As water is removed from the capillary fringe by evaporation, it will be replaced from the underlying aquifer. This process is termed as 'revap'. 'Revap' is allowed to occur only if the amount of water stored in the shallow aquifer exceeds a threshold value, $aq_{shthr,rev}$.

The maximum amount of water that will be removed from the aquifer via 'revap' on a given day is as in Eqn 14.

$$\mathbf{w_{revap,mx} = \beta_{rev} * E_0} \text{ … … … … … … … … … … … … … … … … …Eqn 14}$$

where: $w_{revap,mx}$ is the maximum amount of water moving into the soil zone in response to water difficiences (mm H_2O)

β_{rev} is the revap coefficient

E_0 is the potential evapotranspiration for the day (mm H_2O)

The water balance for the deep aquifer is caluculated by Eqn 15.

$$\mathbf{aq_{dp,i} = aq_{dp,i-1} + w_{deep} - w_{pump,dp}} \text{ … … … … … … … … … …..Eqn 15}$$

where: $aq_{dp,i}$ is the amount of water stored in the deep aquifer on day i (mm H_2O)

$aq_{dp,i-1}$ is the amount of water stored in the deep aquifer on day $i-1$ (mm H_2O)

w_{deep} is the amount of water percolating from the shallow aquifer in to the deep aquifer on day i (mm H_2O)

$w_{pump,dp}$ is the amount of water removed from the deep aquifer by pumping on day i (mm H_2O)

In SWAT, the amount of water entering to the deep aquifer is not considered in water budget calculations and can be considered to be lost from the system.

SWAT uses manning's equation to define the rate and velocity of flow. Water is routed through the channel network using the variable storage routing method or the Muskingum river routing method. Both of the methods are variations of the kinematic wave model. In this study due to its simplicity, the variable storage model was selected. SWAT assumes the main channels are a trapezoidal shape.

Storage routing is based on the continuity equation for a given reach:

$$\mathbf{V_{in} - V_{out} = \Delta V_{stored}} \ldots\ldots\ldots\ldots\ldots\ldots\ldots\ldots\ldots\ldots\ldots\ldots\ldots\ldots\ldots\text{Eqn 16}$$

where: V_{in} is the volume of inflow during the time step (m^3 H_2O)

V_{out} is the volume of outflow during the time step (m^3H_2O)

$\Delta V_{storage}$ is the change in the volume of storage during time step (m^3 H_2O)

The Eqn 16 can be written as:

$$\mathbf{\Delta t * \left(\frac{q_{in,1}+q_{in,2}}{2}\right) - \Delta t * \left(\frac{q_{out,1}+q_{out,2}}{2}\right) = V_{stored,2} - V_{stored,1}} \ldots\ldots\ldots\ldots\ldots\ldots\ldots\text{Eqn 17}$$

where: Δt is the time step (s)

$q_{in,1}$ is the inflow rate at the begining of the flow rate $\left(\frac{m^3}{s}\right)$

$q_{in,2}$ is the inflow rate at the end of the flow rate $\left(\frac{m^3}{s}\right)$

$q_{out,1}$ is the outflow rate at the begining of the flow rate $\left(\frac{m^3}{s}\right)$

$q_{out,2}$ is the outflow rate at the end of the flow rate $\left(\frac{m^3}{s}\right)$

$V_{stored,1}$ is the storage volume at the biginning of the time step (m^3 H_2O)

$V_{stored,2}$ is the storage volume at the end of the time step (m^3 H_2O)

Rearranging Eqn 17, all the known variable are on the left side of the equation,

$$\mathbf{q_{in,ave} + \frac{V_{stored,1}}{\Delta t} - \frac{q_{out,1}}{2} = \frac{V_{stored,2}}{\Delta t} + \frac{q_{out}}{2}} \ldots\ldots\ldots\ldots\ldots\ldots\ldots\text{....Eqn 18}$$

where: $q_{in,ave}$ is the average inflow rate during the time step

The time in the reach is computed by dividing the volume of water in the channel by the flow rate.

$$\mathbf{TT = \frac{V_{stored}}{q_{out}} = \frac{V_{stored,1}}{q_{out,1}} = \frac{V_{stored,2}}{q_{out,2}}} \ldots\ldots\ldots\ldots\ldots\ldots\ldots\ldots\ldots\ldots\text{..Eqn 19}$$

where: TT is the travel time and others are as defined before

By substituting Eqn 19 is substituted in to Eqn 18 to develop a relationship between travel time and storage coefficient.

$$\mathbf{q_{in,ave} + \frac{V_{stored,1}}{\left(\frac{\Delta t}{TT}\right)*\left(\frac{V_{stored,1}}{q_{out,1}}\right)} - \frac{q_{out,1}}{2} = \frac{V_{stored,2}}{\left(\frac{\Delta t}{TT}\right)*\left(\frac{V_{stored,2}}{q_{out,2}}\right)} + \frac{q_{out,2}}{2}} \ldots\ldots\ldots\ldots\ldots\ldots\text{...Eqn 20}$$

which simplifies to

$$\mathbf{q_{out,2}} = \left(\frac{\mathbf{2*\Delta t}}{\mathbf{2*TT+\Delta t}}\right) * \mathbf{q_{in,ave}} + \left(\mathbf{1} - \frac{\mathbf{2*\Delta t}}{\mathbf{2*TT+\Delta t}}\right) * \mathbf{q_{out,1}} \quad \text{...Eqn 21}$$

This equation is similar to the coefficient method equation

$$\mathbf{q_{out,2}} = \mathbf{SC} * \mathbf{q_{in,av}} + (\mathbf{1} - \mathbf{SC}) * \mathbf{q_{out,1}} \quad \text{...Eqn 22}$$

where SC is the storage coefficient. Eqn 22 is the basis for the SCS convex routing method and the Muskingum method. From equation Eqn 21 the storage coefficient in Eqn 22 is defined as

$$\mathbf{SC} = \frac{\mathbf{2*\Delta t}}{\mathbf{2*TT+\Delta t}} \quad \text{...Eqn 23}$$

It can be shown that

$$(\mathbf{1} - \mathbf{SC}) * \mathbf{q_{out}} = \mathbf{SC} * \frac{\mathbf{V_{stored}}}{\mathbf{\Delta t}} \quad \text{...Eqn 24}$$

Substituting Eqn 24 into Eqn 22 gives

$$\mathbf{q_{out,2}} = \mathbf{SC} * \left(\mathbf{q_{in,av}} + \frac{\mathbf{V_{stored}}}{\mathbf{\Delta t}}\right) \quad \text{...Eqn 25}$$

To express all values in units of volume, both sides of the equation are multiplied by the time step and Eqn 26 obtained.

$$\mathbf{V_{out,2}} = \mathbf{SC} * (\mathbf{V_{in}} + \mathbf{V_{stored,1}}) \quad \text{...Eqn 26}$$

4.2.2 SWAT Model Inputs

4.2.2.1 Digital Elevation Model

The digital elevation model (DEM) data was used to delineate the sub-watersheds in the ArcSWAT interface. The DEM data was downloaded from the CGIAR Consortium for Spatial Information (CGIAR-CSI) website[7]; infact the DEM data was the property of NASA shuttle Radar Topographic Mission (SRTM). The SRTM digital elevation data provided on this site has been processed to fill data voids. The DEM data used for this study was downloaded in GeoTiff format for the coordinates of the study area (latitude: 10.95^{o}N to 12.78^{o}N and Longitude: 36.89^{o}E to 38.25^{o}E). The Downloaded DEM data was shown in Figure 8. It had a resolution of 90m and was provided in mosaiced 5 deg x 5 deg tiles for easy download and use. The vertical error of the DEM data was reported to be less than 16m. Before the DEM data was loaded in to ArcSWAT interface, it was projected into projected coordinate system. The projection of the DEM data was done using the Arctool box operation

[7] http://srtm.csi.cgiar.org/SELECTION/inputCoord.asp

in ArcGIS. The projected coordinate system parameters of Ethiopia (study area) are: UTM—other GCS—Adindan UTM zone 37N.prj.

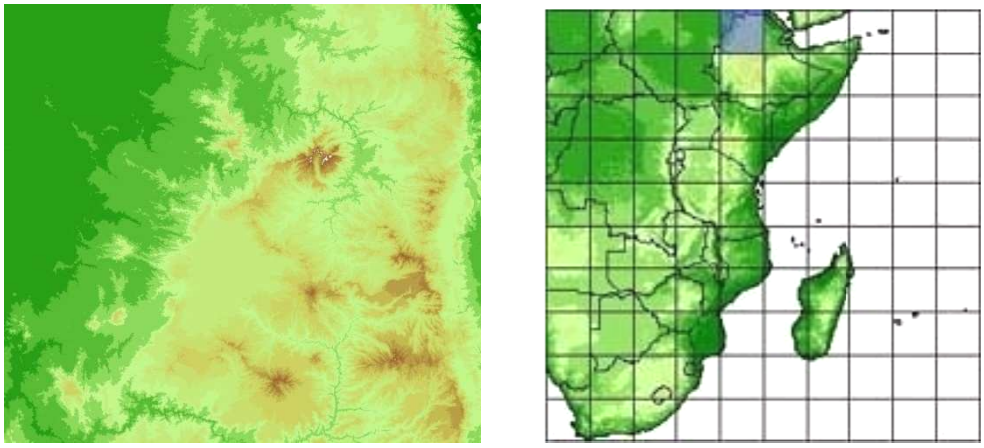

Figure 8: DEM data for the study area (left side) and region in the world map for which the DEM is downloaded (right side) (source: http://srtm.csi.cgiar.org/SELECTION/inputCoord.asp)

As the downloaded DEM covered a larger area in which part of it was not required for the modeling work but reduced the processing time of the GIS functions, a mask was created for the study area. Hence, only the portion of the DEM covered by the mask processed by the interface.

4.2..2.2 Stream Network

The stream network data set was collected from the Ethiopian Ministry of Water Resources (MoWR), GIS department during field visit. The stream network was in a shape file format consisting of the major and minor river systems in the study area (shown in Figure **9**). The stream network dataset was superimposed onto the DEM to define the location of the stream network. Burning-in stream network operation is most important in situations where the DEM does not provide enough detail to allow the interface to accurately predict the location of the stream network.

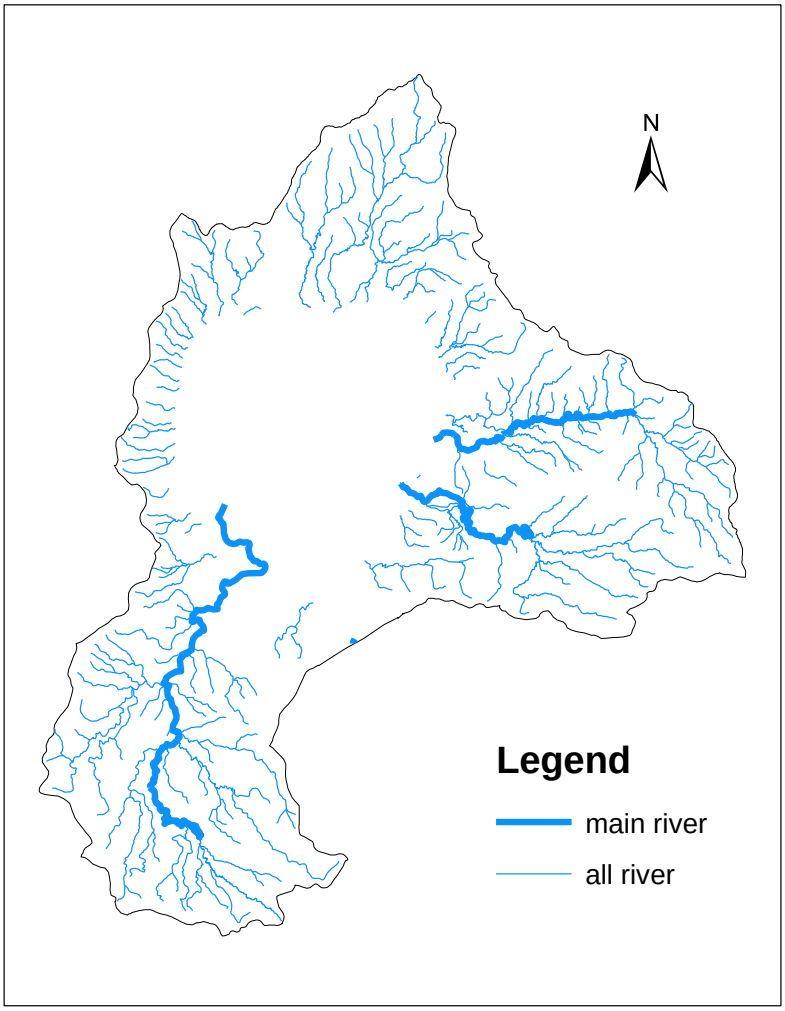

Figure 9: Stream network map in the study area (Source: shape file obtained from the MoWR)

4.2.2.3 Land Use/Land Cover

The land use/land cover map of the study area was collected from MoWR GIS department which was obtained in shape file format. The land use/cover data reclassified according to the SWAT land use/cover type. Redefining was done based on the data collected from physical observation during field visit and personal judgment. A widely cultivated cereal crop locally called ‘’teff’’ was not included in the SWAT crop database. This is due to that fact that teff is growing only in Ethiopia. Hence, the characteristics of this intriguing grain were set after having a discussion with the model developers. A look up table that identifies the 4-letter SWAT code for the different categories of land cover/land use were prepared so as to relate the grid values to SWAT land cover/land use classes. SWAT calculated the area covered by each land use. The different land use/cover types are presented in Table 2 and Figure 10. The characteristic land use parameter values were enclosed in Appendix 3.

Table 2: Land use/land cover types in the study area and redefinition according to SWAT code

Original land use/land cover	Redefined Land use according to SWAT Database	SWAT Code
Afro alpine	Forest deciduous	FRSD
Forest	Forest evergreen	FRSE
Dominantly cultivated	Teff	TEFF
Grassland	Range-grasses	RNGE
Moderately cultivated	Agricultural Land-Row crops	AGRR
Plantation	Agricultural Land-Generic	AGRL
Shrub land	Range-brush	RNGB
Swamp	Wetlands-non forested	WETN
Water body	Water	WATR
Urban	Urban	URBN

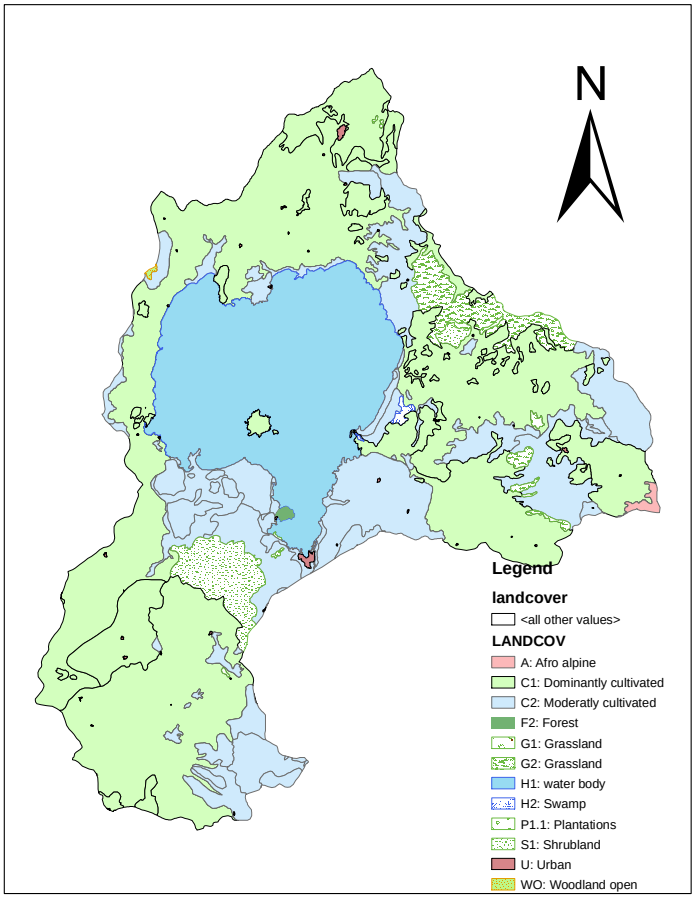

Figure 10: Land use/land cover map of the study area (Source: shape file obtained from MoWR)

4.2.2.4 Soil Data

Soil data was also collected from the Ethiopian MoWR GIS department during field visit. However, this data (Figure 11) was only in shape file format and the characteristics of the soils needed by the SWAT couldn't be found. The soil data used for this study was rather downloaded from the digital soil map of the world CD-ROM Africa map sheet clipped to the extent of the region under study. Chromic Luvisols, Eutric Cambisols, Eutric Fluvisols, Eutric Leptosols, Eutric Regosols, Eutric Vertisols, Haplic Alisols, Haplic Luvisols, Haplic Nitisols, and Lithic Leptosols are the major soils in the study area. However, FAO merges these soil types into four soil classes as I-Y-ab-#92, I-Y-ab-#91, I-Rd#79 and Qc15-1a#169. This data was found in raster format and has a resolution of 10km. The basic characteristics of the soils and the look up table which links the grid size with the soil type was obtained from Katholic University of Leuven, Water Resources Engineering department research team.

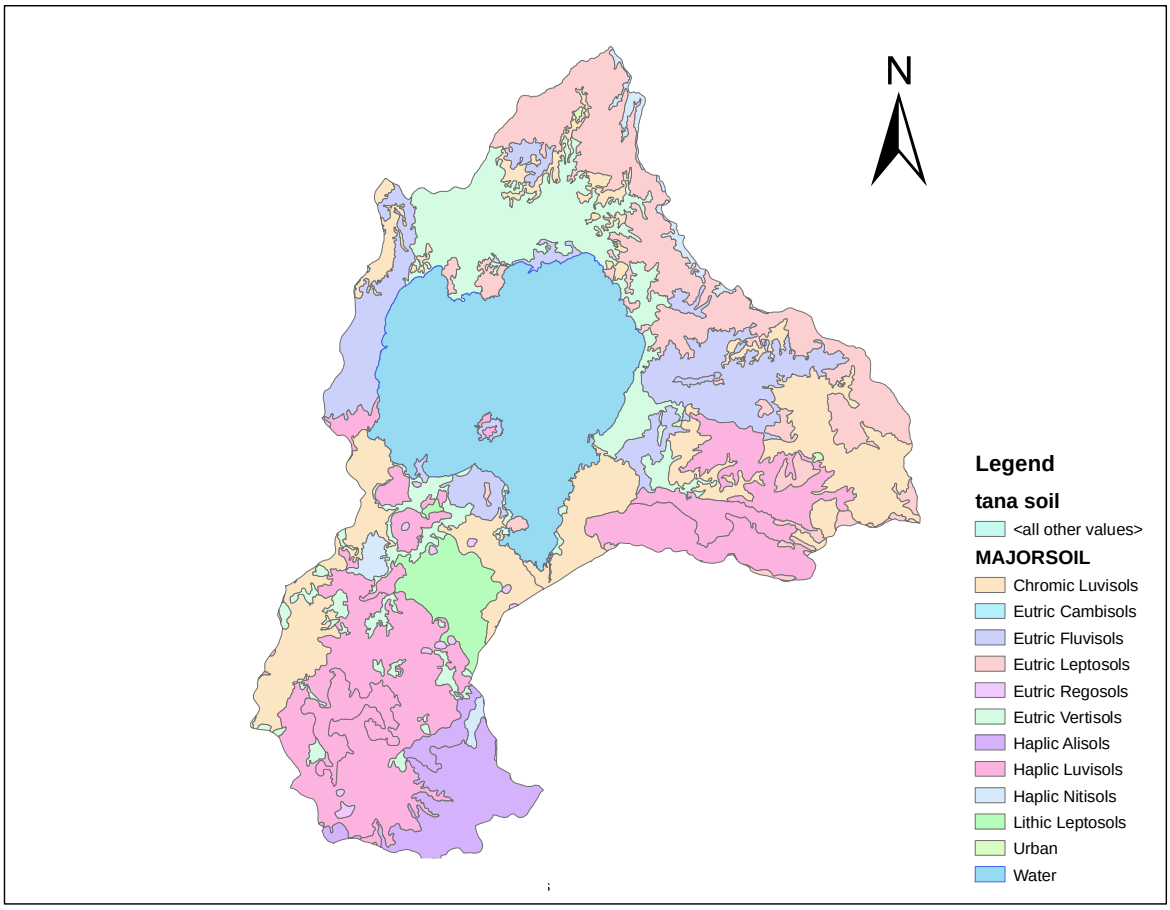

Figure 11: Soil map of the study area (Source: shape file obtained from MoWR)

4.2.2.5 Meteorological Data

Meteorological data is needed by the SWAT model to simulate the hydrological conditions of the basin. The meteorological data required for this study were collected from the Ethiopian National Meteorological Services Agency (NMSA). The meteorological data collected were precipitation, maximum and minimum temperature, relative humidity, wind speed and sunshine hours. Data from ten stations, which are within and around the study area, were collected. However, most of the stations have short length of record periods. Six of the stations have records within the range of 1988-2004 but most of them have missing data especially during 1991-1992 where there was government transition in Ethiopia. In some stations the missing data extends to 1995. The other problem in the weather data was inconsistency in the data record. In some periods there is a record for precipitation but there will be a missing data for temperature, and vice versa. As the SWAT model requires data of the same periods of record, the weather data used for the study was set from 1995-2004.

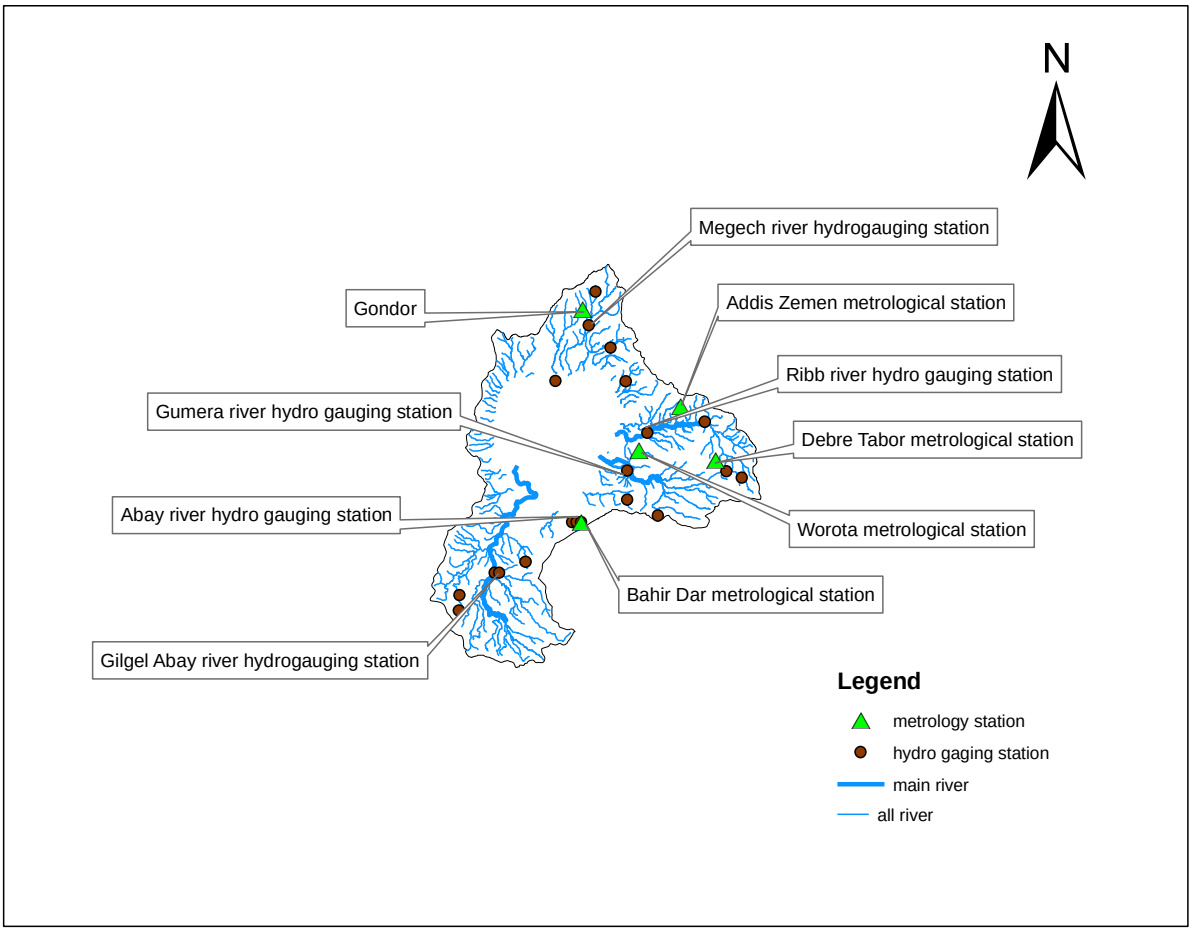

Figure 12: Meteorological and hydrological gauging stations in the study area (Source: shape file obtained from MoWR)

Data quality analysis was performed using SDSM quality control operation. Based on the SDSM quality control analysis and data availability, the precipitation data from Adet, Bahirdar, Dangila, Debre Markos, Debre Tabor, and Gondor, and the maximum and minimum temperature data of these stations except Debere Markos were used as input to the model. Figure 12 shows the location of some of the stations which are found within the watershed.

4.2.2.6 Hydrological Data

The hydrological data was required for performing sensitivity analysis, calibration and uncertainty analysis and validation of the model. The hydrological data was also collected from the Ethiopian MoWR hydrological section. The hydrological data collected was daily flow for the four major rivers feeding in to Lake Tana and the lake water level. The four rivers draining into Lake Tana are: Gilgel Abay, Gumera, Ribb and Megech. However, due to time limitation to accomplish sensitivity analysis and calibration for the four river basins, it was decided to concentrate on the largest river (Gilgel Abay) for modeling and climate impact analysis. Hence, it was only the hydrological data of the Gilgel Abay used for sensitivity analysis, calibration and validation. The location of the gauging stations is presented in Figure 12.

4.2.3 ArcSWAT Model Setup

4.2.3.1 Watershed Delineation

ArcSWAT uses digital elevation model (DEM) data to automatically delineate the watershed into several hydrologically connected sub-watersheds. The watershed delineation operation uses and expands ArcGIS and Spatial Analyst extension functions to perform watershed delineation. The first step in the watershed delineation was loading the properly projected DEM. To reduce the processing time of the GIS functions, a mask was created over the DEM around the study area. Next, a polyline stream network dataset was burnt-in to force SWAT sub-basin reaches to follow known stream reaches. Burning-in a stream network improves hydrological segmentation, and sub-watershed delineation. After the DEM grid was loaded and the stream networks superimposed, the DEM map grid was processed to remove the non-draining zones.

The initial stream network and sub-basin outlets were defined based on drainage area threshold approach. The threshold area defines the minimum drainage area required to form the origin of a stream. The interface lists a minimum, maximum and suggested threshold area. The smaller the threshold area, the more detailed the drainage network delineated by the

interface but the slower the processing time and the larger memory space required. In this study, defining of the threshold drainage area was done by successive re-run of the stream and outlet definition routine from the suggested to the minimum area until known smaller streams were created. Besides those sub-basin outlets created by the interface, outlets were also manually added at the four hydro gauging stations where sensitivity analysis, calibration and validation tasks were later performed. The watershed delineation activity was finalized by calculating the geomorphic sub-basin parameter.

4.2.3.2 Hydrologic Response Unit Analysis

Hydrologic response units (HRUs) are lumped land areas within the sub-basin that are comprised of unique land cover, soil and management combinations. HRUs enable the model to reflect differences in evapotranspiration and other hydrologic conditions for different land covers and soils. The runoff is estimated separately for each HRU and routed to obtain the total runoff for the watershed. This increases the accuracy in flow prediction and provides a much better physical description of the water balance.

The land use and the soil data in a projected shape file format were loaded into the ArcSWAT interface to determine the area and hydrologic parameters of each land-soil category simulated within each sub-watershed. The land cover classes were defined using the look up table. A look-up table that identifies the 4-letter SWAT code for the different categories of land cover/land use was prepared so as to relate the grid values to SWAT land cover/land use classes. After the land use SWAT code assigned to all map categories, calculation of the area covered by each land use and reclassification were done. As of the land use, the soil layer in the map was linked to the user soil database information by loading the soil look-up table and reclassification applied. The land slope classes were also integrated in defining the hydrologic response units. The DEM data used during the watershed delineation was also used for slope classification. The multiple slope discretization operation was preferred over the single slope discretization as the sub-basins have a wide range of slopes between them. Based on the suggested min, max, mean and median slope statistics of the watershed, five slope classes (0-3, 3-6, 6-10, 10-15 and >15) were applied and slope grids reclassified. After the reclassification of the land use, soil and slope grids overlay operation was performed.

The last step in the HRU analysis was the HRU definition. The HRU distribution in this study was determined by assigning multiple HRU to each sub-watershed. In multiple HRU definition, a threshold level was used to eliminate minor land uses, soils or slope classes in

each sub-basin. Land uses, soils or slope classes which cover less than the threshold level are eliminated. After the elimination process, the area of the remaining land use, soil, or slope class was reapportioned so that 100% of the land area in the sub-basin is modeled. The threshold levels set is a function of the project goal and amount of detail required. In the SWAT user manual it is suggested that it is better to use a larger number of sub-basins than larger number of HRUs in a sub-basin; a maximum of 10 HRUs in a sub-basin is recommended. Hence, taking the recommendations in to consideration, 2%, 10%, and 20% threshold levels for the land use, soil and slope classes were applied, respectively so as to encompass most of spatial details.

4.2.3.3 Importing Climate Data

The climate of a watershed provides the moisture and energy inputs that control the water balance and determine the relative importance of the different components of the water cycle. The climatic variables required by SWAT consist of daily precipitation, maximum/minimum temperature, solar radiation, wind speed and relative humidity. However, the data to be used by the model depends on the type of method chosen for estimation of potential evapotranspiration. Due to data availability and quality, daily precipitation, and maximum/minimum temperature in dbase format were the climatic input variables imported together with their weather location. And as discussed above it was the Hargraves method which was used to determine the potential evapotranspiration.

4.2.3.4 Sensitivity Analysis

SWAT is a complex model with many parameters that makes manual calibration difficult. Hence, sensitivity analysis was performed to limit the number of optimized parameters to obtain a good fit between the simulated and measured data. Sensitivity analysis helps to determine the relative ranking of which parameters most affect the output variance due to input variability (van Griensven et al., 2002) which reduces uncertainty and provides parameter estimation guidance for the calibration step of the model. SWAT model has an embedded tool to perform sensitivity analysis and provides recommended ranges of parameter changes. SWAT2005 uses a combination of Latine Hypercube Sampling and One-At-a-Time sensitivity analysis methods (LH-OAT method) (van Griensven, 2005). The concept of the Latin-Hypercube Simulation is based on the Monte Carlo Simulation to allow a robust analysis but uses a stratified sampling approach that allows efficient estimation of the output statistics while the One-Factor-At-a-Time is an integration of a local to a global sensitivity method (van Griensven, 2005). In local methods, each run has only one parameter changed

per simulation which aides in the clarity of a change in outputs related directly to the change in the parameter altered (Green and van Griensven, 2007).

4.2.3.5 Model Calibration

Even though the target of this study was to calibrate the model at four of the gauging stations in the Lake Tana basin, calibration was performed only at Gilgel Abay gauging station due to time limitation.

There are three calibration approaches widely used by the scientific community. These are the manual calibration, automatic calibration and a combination of the two. Manual calibration is the most widely used approach. However it is tedious, time consuming, and success of it depends on the experience of the modeler and knowledge of the watershed being modeled (Eckhardt & Arnold, 2001). Automatic calibration involves the use of a search algorithm to determine best-fit parameters. It is desirable as it is less subjective and due to extensive search of parameter possibilities can give results better than if done manually.

SWAT has two built-in calibration tools: the manual calibration helper and the auto-calibration. The manual calibration approach helps to compare the measured and simulated values, and then to use the expert judgment to determine which variable to adjust, how much to adjust them, and ultimately assess when reasonable results have been obtained. The auto-calibration technique is used to obtain an optimal fit of process parameters which is based on a multi-objective calibration and incorporates the Shuffled Complex Evolution Method algorithms (Green and van Griensven, 2007). In this study both of the techniques were employed to get the best model parameters.

First, the manual calibration was performed and when the model evaluation parameters reached to an unchanged level, the model was run automatically. Parameter changes in SWAT affecting hydrology were done in a distributed way for selected sub-basins and HRU's. They were modified by replacement, by addition of an absolute change and by multiplication of a relative change depending on the nature of the parameter. However, a parameter was never allowed to go beyond the predefined parameter ranges during the calibration process. In the manual calibration, first the water balance was calibrated followed by temporal flow calibration. The procedure followed for calibrating the SWAT model is shown in Figure 13.

The calibration for the water balance was done first for average annual conditions. Once the run was calibrated for the average annual conditions, the average monthly followed by daily

records was performed to fine-tune the calibration. The calibration was done separately for the surface runoff and base-flow as the parameters affecting them were different. A base-flow filter programe was used to determine the relative proportion of annual flow contribution from surface runoff or base-flow. The automated web GIS based hydrograph analysis tool (WHAT) was used to separate the surface runoff from the base-flow. WHAT, accessed from http://cobweb.ecn.purdue.edu/~what/ can also compute R^2 and Nash-Sutcliff coefficient. After the base flow and surface runoff were separated, the surface runoff was calibrated by adjusting the sensitive parameters which affect surface runoff like CN2 (Initial SCS runoff curve number for moisture condition II), Ch_N2 (Manning's ''n'' value for the main channel) and Esco (Soil evaporation compensation factor). The simulated versus observed values for each adjustment were evaluated with coefficient of determination (R^2) and Nash-Sutcliffe efficiency (E_{NS}) and when the values of R^2 and E_{NS} were above 0.5, calibration of base-flow was followed. Base-flow calibration was performed by adjusting the sensitive parameters which affects groundwater contribution. The most sensitive base-flow parameters which were adjusted were GW_REVAP (Groundwater ''revap'' coefficient), REVAPMN (threshold depth of water in the shallow aquifer for ''revap'' or percolation to occur), and GWQMN (depth of water in the shallow aquifer required for return flow to occur). Like surface runoff calibration, the simulated versus observed values were evaluated with R^2 and E_{NS}. The parameters were adjusted until the R^2 and E_{NS} results were above 0.5. However, after adjustments of base-flow parameters were done the surface runoff was checked because the adjustments of the base-flow parameters will affect the surface runoff in some way.

Once the water balance was calibrated temporal flow calibration was performed at each step by adjusting parameters which affects the shape of the hydrograph. The parameters adjusted were Ch_K (effective hydraulic conductivity in main channel alluvium), alpha_BF (baseflow alpha factor), Surlag (Surface runoff lag coefficient) and GW-delay (Groundwater delay time).

After the parameters were manually calibrated and were reached to acceptable value as per the R^2 and E_{NS}, the final parameter values that were manually calibrated were used as the initial values for the auto-calibration procedure. Maximum and minimum parameter value limits were used to keep the output values within a reasonable value range. Finally, the auto-calibration tool was run to provide the best fit between the measured and simulated data.

4.2.3.6 Model Validation

In order to utilize the calibrated model for estimating the effectiveness of future potential management practices, the model tested against an independent set of measured data. This testing of a model on an independent set of data set is commonly referred to as model validation. As the model predictive capability was demonstrated as being reasonable in both the calibration and validation phases, the model was used for future predictions under different management scenarios.

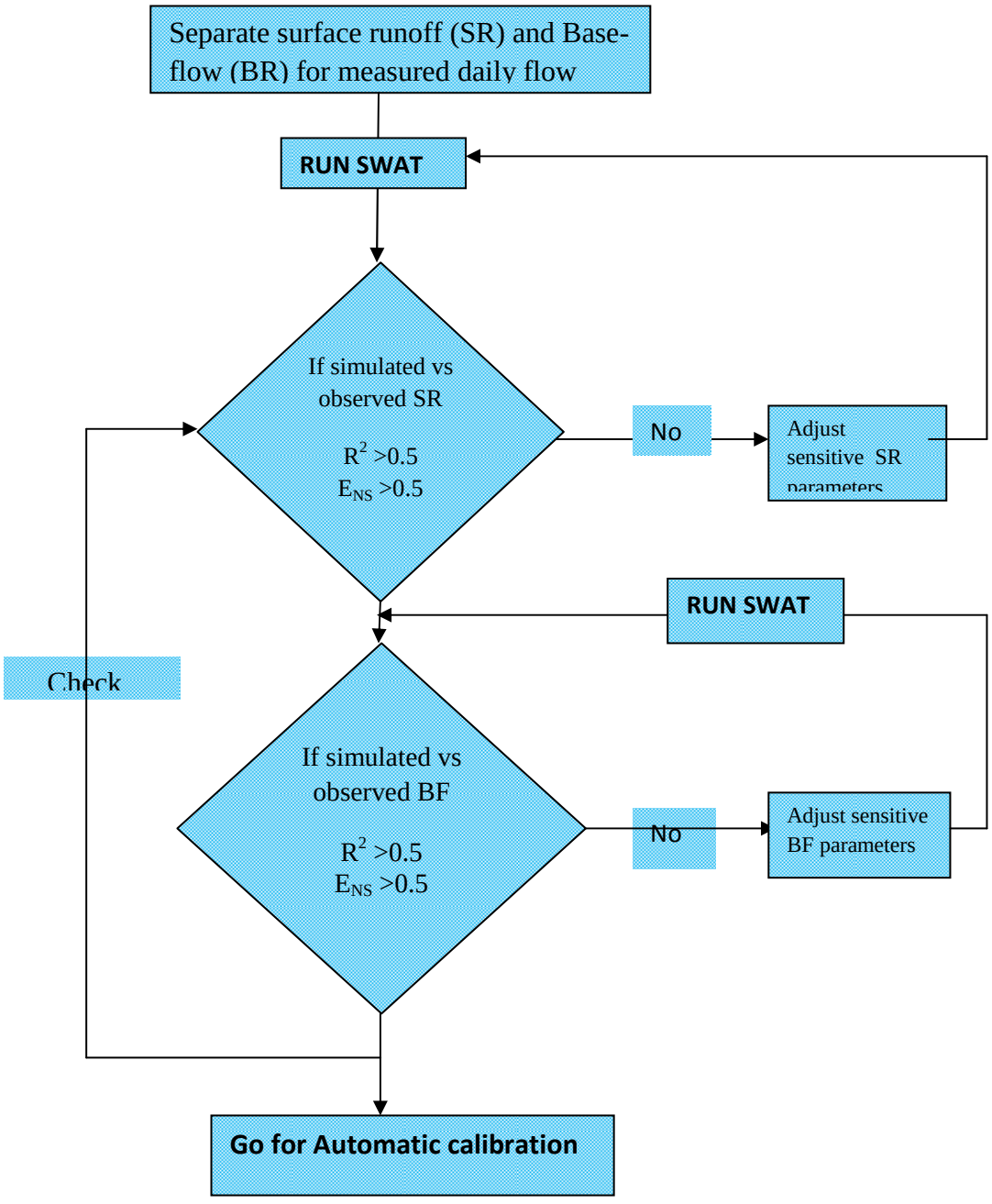

Figure 13: Calibration procedure for flow

4.2.3.7 Determination of impacted flow

SWAT model helps to simulate climate change impact by manipulating the climatic input that is read in to the model (precipitation, temperature, solar radiation, relative humidity, wind speed, carbon dioxide level and potential evapotranspiration). In this study changes in precipitation and temperature were adjusted to see the effect of climate change in the river flow. It was assumed that other climatic variables will be constant. In fact, their omission or inclusion doesn't affect the hydrological process as the Hargreaves method was used to determine the potential evapotranspiration. The changes were applied by setting adjustment factors in to the interface. The model calculates the change in precipitation, maximum and minimum temperature using equations 27, 28 and 29 respectively. The adjustment terms were applied from month to month so as to simulate seasonal changes in climatic conditions.

$$\mathbf{R_{day,adj}} = \mathbf{R_{day}} * \left(\mathbf{1} + \frac{\mathbf{adj_{pcp}}}{\mathbf{100}}\right) \text{... ... ...Eqn 27}$$

where: $R_{day,adj}$ is the adjusted precipitation falling in the sub − basin on a given day (mm H_2O)

$R_{day,adj}$ is the precipitation falling in the sub − basin on a given day (mm H_2O)

adj_{pcp} is the percent change in rainfall

$$\mathbf{T_{max,adj}} = \mathbf{T_{mx}} + \mathbf{adj_{tmp}} \text{ ... ...Eqn 28}$$

where: $T_{max,adj}$ is the adjusted daily maximum temprature (^{0}C)

T_{max} is the daily maximum temprature (^{0}C)

adj_{tmp} is the change in temprature (^{0}C)

$$\mathbf{T_{mn,adj}} = \mathbf{T_{mn}} + \mathbf{adj_{tmp}} \text{ ... ...Eqn 29}$$

where: $T_{min,adj}$ is the adjusted daily minimum temprature (^{0}C)

T_{min} is the daily minimum temprature (^{0}C)

adj_{tmp} is the change in temprature (^{0}C)

4.2.4 Model Evaluation

The performance of SWAT was evaluated using statistical measures to determine the quality and reliability of predictions when compared to observed values. Coefficient of determination (R^2) and Nash-Sutcliffe simulation efficiency (E_{NS}) were the goodness of fit measures used to evaluate model prediction. The R^2 value is an indicator of strength of relationship between the observed and simulated values. The Nash-Sutcliffe simulation efficiency (E_{NS}) indicates how well the plot of observed versus simulated value fits the 1:1 line. If the measured value is the same as all predictions, E_{NS} is 1. If the E_{NS} is between 0 and 1, it indicates deviations between measured and predicted values. If E_{NS} is negative, predictions are very poor, and the average value of output is a better estimate than the model prediction (Nash and Sutcliffe, 1970). The R^2 and E_{NS} values are explained in equations 30 and 31 respectively.

$$\mathbf{R^2} = \frac{\left(\sum_{i=1}^{n}(O_i-\bar{O})(P_i-\bar{P})\right)^2}{\sum_{i=1}^{n}(O_i-\bar{O})^2 \sum_{i=1}^{n}(P_i-\bar{O})^2} \text{ … … … … … … … … ..Eqn 30}$$

$$\mathbf{E_{NS}} = \frac{\sum_{i=1}^{n}(O_i-\bar{O})^2-\sum_{i=1}^{n}(P_i-O_i)^2}{\sum_{i=}^{n}(O_i-\bar{O})^2} \text{ … … … … … … ..Eqn 31}$$

where: n is the number of observations during the simulation period

O_i and P_i are the observed and pridicted values at each comparison point i

$\bar{O}$ and $\bar{P}$ are the arithimetic means of the observed and predicted values

5. Results

5.1 Climate Projection

5.1.1 Predictor Variables Selection

The best correlated predictor variables selected for precipitation, maximum temperature and minimum temperature are listed in Table 3. The description of the predictors is presented in Table 1.

Table 3: Selected predictor variables for the predictands (precipitation, maximum and minimum temperature) at Dangila station

Predictor	predictand		
	PRCP	TMAX	TMIN
Mslp		✓	
P_v			✓
P_zh			✓
r500	✓		
P8_z	✓	✓	✓
P_z		✓	
P500	✓	✓	✓
P8_u	✓	✓	
Rhum		✓	
P_f	✓		
P_th			✓

The strongest correlation was obtained between the predictands and each predictor for each month. The precipitation showed a better correlation with p8_z in the months May, June, October and November. The correlation of maximum temperature with the predictor variables was exceptionally strong for all the selected predictors. Most of the predictors gave better correlation from May to August. P8_z also showed a good correlation from October to December. The correlation between minimum temperature and p500 was strongly correlated for all months except March and October. P_zh also showed good correlation with the minimum temperature from September to December.

5.1.2 Calibration and Validation

The calibration was carried out from 1990-1997 for eight years and the withheld data from 1998-2001 were used for model verification. The model develops a better multiple regression equation parameters for the maximum and minimum temperature than the precipitation. This

is mainly due to the conditional nature of precipitation. In conditional models, there is an intermediate process between regional forcing and local weather (e.g., local precipitation amounts depend on wet–/dry–day occurrence, which in turn depend on regional–scale predictors such as humidity and atmospheric pressure) (Wilby and Dawson 2004). This can clearly be seen in the R^2 values presented in Table 4.

Table 4: Calibration and Validation R2 values of the SDSM downscaling of precipitation, maximum and minimum temperature at Dangila station

	R^2		
	Precipitation	Max Temperature	Min Temperature
Calibration	0.418	0.49	0.47
Validation	0.31	0.52	0.46

Twenty ensembles of synthetic daily weather series generated using NCEP-reanalysis data for the verification of the calibrated model. The mean of the 20 ensembles of maximum temperature and minimum temperature values gave a better R^2 values, inferring that future projections would also be well replicated. The precipitation verification showed that the calibrated model couldn't able to replicate the independent data set. This is due to complicated nature of precipitation processes and its distribution in space and time. Climate model simulation of precipitation has improved over time but is still a problematic (Bader et al., 2008). Thorpe (2005) also added that rainfall predictions have a larger degree of uncertainty than those for temperature. This is because rainfall is highly variable in space and so the relatively coarse spatial resolution of the current generation of climate models is not adequate to fully capture that variability. The summarized monthly values of the observed precipitation, maximum temperature and minimum temperature *vs* the corresponding modeled values are shown in Figure 14, Figure 15, and Figure 16 respectively.

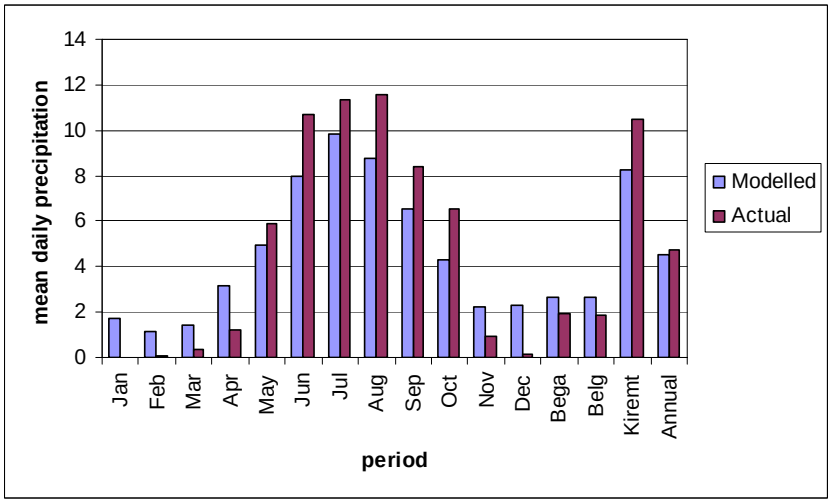

Figure 14: Observed and generated mean daily precipitation for the Dangila station

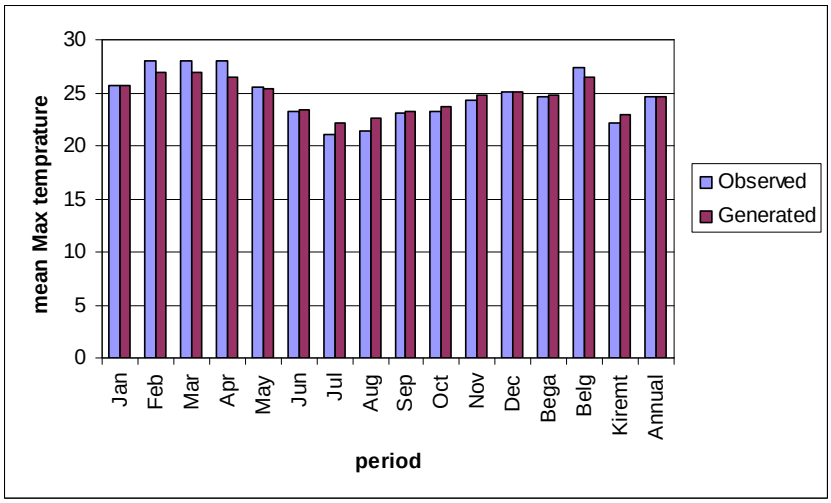

Figure 15: Observed and generated mean daily maximum temperature for the Dangila station

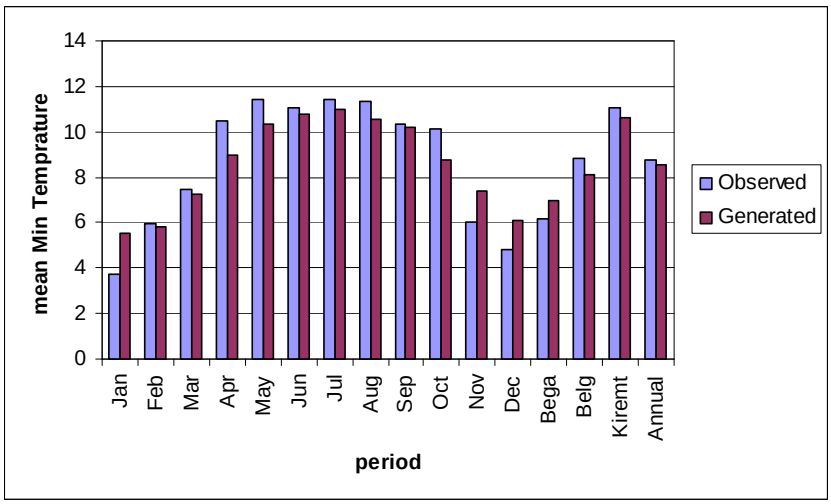

Figure 16: Observed and generated mean daily minimum temperature for the Dangila station

It is easily seen from the graphs that SDSM able to replicate the maximum and minimum temprature values well; however, it didn't give satisfactory results for the precipitation values.

5.1.3 Scenario Generation

Predictors from HadCM3 experiment for the period 1961-2099 were used to downscale the present and future climate forcing. The calibrated model was then used for the scenario generation from 2010 to 2099. The scenario generator produces 20 ensembles of synthetic weather series and the mean of the ensembles was used here in the analysis. The generated scenario was divided in to three 30 years of data ranges based on the recommendation of the WMO as the 2020s, being 2020's in the middle; 2050s, being 2050's in the middle and 2080s, being 2080's in the middle. For the ease of simplicity the generated scenarios were dealt individually for each predictand as below. All the comparisons in the following analysis were done with respect to the baseline period (1990-2001) data. The summarized SDSM result is presented in appendix 4.

5.1.3.1 Precipitation

The precipitation projection exhibited a decrease in annual mean precipitation in the 2020s and an increase in the 2050s and 2080s. As can be seen in Figure 17, in 2020s there may be a decrease in precipitation for all months except May, June and July for both scenarios (A2a and B2a). In 2020s, the A2a scenario showed a monthly mean precipitation decrease up to 29 % and B2a showed a decrease up to 30%. In 2020s the monthly mean precipitation increase may reach up to 19 % in A2a scenario and 18 % for the B2a scenario. In the 2050s, there may be an early occurrence and early end of precipitation compared with the normal situation. This is reflected by an increase of precipitation in April and a decrease in September. The overall effect in 2050s may be an increase of mean annual precipitation by 3.8% in the A2a scenario and 2.2% in the B2a scenario. In 2050s, the increase in monthly mean precipitation may reach up to 29% in the A2a scenario and 28% in the B2a scenario. In the 2050s, the decrease in monthly mean precipitation may reach up to 12% in the A2a scenario and 14% in the B2a scenario. In 2080s, there may be an increase in mean annual precipitation in all months except September in the A2a scenario and, September and October in the B2a scenario. The A2a and B2a scenarios showed an increase in mean annual precipitation amount by 19% and 12% respectively. The increase in monthly mean precipitaton may reach up to 34% for the A2a scenario and 31% for the B2a scenario. Figure 17 a & b show the monthly percentage change in precipitation for the coming 90 years for each month and season.

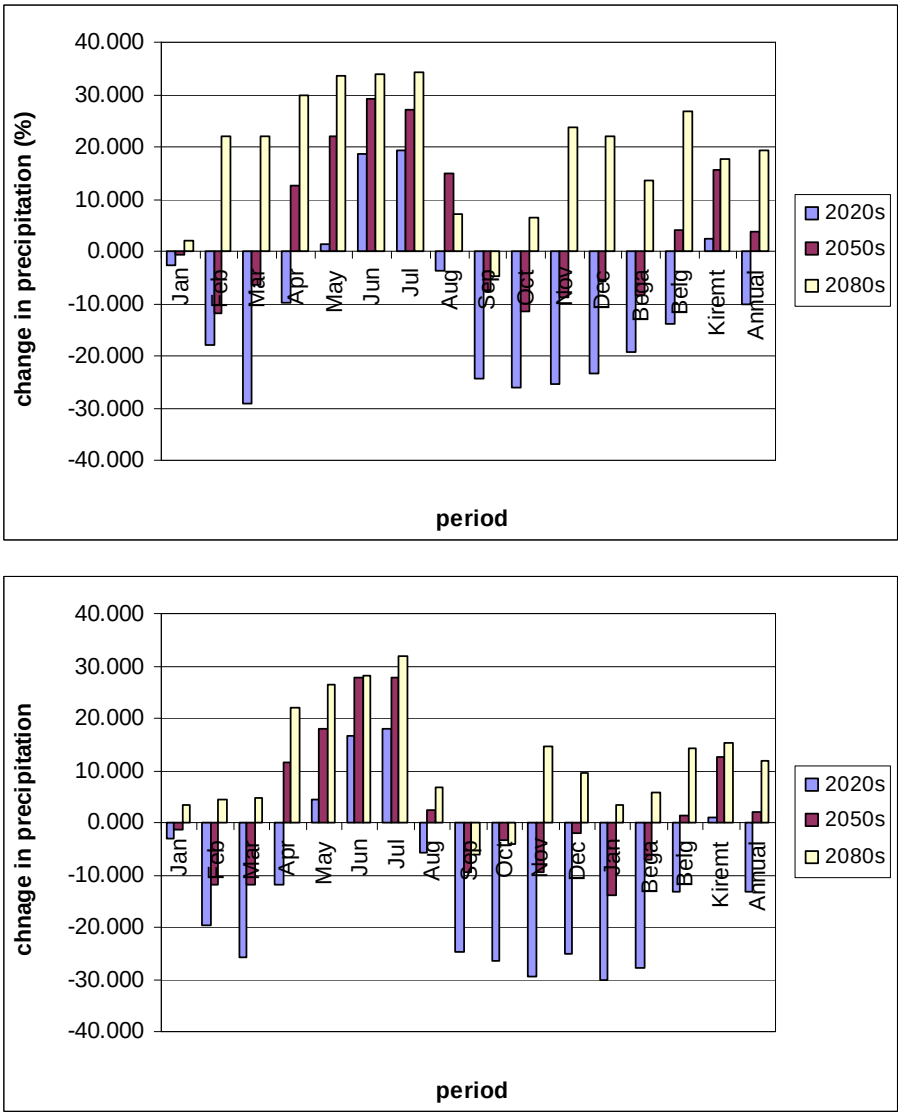

Figure 17: (a & b) Percentage change in monthly precipitation in the future from the baseline period average precipitation

As shown in the Figure 17, there may be an increase in precipitation in Kiremt season in the next 90 years. And there may be a corrosponding increase in precipitation amount in Belg season for the next 60 years (2050s and 2080s). Kiremt (wet season) and Belg(less rainy season) are the cropping seasons in Ethiopia. Hence this study can give us an insight on the possible impact of climate change on the agriculture in the study area.

5.1.3.2 Maximum Temperature

The maximum temperature scenario generation showed that there may be an increase in mean maximum temperature in all the months except April, May and June in the 2020s and 2050s. However, there may be an increase in temperature in all the months in the 2080s. The change

in monthly mean maximum temperature ranges between -2.4^{0}c in May (2020s) and 5^{0}c in September (2080s) for the A2a scenario; and between -2.5^{0}c in May (2020s) and 4.3^{0}c in September (2080s) for the B2a scenario. Seasonally, a pronounced increase in mean maximum temperature is observed in the Bega (dry season) and Kiremt (rainy season). The monthly change mean daily maximum temperature from the baseline period data is shown in Figure 18 a &b.

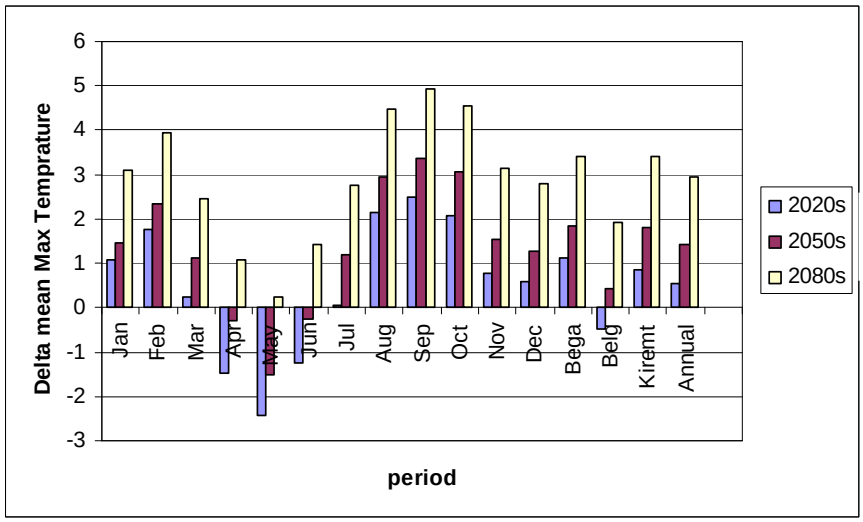

a) A2a scenario

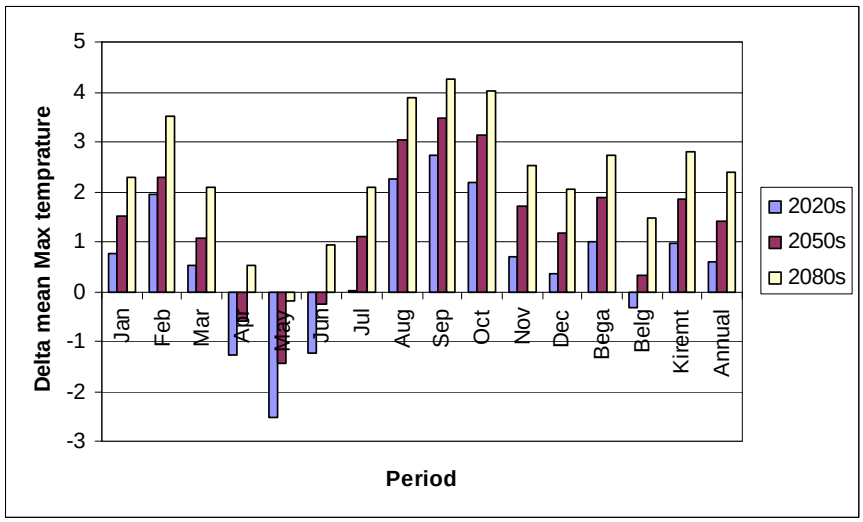

b) B2a scenario

Figure 18: (a & b) change in mean maximum temperature for the period 2010-2099 from the baseline period mean maximum temperature

The overall analysis (2010-2099) of the mean maximum temperature showed that there may be an increasing trend in both scenarios (A2a and B2a). It is observed that there may also be an increase of mean maximum temperature by 0.52^{0}c/decade and 0.34^{0}c/decade for A2a and

B2a scenarios respectively. Figure 19 clearly shows the increasing trend in mean annual maximum temperature for both scenarios.

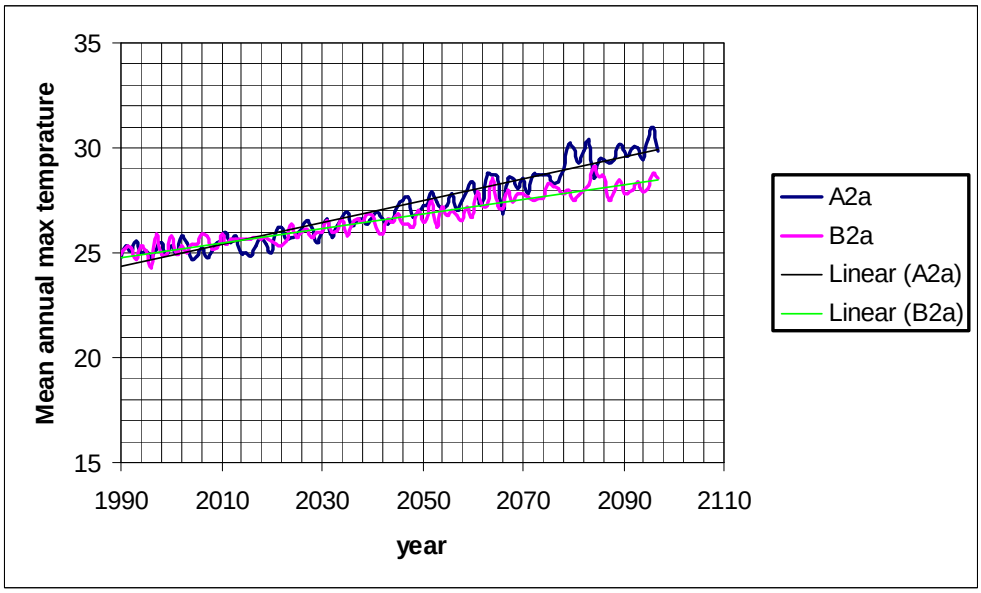

Figure 19: Trend for mean annual maximum temperature from 1990-2099 at Dangila station

5.1.3.3 Minimum Temperature

The annual mean minimum temperature trend in the long run may be increasing as compared to the baseline period for both scenarios. In 2020s the net annual mean minimum temperature change may be negligible as resulting from both scenarios since the decrease and increase from the baseline period is shared equally among the months. However, in 2050s all the months except September, October and November show a possible increase in mean minimum temperature for both scenarios. In this period the net effect may result in an increase in mean minimum temperature in the Belg season. In 2080s, there may be an increase in mean minimum temperature in all months of the year and the effect will be significant in the Belg season.

No table of figures entries found.

As shown in Figure 20 a & b, the change in mean minimum temperature ranges between -1.4^{0}c in October in the 2020s and +4.2^{0}c in March in the 2080s for the A2a scenario; and -1.3^{0}c in October in the 2020s and + 3.8^{0}c in March in the 2080s for the B2a scenario.

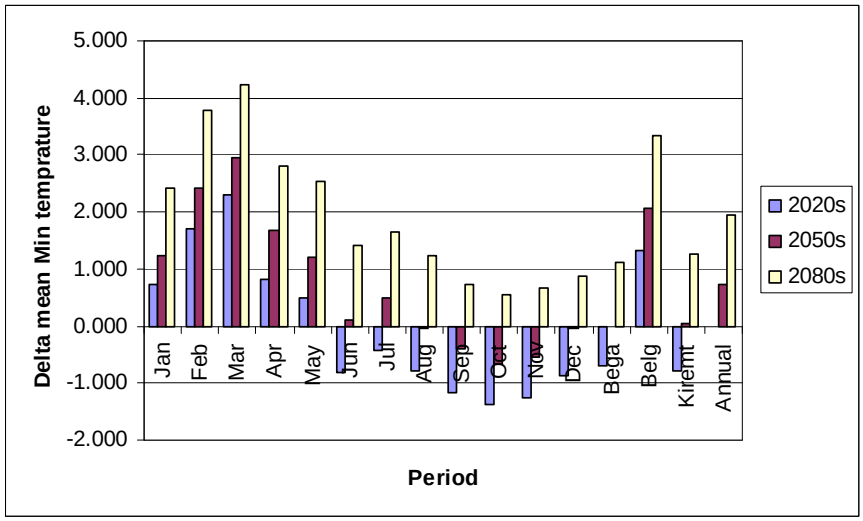

a) A2a scenario

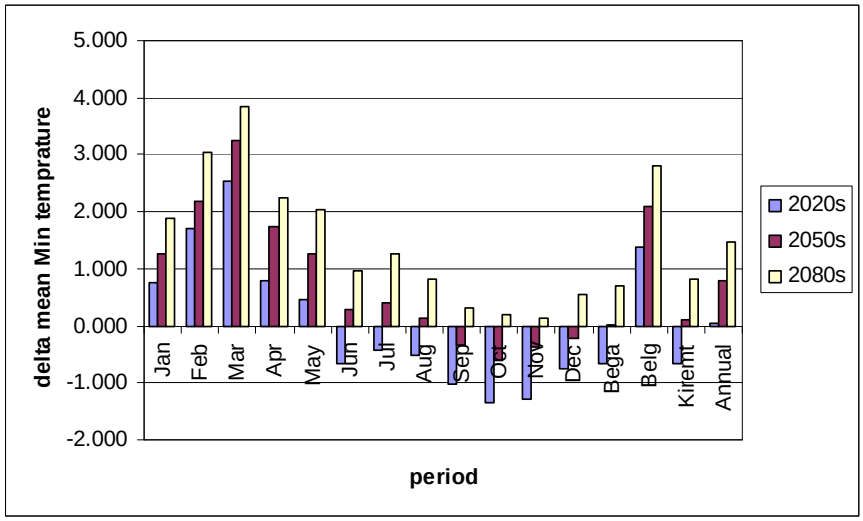

b) B2a scenario

Figure 20: (a & b) Change in mean minimum temperature (2010-2099) from the baseline period mean minimum temperature at Dangila station

The long term trend analysis is exhibited in Figure 21 which shows that the mean minimum temperature may increase by 0.43^0c/decade and 0.27^0c/decade for the A2a and B2a scenarios respectively.

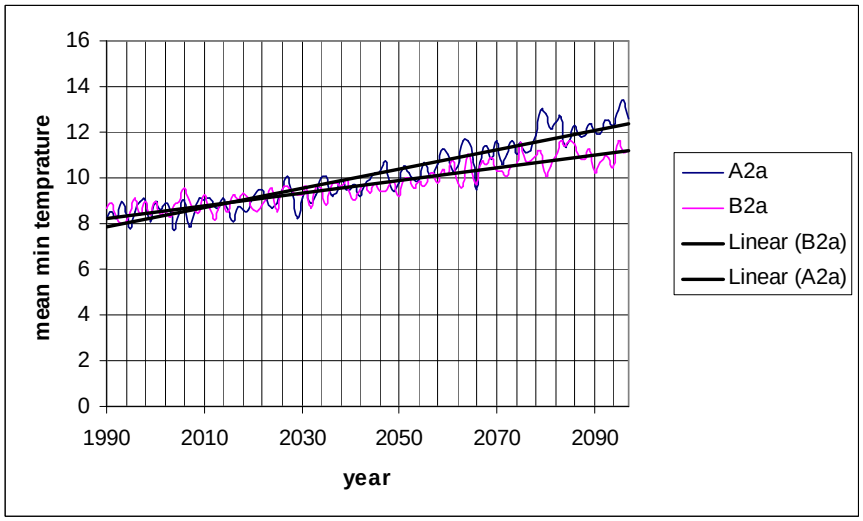

Figure 21: Trend graph for mean minimum temperature from 1990-2099

5.2 Hydrological Modeling

5.2.1 Simulation for Lake Tana Watershed

The overall watershed delineation and HRU definition simulation in the Lake Tana basin gave a watershed area of 14952 km^2 which resulted in 34 sub-basins and 189 HRUs. The watershed delineation of the area gave minimum, maximum and mean elevations in the basin of 1759, 4109, and 2025 masl respectively. The area coverage by each land use type is presented in Table 5.

Table 5: Land use types and their areal coverage in Lake Tana Basin

Land Use	SWAT code	Area (km^2)	% of total area
Forest Decidious	FRSD	1034.73	6.92
Ethiopian Teff	TEFF	6124.14	40.96
Wetlands-Non forested	WETN	679.20	4.54
Ranged Grasses	RNGE	931.31	6.23
Agricultural Land-Row Crops	AGRR	1725.12	11.54
Residential	URBN	427.86.48	2.86
Range Brush	RNGB	347.54.39	2.32
Water	WATR	3248.74	21.73
Forest ever green	FRSE	410.43	2.74
Agricultural Land-Generic	AGRL	22.86	0.15

Most of the area in the watershed is covered by Teff and Water (the lake). Teff is the most stable crop in Ethiopia and highly cultivated in this region and covers about 41% of the watershed. The lake covers 3249 km^2 which is 22% of the watershed.

Due to larger resolution of the FAO digital soil map of the world CD-ROM Africa map sheet, only four soil types extracted in the study area. And the majority of the land was covered by soil type I-Y-ab#92. The SWAT result for the soils' area coverage in the watershed is shown in Table 6.

Table 6: Soil types/ slope classes and their areal coverage in lake Tana basin

	Soil type/slope class	Area (km^2)	% of total area
Soil types	I-Y-ab#92	13044.68	87.24
	I-Y-ab#91	743.03	4.97
	I-Rd#79	1164.25	7.79
Slope classes in %	0-3	7557.87	50.55
	3-6	2598.22	17.38
	6-10	1343.25	8.98
	10-15	424.27	2.84
	>15	3028.35	20.25

SWAT slope computation using the DEM data indicated that half of the watershed has a slope of less than 3% and 20% of the watershed have a slope greater than 15%. The slope classes and their areal coverage are shown in Table 6.

Though simulation was done for the entire basin, calibration and subsequent impact assessment was done in a gauging station at Gilgel Abay and only sub-basins above the gauging station were given a due attention. According to SWAT definition, the sub-basins 26 to 34 were above the gauging station. These sub-basins cover 2878 km^2 which is 19% of the total watershed.

5.2.2 Sensitivity Analysis

The results of the sensitivity analysis gave the degree of sensitivity of 26 parameters and the parameter bound which was important for the manual and auto-calibration activities. Alpha_Bf, and Gw_Delay were the most sensitive parameters which has effect on base-flow contribution while Cn2, Esco, Ch_N2, and Surlag were among the most sensitive parameters which has effect on the surface runoff. The ten most sensitive parameters, their ranking and description is exhibited in Table 7.

Table 7: Sensitive parameter ranking and final auto-calibration result

Rank	Parameter	description	Range	Auto-calibrated resut
1	Alpha_Bf	Baseflow alpha factor	0 - 1	0.38
2	Cn2	Initial SCS runoff curve number for moisture condition II	-25% to +25%	-5%
3	Ch_N2	Manning's ''n'' value for the main channel	0 - 1	0.059
4	Ch_K2	Effective hydraulic conductivity in main channel alluvium	0 - 150	122.86
5	Surlag	Surface runoff lag coefficient	0 - 10	0.61
6	Esco	Soil evaporation compensation factor	0 - 1	1
7	Gw_Delay	Groundwater delay time	-10% to +10%	-10%
8	Sol_Z	Depth from soil surface to bottom of layer	-25% to +25%	24.41%
9	GW_REVAP	Groundwater ''revap'' coefficient	-0.036 to +0.036	0.06
10	Revapmn	the threshold depth of water in the shallow aquifer for ''revap'' or percolation to the deep aquifer to occur	-100 to +100	

5.2.3 Model Calibration

The calibration of the model was performed for six years (1995 to 2000) using Gilgel Abay river flow data at Merawi runoff station. The performance of the model was evaluated using R^2 and E_{NS} statistical measures for both manual and auto-calibration. After manual calibration the model R^2 and E_{NS} values reached to 0.66 and 0.54 respectively as shown in Figure 22.

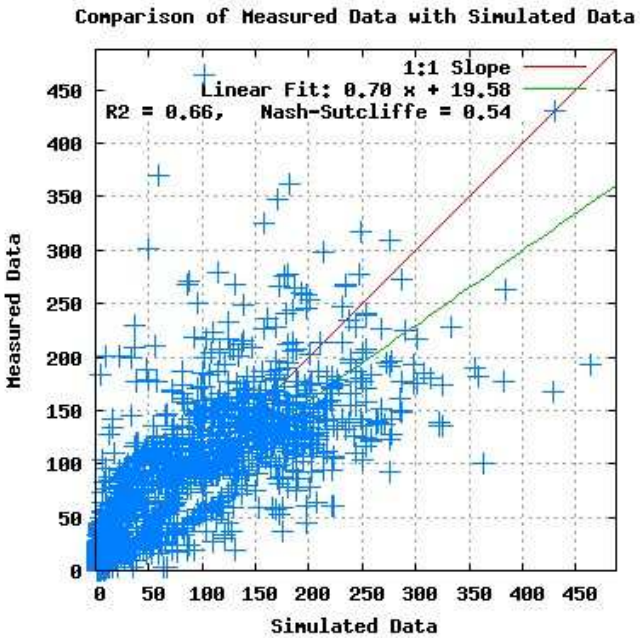

Figure 22: Comparison of measured data at Gilgel Abay runoff station with simulated data after manual calibration (WHAT R^2 and E_{NS} computation)

The manual calibration followed by auto-calibration improved the R^2 and E_{NS} values to 0.74 as can be seen from Figure 23. Santhi et al. (2001) stated that efficiency values greater than or equal to 0.50 are considered adequate for SWAT model application. Hence, it is observed that SWAT exhibited strong performance in representing the hydrological conditions of the watershed.

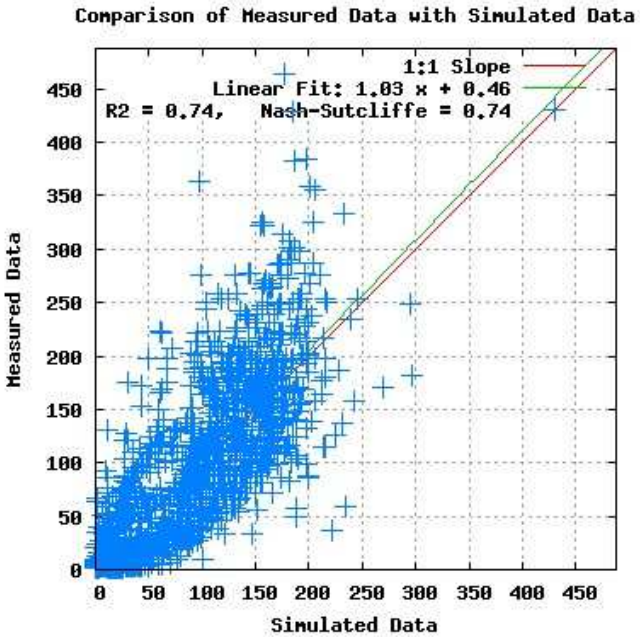

Figure 23: Comparision of measured data at Gilgel Abay runoff station with simulated data after auto-calibration (WHAT R^2 and E_{NS} computation)

Other statistical measures, as shown

Table **8**, also exhibit a descent agreement between the simulated and measured data.

Table 8: Calibration and validation period statistics for measured and simulated flows at Gilgel Abay runoff station

Period	Total flow (m^3/s)		Average flow (m^3/s)		% error
	Observed	Simulated	Observed	simulated	
Calibration (1995-200)	129077	124757	58.88	56.91	3.34
Validation (2001-2005)	71196	70657	48.73	48.36	0.75

It can be seen from the flow hydrograph (Figure 24) that the simulated flows well replicate the observed flows except that the peak values couldn't be caught. This might be due to the fact that greater attention was paid for the water balance calibration than shape of the hydrograph.

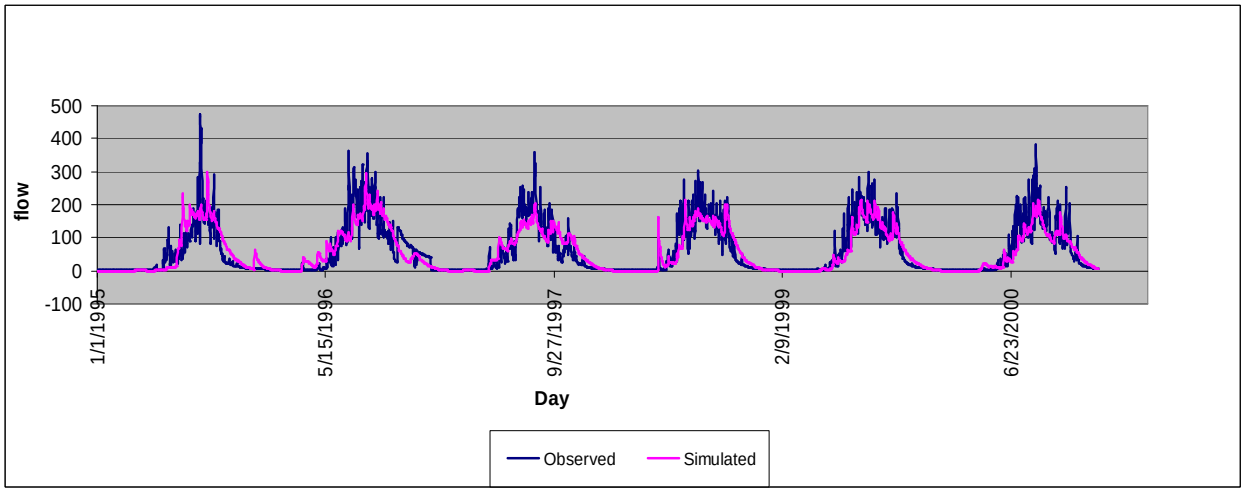

Figure 24: Observed and simulated flow hydrograph for the calibration period (1995 - 2000)

5.2.4 Model Validation

The validation of the model at the Gilgel Ababy gauging station was done for an independent data set of four years from 2001 to 2004. Validation of the model showed the model's strong predictive capability through R^2 and E_{NS} value of 0.78 each. Other statistical measures shown in

Table 8 also proved the model's strong performance. As can be seen from Figure 25, the model replicated the observed flows well. However, it couldn't able to catch the peak flows.

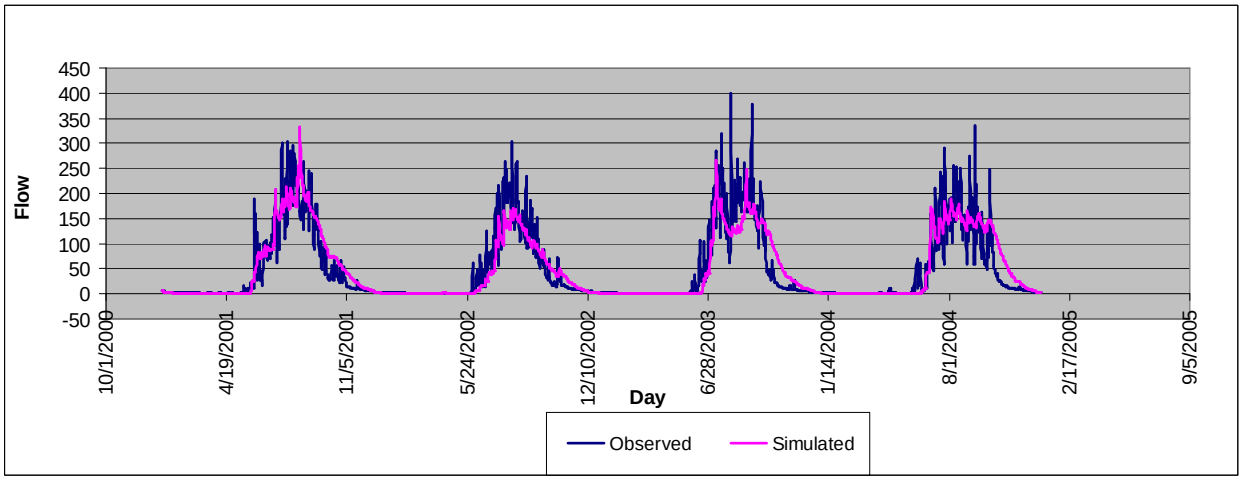

Figure 25: Observed and simulated flow hydrographs for the validation period (2001 - 2005)

From the calibration and the validation results, it is deduced that the model represented the hydrological characteristics of the watershed and hence it can be used for further analysis.

5.3 Impact of Climate Change on the Flow Volume

The impact of climate change on flow volume was analyzed on a monthly, seasonal and annual basis. The effect of climate change on low flow was also analyzed. The results for the analysis were discussed in the following sections and the summarized results are enclosed in appendix 5.

5.3.1 Impact on Monthly Flow Volume

The impact of climate change was analyzed taking the 1990-2001 river flow as the baseline flow against which the future flows for the 2020s, 2050s and 2080s compared. Precipitation, minimum and maximum temperature were the climate change drivers considered for the impact assessment. The inputs for the change in precipitation, maximum and minimum temperature are discussed in section 5.1.3 and presented in appendix 4. The monthly percentage change in flow volume in both scenarios for the period 2020s, 2050s and 2080s are presented in Figure 26 and Figure 27.

In the 2020s for the A2a scenario, the flow volume may show a decrease for all the months except May, June, July and August. In this period a decrease up to 43% and an increase up to 58% in monthly flow volume may be expected. Increase in flow volume may be observed in

months which showed an increase in monthly precipitation. However, in August there may be a decrease in monthly precipitation by 4% but an increase in monthly flow volume by about 7% will be observed. The increase flow volume might be due to catchment and groundwater lag time effects. In the 2020s for B2a scenario, the same effect as the A2a scenario of 2020s may be observed. But the decrease in monthly flow volume is expected to reach up to 46% and the increase might reach up to 57%.

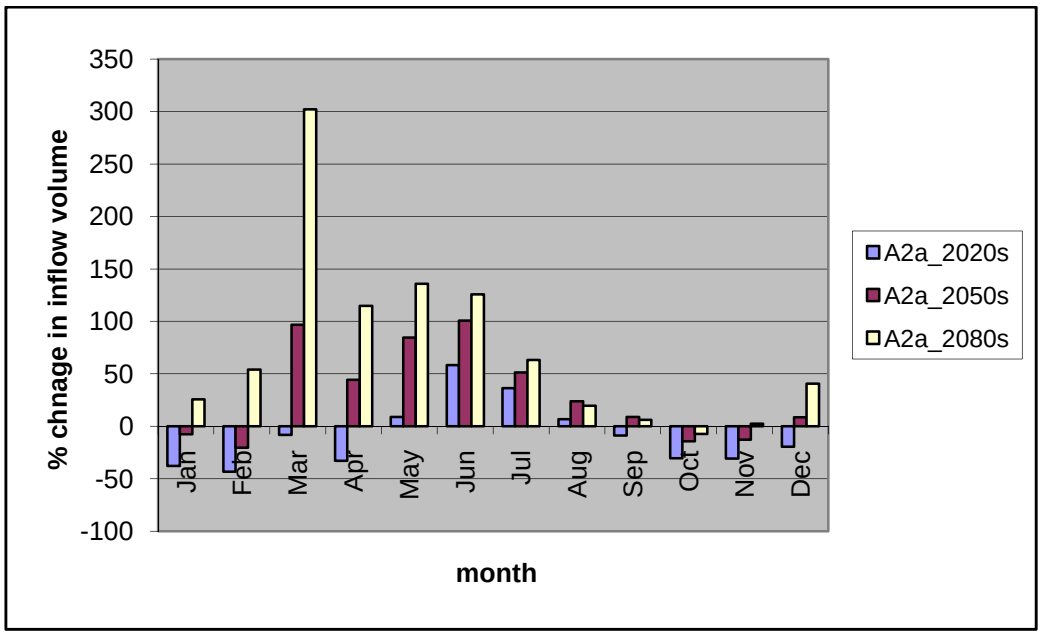

Figure 26: Monthly percentage change in flow volume for the A2a scenario for the periods 2020s, 2050s and 2080s against the baseline flow volume

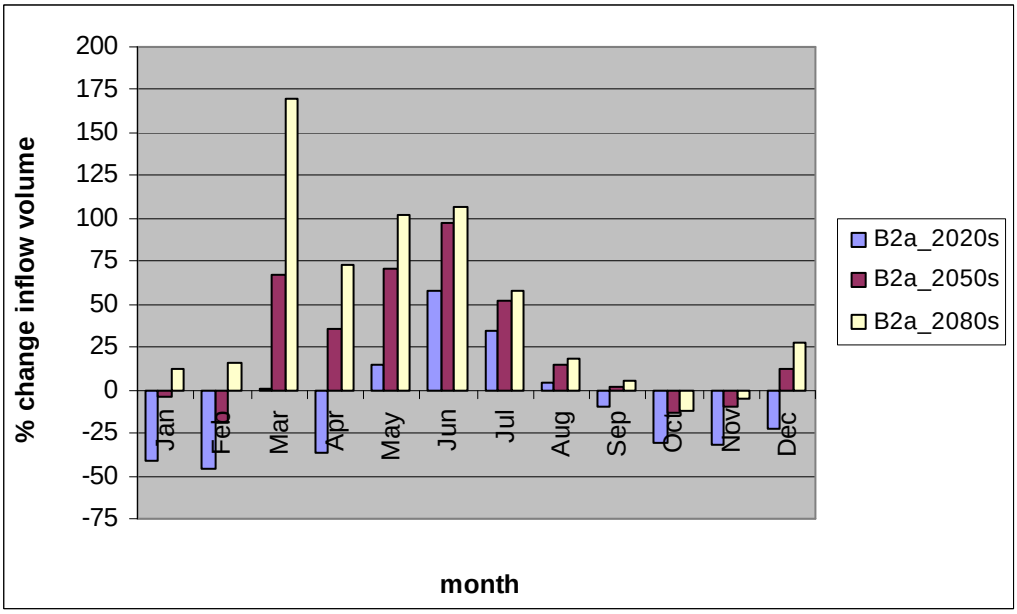

Figure 27: Monthly percentage change in flow volume for the B2a scenario for the periods 2020s, 2050s and 2080s against the baseline flow volume

In 2050s for both scenarios, the increase in precipitation is reflected in an increase in flow volume and a decrease in precipitation is reflected in a decrease in flow volume. But in March and September, though there may be a decrease in precipitation, the flow volume may increase. In September it is attributed to the effect of increase in precipitation in the previous months but, it is hard to explain the reason behind the March's exceptional increase in flow volume while there may be a decrease in precipitation. This might arise from problem of the input data. In the 2050s, monthly flow volume would increase up to 100% and decrease up to 20% for the A2a scenario and increase up to 97% and decrease up to 19% for the B2a scenario were expected.

In 2080s for the A2a scenario an increase in flow volume in all months except October may be observed. The increase in monthly flow volume may reach up to 135%. But a decrease in precipitation in September by 4.6% may be reflected in a decrease in flow volume by 7% in October. In 2080s B2a scenario, the pattern of monthly flow volume change may be more or less the same as the A2a scenario and the increase in flow volume may reach up to 106%. But a decrease in precipitation in September and October by 6.3% and 4% respectively may be reflected in a decrease in flow volume in October and November by 12.5% and 5.2% respectively. However, as shown in Figure 26 and Figure 27 exceptionally high increase in

flow volume is observed in March. This indicates that the model couldn't simulate the hydrological condition in March for an unknown reason.

5.3.2 Impact on Seasonal and Annual Flow Volume

In this section, the impacts of climate change on the seasonal and annual flow volume are presented so as to foresee its consequence on the socio-economic condition of the area. As discussed in the section 2.3, there are three seasons in the study area: Kiremt (rainy and cropping season), Belg (small rain season) and Bega (dry season). Figure 28 and Figure 29 exhibit the implication of climate change on the river flow in these seasons.

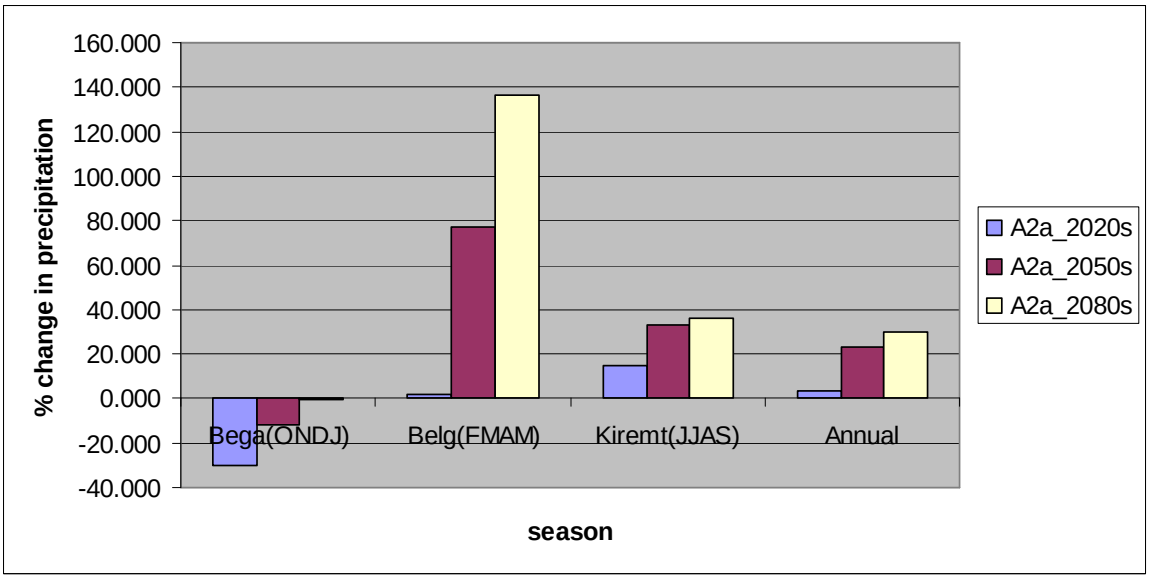

Figure 28: Percentage change in seasonal and annual flow volume in respect to baseline climate for the A2a scenario

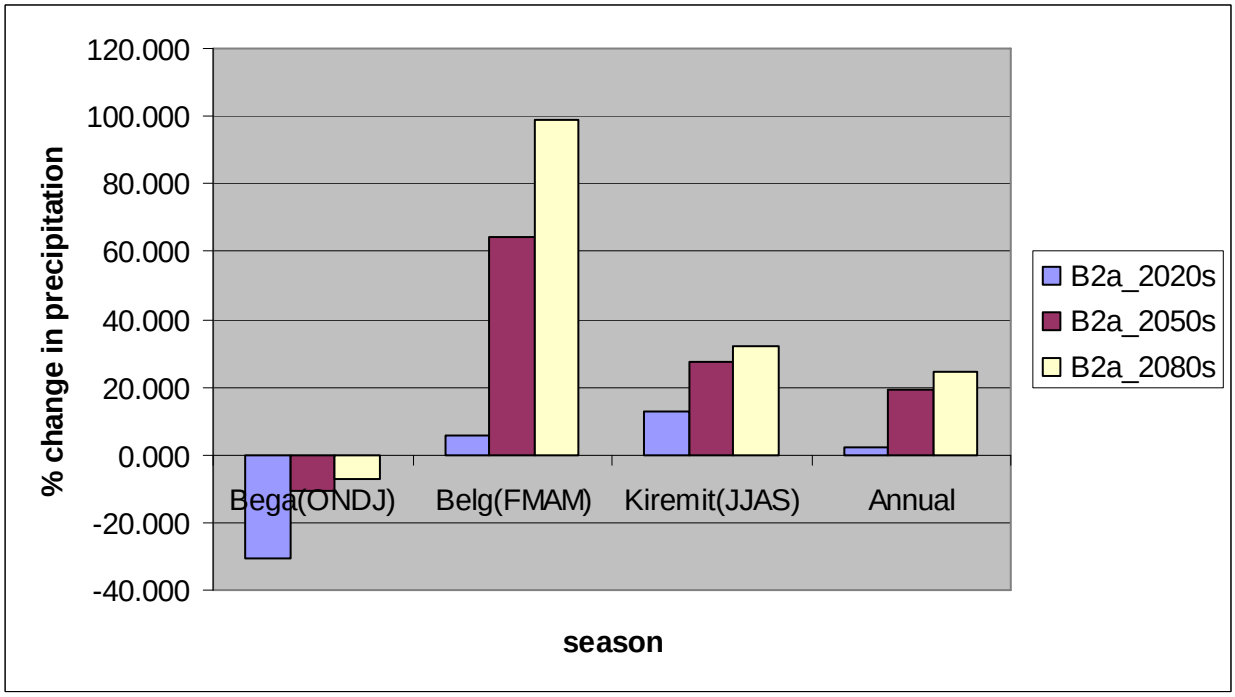

Figure 29: Percentage change in seasonal and annual flow volume in respect to baseline climate for the B2a scenario

As can be seen from Figure 28 and Figure 29, there may be an annual increase in flow volume for the next 90 years. Belg season is expected to show the larger share in increased flow volume. The increase may reach up to 136% in 2080s for the A2a scenario and 99% in 2080s for the B2a scenario. Kiremit season also shows a descent increase in flow volume. The increase ranges from 15% to 36% for the A2a scenario and 12% to 32% for the B2a scenario. However, both scenarios show that there might be a decrease in flow volume in Bega season. The decrease would reach up to 30% for the A2a scenario and 31% for the B2a scenario.

5.3.3 Low Flow Analysis

Analyzing low flow statistics is important for water quality and aquatic habitat needs. Climate change affects both the high flows and low flows owing to variability in the precipitation and temperature. In this study a 95 percent exceedance probability was considered to characterize low flow conditions in the stream. It is found that there may be no significant effect in the low flows at this probability of exceedance. However, the effect is significant at 70 percent exceedance probability which shows that in 2020s and 2050s the low flow may decrease but it may increase in the 2080s for both scenarios in respect to the baseline situation. Table 9 and Figure 30 & 31 exhibit the low flow statistics at 70% exceedance probability and flow duration curve respectively.

Table 9: Low flow statistics at 70% exceedence probability for both scenarios at different time periods

Scenario	Period			
	Baseline*	2020s	2050s	2080s
A2a	1.89	0.79	1.61	2.50
B2a	1.89	0.77	1.35	1.98

*baseline period is not under any of the scenarios

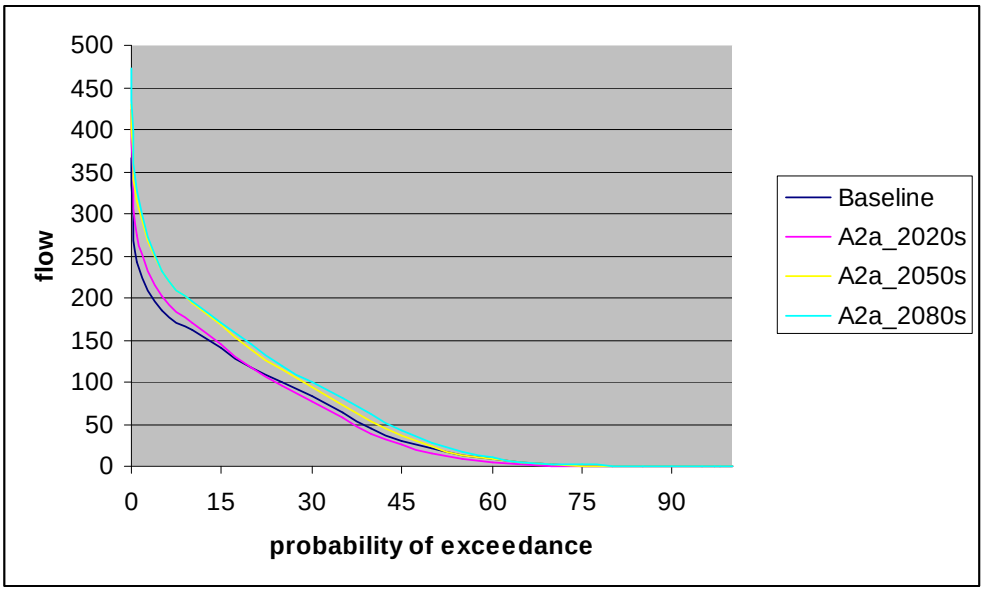

Figure 30: Flow duration curve for the A2a scenario for different time periods

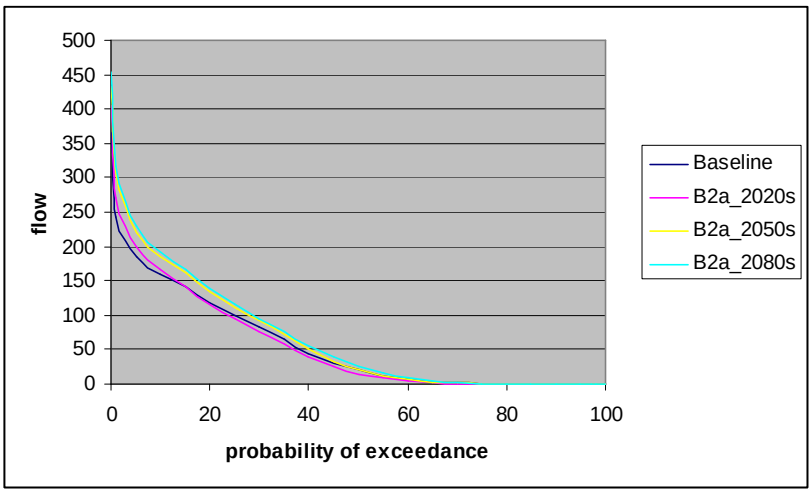

Figure 31: Flow duration curve for the B2a scenario for different time periods

5.4 Uncertainities in the study

There are various sources of uncertainties which arise from data quality, associated with model assumptions and level of understanding specially in the climate system. The uncertainities related to climate change studies in general are discussed in section 3.4. In the hydrological model the impact of climate change was done only considering the changes in the precipitation, maximum and minimum temperature. However, in real world, other climatic variables will also change. And the scope of this study was limited to change in climate assuming land use pattern keeps the same in the future. The resolution of the soil data was so coarse that it also adds another uncertainity with the hydrological model estimation.

This study is done with a climate data which is too short and having lots of gaps. Besides the SDSM model prediction assumes that the relationship developed between the predictands and predictors at recorded climatic conditions will hold the same in the future. However, this assumption may not be true.

The commulative assumptions and poor data quality stated above will certainly reduce the reliability of the results. This is clearly seen in the SDSM downscaling result of precipitation projection. As precipitation is one of the main inputs of the SWAT model it will result in uncertainity in the estimations of flow volumes in the long run.

6. Conclusion and Recommendation

6.1 Conclusions

It was difficult to get high quality input data to perform the modeling work; however every single effort was exerted to produce good output. A cascade of models was used in this study and the result was really satisfactory. However, it is undeniable that there are some uncertainties due to unavoidable assumptions taken.

The results of the climate projection showed that SDSM is able to replicate the observed maximum and minimum temperature well; however, SDSM couldn't able to replicate well the observed precipitation with the simulated precipitation due its conditional nature and high variability in space. Still the simulated precipitation values follow the same trend as the observed precipitation. Hence, the overall performance of SDSM was considered satisfactory.

SDSM downscaling showed that in 2020s the mean annual precipitation may show a decrease up to 10% (A2a scenario) and 13.3% (B2a scenario) but it may show an increase in the 2050s and 2080s up to 19.3% (A2a scenario) and 11.8% (B2a scenario). Seasonally, there may be an increase in precipitation in Kiremit for the next 90 years, and Belg may show an increase in precipitation after 2040. As Kiremit and Belg are the cropping seasons in Ethiopia, climate change may have positive implication to the agricultural sector even if the increase in the maximum and minimum temperature has a contradictory effect by increasing evapotranspiration condition. The results of precipitation simulation showed that the A2a scenario will be wetter than the B2a scenario.

The SWAT2005 calibration and validation simulations well replicated the observed values; however it couldn't able to simulate the peak values. This was due to the fact that greater attention was given to water balance calibration than the temporal flow calibration. It was also observed that peaks were due to flash floods occurring in June, July and August, which were difficult to consider in the modeling work. The statistical measures showed that the validation results were better than calibration results. This was most likely due to better input data quality for the validation simulation. Input data analysis showed that recently collected data had relatively less missing data values than the older ones. The other possible reason would be the fact that recent data may be collected using relatively advanced equipments. Goodness of fit evaluation results of 0.74 both for R^2 and E_{NS} was found during the calibration which is comparable to the performance reported by SWAT model developers (Santhi et al. 2001).

Therefore, based on these satisfactory results the model was used to assess the impact of climate change on the hydrological conditions of the watershed.

The calibrated and validated model was used for impact assessment. In the coming 90 years a decrease in monthly flow volume up to 46% in the 2020s and an increase up to 135% in the 2080s may be expected. There may be a significant increase in flow volume in Belg season up to 136% and there may also be a descent increase in flow volume in Kiremit season up to 36%. The increase in Belg season flow may have paramount importance for small scale irrigation activities practiced by the local farmers. It is generally observed that the increase in precipitation will be accompanied by a corresponding increase in inflow volume and vice versa. It was also observed that the flow volume was affected more by a change in precipitation than a change in temperature.

This study showed that there may be a net annual increase in flow volume in Gilgel Abay river flow due to climate change. As Gilgel abay is the largest tributary river feeding in to Lake Tana, any effect on this river is easily reflected into the Lake. Besides as the basin is small, it is believed that the impact of climate change will be more or less the same in other tributary rivers as well. Hence, it can be concluded that climate change may result in an increase in flow volume into Lake Tana. This may have a positive as well has a negative implication to the socio-economic condition of the region. The increase in flow will help to harness a significant amount of water for the ongoing dam projects in the Gilgel Abay river basin. However, it may also aggravate the recurrent flooding problems in the Lake Tana surrounding area.

6.2 Recommendations

This study was done in a limited time and resource. Hence the results of this study should be taken as a starting point for further studies. One of the limitations of this study was that the downscaling accuracy of SDSM is based on the assumption that the predictor-predictand relationships developed for the historical period are time-invariant. However, latest research results indicate that this assumption has already been violated in the observational data (Wilby, 1997). Besides, downscaled scenarios in this study were generated using only one GCM model experiment. Downscaled scenarios using other GCM models running the same experiment may likely produce slightly different, but equally plausible results. Hence, it is recommended to assess the impact of climate change in the region using different GCM model outputs. In this study, downscaling of the large scale variables was done at Dangila station, and it was assumed that this change will be applicable to other stations as well. However, it is recommendable if climate change assessment will be done downscaling large scale variables at each station considered in this study.

The hydrological modeling was done for the entire Lake Tana basin; however, due to time limitation, calibration, validation and impact assessment was done at Gilgel Abay river only. The author recommends the work to be continued so as to show the overall climate change effect on the entire Lake Tana basin.

References

Allali A, R. Bojariu, S. Diaz, I. Elgizouli, D. Griggs, D. Hawkins, O. Hohmeyer, B. Jallow, L. Bogataj, N. Leary, H. Lee, D. Wratt, Eds., 2007: An Assessment of the Intergovernmental Panel on Climate Change, Synthesis Report. Valencia, Spain, 12-17 November 2007.

Bates, B.C., Z.W. Kundzewicz, S. Wu and J.P. Palutikof, Eds., 2008: Climate Change and Water. Technical Paper of the Intergovernmental Panel on Climate Change, IPCC Secretariat, Geneva, 210 pp.

BCEOM, 1999. Abay River Basin Integrated Development Master Plan Project: phase 2 data collection-site Investigation Servey and Analysis.

Beven, K.J., 2000. Rainfall-Runoff Modeling. The Primer. Wiley.

CCSP, 2008: Climate Models: An Assessment of Strengths and Limitations. A Report by the U.S. Climate Change Science Program and the Subcommittee on Global Change Researce [Bader D.C., C. Covey, W.J. Gutowski Jr., I.M. Held, K.E. Kunkel, R.L. Miller, R.T. Tokmakian and M.H. Zhang (Authors)]. Department of Energy, Office of Biological and Environmental Research, Washington, D.C., USA, 124 pp.

Cunderlik M. Juraj, October 2003. Hydrologic model selection fort the CFCAS project: Assessment of Water Resources Risk and Vulnerability to Changing Climatic Conditions, Project Report I, 40pp.

Eckhardt K. and J. G. Arnold, "Automatic calibration of a distributed catchment model", Journal of Hydrology, vol. 251, no. 1/2, 2001, pp. 103-109.

Ethiopian National Metrological Services Agency. 2001, Initial National Communication of Ethiopia to the United Nations Framework Convention on Climate Change (UNFCCC, Addis Ababa.

IPCC 1997-R.T.Watson, M.C.Zinyowera, R.H.Moss Eds., 1997: The Regional Impacts of Climate Change: An Assessemnt of Valunerability. Cambridge University Press, UK. pp 517

IPCC, 2001: Climate Change 2001. The Scientific Basis. Contribution of Working Group I to the Third Assessment Report of the Intergovernmental Panel on Climate Change [Houghton, J.T.,Y. Ding, D.J. Griggs, M. Noguer, P.J. van der Linden, X. Dai, K. Maskell, and C.A. Johnson (eds.)]. Cambridge University Press, Cambridge, United Kingdom and New York, NY, USA, 881pp.

IPCC-TGCIA (1999): Guidelines on the Use of Scenario Data for Climate Impact and Adaptation Assessment. Version 1. Prepared by Carter, T.R., Hulme, M. and Lal, M., Intergovernmental Panel on Climate Change, Task Group on Scenarios for Climate Impact Assessment, 69pp.

Lijalem, Z., 2007. Climate Change Impact on Lake Ziway Watershed Water Avilability, Ethiopia. MSc. Cologne: University of Applied Sciences Cologne, Institute for Technology in the tropics.

Mearns, L.O., F. Giorgi, P. Whetton, D. Pabon, M. Hulme and M. Lal, (2003): Guidelines for use of climate scenarios developed from Regional Climate Model experiments. Data Distribution Centre of the International Panel of Climate Change, 38 pp. Available for download from: http://ipcc-ddc.cru.uea.ac.uk

Nakicenovic N. and R. Swart Eds., 2000. Emissions Scenarios of the Intergovernmental Panel on Climate: A Special Report of IPCC Working Group III. Cambridge University Press, UK. Pp570

Nash J.E., Sutcliff, J.V. 1970. River Flow Forcasting through Conceptual Models Part I- A discussion of Principles. Journal of Hydrology, 10:282-290.

Neitsch S.L., J.G. Arnold, J.R. Kiniry, J.R. Williams, 2005. Soil and Water Assessment Tool (SWAT) Theoretical Documentation, Version 2005, Grassland Soil and Water Research Laboratory, Agricultural Research Service, Blackland Research Center, Texas Agricultural Experiment Station.

Neitsch S.L., J.G. Arnold, J.R. Kiniry, J.R. Williams, 2005. Soil and Water Assessment Tool (SWAT) Input/Output File Documentation, Version 2005, Grassland Soil and Water Research Laboratory, Agricultural Research Service, Blackland Research Center, Texas Agricultural Experiment Station.

Ringius, L., Downing, T.E., Hulme, M., Waughray, D., Selrod, R., 1996. Climate change in Africa: Issues and challenges in Agriculture and Water for Sustainalbe Development. CICERO Report, 8. University of Oslo, Norway, p. 151.

Santhi, S., Arnold, J.G., Williams, J.R., Dugas, W.A., Srinivasan, R., and L.M. Hauck. 2001. Validation of SWAT model on a large river basin with point and nonpoint sources. Journal of the American Water Resources Association 37:1169-1188.

Setegn Shimelis G., Ragahavan Srinivasan, Bijan Dargahi (2008).Hydrological Modelling in the Lake Tana Basin, Ethiopia using SWAT model. The Open Hydrology Journal Vol 2(2008): pp 25-38

Smith, J.B. and Hulme, M. (1998): Climate change scenarios; in United Nations Environment Programme (UNEP) Handbook on Methods for Climate Change Impact Assessment and Adaptation Studies, Version 2.0, (ed.) I. Burton, J.F. Feenstra, J.B. Smith and R.S.J. Tol, United Nations Environment Programme and Institute for Environmental Studies, Vrije Universiteit, Amsterdam, p. 3-1-3-40.

Thorpe A.J., 2005, Climate Change Pridiction: A challenging scientific problem. Institute of physics, [online] 4 Apr., available at: http://www.iop.org/activity/policy/Publications/file_4147.pdf [accessed 4 April 2009]

USBR, 1964. Land and Water Resources of the Blue Nile Basin, Ethiopia. United States, department of the Interior.

van Griensven A., 2005. Sensitivity, auto-calibration, uncertainty and model evaluation in SWAT2005. s.l., s.n

van Griensven, A., Francos, A., Bauwens, W., 2002. Sensitivity analysis and autocalibration of an integral dynamic model for river water quality. Water Sci. Technol. 45, 325-332.

van Griensven, A., Green C.H., 2007. Auto-calibration in Hydrological Modeling: Using SWAT2005in small-scale watersheds. Science Direct, Environmental Modeling & Software 23 (2008), 422-434, available at: www.sciencedirect.com [Accessed 27 April 2009]

Vörösmarty, C.J., E.M. Douglas, A.A. Green and C. Ravenga, 2005: Geospatial indicators of emerging water stress: an application to Africa. Ambio, 34(3), 230–236.

Ward R. C. & M. Robinson, 2000. Principles of Hydrology. 4th ed. London: McGraw-Hill Publishing Company.

Winchell M., R. Srinivasan, M. Di Luzio, J. Arnold, 2007. ArcSWAT Interface for SWAT2005, User's Guide. Blackland Research Center, Texas Agricultural Exprimentation Station; Grassland, Soil and Water Research Laboratory; USDA Agricultural Research Service.

Wilby, R.L., 1997. Non-stationarity in daily precipitation series: implications for GCM downscaling using atmospheric circulation indices. International Journal of Climatology 17, 439-454.

WILBY, Robert L., and Christian W. Dawson, August 2007. Using SDSM Version 4.1 SDSM 4.2 – A decision support tool for the assessment of regional climate change impacts, User Manual, Leics., LE11 3TU, UK

Website References

Environment Canada, Canadian Climate Change Scenarios Network – National Node [Online] (updated 20 March 2007) Available at: http://www.cccsn.ca/Download_Data/HadCM3_Predictors-e.html [Accessed 2 March 2009]

Intergovernmental Panel on Climate Change, the IPCC Data Distribution Center. [Online] (updated 05 February 2009) Avilable at: http://www.ipcc-data.org/ [Acessed 2 March 2009]

Kyoto Protocol[Online] Avilable at: http://unfccc.int/kyoto_protocol/items/2830.php [Accessed 04 April]

SWAT Official Web Site [Online]: Avilable at: http://www.brc.tamus.edu/swat/ [Acessed February – April 2009]

The CGIAR Consortium for Spatial Information (CGIAR – CSI) [Online] Avilable at: http://srtm.csi.cgiar.org/SELECTION/inputCoord.asp [Acessed 12 February 2009]

U.S. Environmental Protection Agency. 2008. Climate Change. [Online] (updated March 22, 2009) Available at: http://www.epa.gov/climatechange/basicinfo.html [Acessed 2 April 2009]

WHAT: Web Based Hydrograph Analysis Tool. [Online] Avilable at: http://cobweb.ecn.purdue.edu/~what/ [Accessed 1 March 2009]

World Meteorological Organization. [Online] Avilable at: http://www.wmo.int/pages/index_en.html [Acessed 04 April 2009]

Appendix

Appendix 1: Summary of Average Monthly Meteorological Variables from 1995-2004 for Stations Considered in the Modeling Work

i) Monthly precipitation in mm

Adet Station

year	Jan	Feb	Mar	Apr	May	Jun	Jul	Aug	Sep	Oct	Nov	Dec
1995	0	0	34.00	36	136	154	396	332	146	28	19	78
1996	6	3	95	167	174	208	334	285	277	20	106	1
1997	3	0	51	21	248	160	258	196	238	170	45	0
1998	3	0	24	19	182	154	330	265	171	198	10	1
1999	27	0	2	25	96	131	337	244	113	145	27	16
2000	0	0	3	134	57	101	250	25	130	161	25	31
2001	0	4	3	33	138	195	343	373	148	95	25	12
2002	12	4	38	35	51	138	283	200	122	54	9	14
2003	0	8	11	7	16	163	341	297	207	53	21	4
2004	8	8	2	32	10	191	288	249	207	122	22	0
AVG	**5.9**	**2.7**	**26.3**	**50.9**	**110.8**	**159.5**	**316**	**246.6**	**175.9**	**104.6**	**30.9**	**15.7**

Bahir Dar Station

year	Jan	Feb	Mar	Apr	May	Jun	Jul	Aug	Sep	Oct	Nov	Dec
1995	0	4	8	19	77	261	419	260	104	21	8	5
1996	0	1	28	49	99	265	299	360	215	41	26	0
1997	0	0	20	29	239	123	233	220	178	137	24	10
1998	0	0	18	1	106	196	387	358	242	116	0	0
1999	9	0	0	8	50	130	395	487	196	199	3	0
2000	0	0	0	92	63	155	315	517	226	178	28	0
2001	0	1	6	35	69	277	382	565	146	99	13	17
2002	0	1	13	16	2	440	465	398	158	17	1	1
2003	0	0	0	0	2	243	620	447	259	75	6	6
2004	9	21	6	39	7	145	484	297	233	90	8	0
AVG	**1.8**	**2.8**	**9.9**	**28.8**	**71.4**	**223.5**	**399.9**	**390.9**	**195.7**	**97.3**	**11.7**	**3.9**

Dangila Station

year	Jan	Feb	Mar	Apr	May	Jun	Jul	Aug	Sep	Oct	Nov	Dec
1995	0.6	0	61.1	41.5	130.2	209.2	20.8	263	177.9	55.8	3.3	21.2
1996	0	1.9	97.4	94.3	182.4	185.6	339.8	385.9	249.7	74.2	43.2	0.3
1997	0	0	35.7	52.5	209.5	205.9	351.4	379.7	175	163.6	90.5	3.4
1998	0	0	22.7	13.9	186.1	307.5	282.3	343.2	254.2	148.3	5.8	0
1999	2	0	0	36.3	243.7	280.8	338.8	370.8	329.5	263.9	35.8	7.8
2000	0	7.1	7.5	77	135.3	344.1	313	436.1	237.8	265.3	70	2.5
2001	0	0	14.5	13.9	157.3	318.3	389.5	259.3	105.3	97.6	3.3	7.1
2002	0	3.6	11.9	14.8	52.1	278.8	298.9	351.7	182.7	123	30.3	2
2003	0	4.5	7.5	2.2	23.1	330.6	338.8	279	301.9	26.8	55	0
2004	0.5	9.1	2.3	90.5	60.7	230.5	488.2	363.8	266.6	94.7	21	0
AVG	**0.31**	**2.62**	**26.06**	**43.69**	**138.04**	**269.13**	**316.15**	**343.25**	**228.06**	**131.32**	**35.82**	**4.43**

Debre Markos Station

year	Jan	Feb	Mar	Apr	May	Jun	Jul	Aug	Sep	Oct	Nov	Dec
1995	0	1	20.3	90.4	146.6	126.4	246.1	344.6	151.2	14.4	12.4	95.5
1996	27.6	4.6	74.1	108	228	291.7	252.3	306.5	152.1	33.1	35.2	23.2
1997	14.3	0	29.6	97.5	17.2	151	286.8	338.8	205.8	183.5	85	6.7
1998	2.9	2.2	21	4.4	142.4	99.2	203.2	252.6	270.7	200.8	6.9	0
1999	72.6	0	2.8	43.2	46.8	180.7	252.1	340.3	164.3	210.5	2.5	28.3
2000	0	0	2.9	110.5	29.5	174.9	295.4	211.1	271	265.9	32.7	12.3
2001	0	3.7	58.1	101.2	129.6	154.7	365.2	322.2	170.3	66.9	0	2.2
2002	57	0	92.2	75.2	11.1	155.9	276.3	335.5	234.6	3.9	2.2	61.5
2003	3.6	57.4	69.6	19.2	5.3	212	205.5	351.6	256.8	10.7	0.3	18.8
2004	4.1	7.6	13.8	120.1	19.8	195	286.6	317.7	205.2	87.5	37.7	23.2
AVG	**18.21**	**7.65**	**38.44**	**76.97**	**77.63**	**174.15**	**266.95**	**312.09**	**208.2**	**107.72**	**21.49**	**27.17**

Debre Tabor Station

year	Jan	Feb	Mar	Apr	May	Jun	Jul	Aug	Sep	Oct	Nov	Dec
1995	0	8	46	95	109	353	355	130	37	20	0	0
1996	1	2	33	59	155	203	282	271	118	23	5	42
1997	7	8	67	110	206	234	310	304	160	45	41	5
1998	3	0	74	43	198	229	449	361	197	324	12	82
1999	14	0	21	7	204	128	404	415	254	80	0	0
2000	34	0	0	24	46	203	459	357	246	252	11	20
2001	0	0	7	124	79	205	423	465	235	147	35	3
2002	0	1	18	24	99	207	496	434	195	70	4	8
2003	0	1	61	45	48	205	255	325	129	3	16	19
2004	0	14	35	19	10	99	440	405	214	17	33	15
AVG	**5.9**	**3.4**	**36.2**	**55**	**115.4**	**206.6**	**387.3**	**346.7**	**178.5**	**98.1**	**15.7**	**19.4**

Gondor Station

year	Jan	Feb	Mar	Apr	May	Jun	Jul	Aug	Sep	Oct	Nov	Dec
1995	0	0	36	24	100	104	283	308	104	12	1	19
1996	0	4	24	84	184	195	250	260	76	68	23	0
1997	0	2	28	42	126	184	242	230	34	199	42	14
1998	0	0	10	4	95	285	383	492	128	128	5	0
1999	36	0	0	42	129	145	448	401	214	351	11	54
2000	0	1	3	73	60	366	453	369	170	268	1	4
2001	1	1	4	48	95	408	570	494	122	145	16	0
2002	15	3	45	17	88	197	317	248	79	44	6	5
2003	0	21	11	0	38	242	317	281	136	22	0	6
2004	2	4	6	38	1	183	380	316	113	68	66	0
AVG	**5.4**	**3.6**	**16.7**	**37.2**	**91.6**	**230.9**	**364.3**	**339.9**	**117.6**	**130.5**	**17.1**	**10.2**

ii) Average monthly maximum temperature

Adet Station

year	Jan	Feb	Mar	Apr	May	Jun	Jul	Aug	Sep	Oct	Nov	Dec
1995	28.06	28.43	29.26	29.53	28.9	27.3	22.13	22.42	23.83	25.77	26.7	26.65
1996	26.71	29.14	29.42	28.67	26.32	23.53	22.52	22.32	24.57	25.74	25.5	25.97
1997	26.16	28.79	29.42	29.37	27.52	24.93	22.23	23.45	25.27	24.77	25.3	26.77
1998	27.55	28.21	29.52	31.13	28.06	25.77	21.26	21.23	23.4	24.29	25.07	25.27
1999	25.77	29.04	29.39	30.03	28.19	26.1	21.55	22.19	23.87	23.23	24.83	25.32
2000	26.71	28.21	30.1	26.27	27.94	26	22.68	22.16	23.8	23.68	24.67	25.42
2001	26.1	28.61	28.65	29.8	28.13	23.8	23.1	22.94	24.87	26.13	26.1	26.74
2002	26.77	29	29.35	30.2	29.65	26.3	24.42	23.39	24.42	25.74	26.03	26
2003	27.29	29	29.81	30.4	30.94	26.63	22.61	22.65	23.73	25.23	25.67	26.03
2004	27.32	28.14	30.03	28.97	29.77	25.53	23.55	23.1	23.93	24.48	25.6	26.29
AVG	**26.84**	**28.66**	**29.50**	**29.44**	**28.54**	**25.59**	**22.61**	**22.59**	**24.17**	**24.91**	**25.55**	**26.05**

Bahirdar Station

year	Jan	Feb	Mar	Apr	May	Jun	Jul	Aug	Sep	Oct	Nov	Dec
1995	27.13	27.25	27.94	29.5	30.32	29.23	27.52	24.26	24.33	25.68	27.23	26.77
1996	26.77	26.76	29.52	29.23	29.97	27.1	26.16	25	24.73	26.29	27.6	26.84
1997	26.94	27.11	29.35	30.5	29.81	28.03	26.58	25.13	25.83	27.55	27.2	27.58
1998	27.81	28.82	29.9	32.47	33.55	30.73	28.16	22.87	23.77	25.77	27	27.71
1999	26.97	26.86	30.29	29.47	31.03	29.13	27.65	23.43	24.17	25.26	25.3	26.26
2000	26.06	27.38	29.26	30.73	28.23	29.63	27.13	24.77	24.63	25.77	25.97	26.45
2001	26.48	26.07	29.02	28.83	30.84	29.47	26	24.45	24.8	26.16	27.1	26.61
2002	27.35	27.04	29.1	29.97	31.1	30.97	27.77	25.84	25.3	26.48	27.9	27.74
2003	26.71	27.71	30.23	31.37	31.58	32.33	27.74	24.74	24.97	26.06	27.77	27.84
2004	27.32	27.28	28.68	30.27	29.26	31.27	27.26	25.52	25.47	26.26	27.43	27.48
AVG	**26.95**	**27.23**	**29.33**	**30.23**	**30.57**	**29.79**	**27.20**	**24.60**	**24.80**	**26.13**	**27.05**	**27.13**

Dangila Station

year	Jan	Feb	Mar	Apr	May	Jun	Jul	Aug	Sep	Oct	Nov	Dec
1995	25.84	26.43	27.13	28.63	27.26	26.93	23.71	21.23	22.03	23.39	25.83	25.61
1996	24.68	26.79	27.13	27.63	27.9	26.53	24.55	21.1	22.1	23.48	24.6	25.68
1997	25.42	26.07	28.26	27.47	27.23	24.27	22.94	21.84	22.3	23.16	24.1	23.94
1998	24.94	25.61	27.39	27.87	26.81	24.07	23.35	22	22.7	24.42	23.33	24.55
1999	25.55	26.21	27.45	28.43	29.68	26.1	23.84	20.77	21.47	24.45	23.93	24.87
2000	25.48	25.86	28.71	28.1	27.84	25.27	23.71	20.77	21.7	22.81	22.63	24.45
2001	25.03	26.54	27.68	29	25.68	25.5	22.71	21.9	21.77	23.29	23.07	24.23
2002	25.1	25.43	27.97	27.33	28.74	25.67	22.61	21.48	21.93	23.45	24	24.65
2003	25.68	26.32	28.1	28.33	29.31	28.33	23.58	23.39	22.5	23.74	25.5	25.52
2004	25.55	27.03	28.52	29.37	29.48	29.67	24.13	21.97	22.63	23.81	24.93	25.97
AVG	**25.33**	**26.23**	**27.83**	**28.22**	**27.99**	**26.23**	**23.51**	**21.65**	**22.11**	**23.60**	**24.19**	**24.95**

Debre Tabor

year	Jan	Feb	Mar	Apr	May	Jun	Jul	Aug	Sep	Oct	Nov	Dec
1995	26.93	23.32	24.52	25	24.55	23.8	23.1	18.13	18.93	20.29	22.03	22.23
1996	21.55	22.76	24.42	24.17	23.45	21	19.9	18.61	18.83	20.48	21.73	21.03
1997	21.55	21.89	23.35	24.27	23.03	21.8	20.48	18.45	19.27	21.45	20.97	21.97
1998	21.58	22.96	24	24.73	26.35	23.03	22.1	17.52	18.13	19.87	20.77	22.16
1999	22.68	22.18	24.84	24.97	25.13	24.7	23.13	17.55	18.17	19.77	19.37	21.52
2000	22.16	22.76	24.39	25.57	22.03	23.77	21.97	18.94	18.7	19.68	19.93	21.52
2001	22.42	22.82	24.97	23.97	25.35	23.3	20.16	18.16	18.7	20.55	21.97	22.03
2002	22.77	22.93	24.97	24.63	24.81	25.47	21.77	19.94	19.83	20.77	22.87	23.06
2003	22.77	23.64	24.42	24.47	25.26	26.13	22	18.42	18.83	20.19	21.93	22.26
2004	22.58	23.62	23.9	24.97	23.03	26.07	21.42	19.52	19.2	21	21.5	22.29
AVG	**22.70**	**22.89**	**24.38**	**24.68**	**24.30**	**23.91**	**21.60**	**18.52**	**18.86**	**20.41**	**21.31**	**22.01**

Gondor Station

year	Jan	Feb	Mar	Apr	May	Jun	Jul	Aug	Sep	Oct	Nov	Dec
1995	26.94	23.32	24.52	25	24.55	23.8	23.1	18.13	18.93	20.29	22.03	22.23
1996	21.55	22.76	24.42	24.17	23.45	21	19.9	18.61	18.9	20.48	21.73	21.03
1997	21.55	21.89	23.35	24.27	23.03	21.8	20.48	18.45	19.27	21.45	20.97	21.97
1998	21.58	22.96	24	24.73	26.35	23.03	22.1	17.52	18.13	19.87	20.84	22.13
1999	22.68	22.18	24.84	24.97	25.13	24.7	23.13	17.55	18.17	19.77	19.37	21.52
2000	22.16	22.76	24.39	25.57	22.03	23.77	21.97	18.94	18.7	19.68	19.93	21.52
2001	22.42	22.82	24.97	23.97	25.35	23.3	20.16	18.16	18.7	20.55	21.97	22.03
2002	22.77	22.93	24.97	24.63	24.81	25.47	21.77	19.94	19.83	20.77	22.87	23.06
2003	22.77	23.64	24.42	24.47	25.26	26.13	22	18.42	18.83	20.19	21.93	22.26
2004	22.58	23.62	23.9	24.97	23.03	26.07	21.42	19.52	19.2	21	21.5	22.29
AVG	**22.70**	**22.89**	**24.38**	**24.68**	**24.30**	**23.91**	**21.60**	**18.52**	**18.87**	**20.41**	**21.31**	**22.00**

iii) Average monthly minimum temperature

Adet station

year	Jan	Feb	Mar	Apr	May	Jun	Jul	Aug	Sep	Oct	Nov	Dec
1995	4.19	5.21	6.32	9.8	11.42	11.47	12.61	11.58	10.03	6.42	4.73	4.32
1996	4.23	5.69	9.35	11.23	12.13	11.73	12.06	11.77	11.33	9.16	7.87	5.87
1997	3.87	5.36	10.19	10.43	12	11.33	11.9	12.03	10.2	10.23	9.33	5.61
1998	5.16	4.71	9.71	8.97	11.68	11.37	12.16	12.32	11.33	11.1	6.97	4.42
1999	5.61	6.61	4.94	7.57	9.35	11.13	11.97	11.94	10.43	10.71	6.63	6.29
2000	5.81	6.62	7	9.77	11.1	10.87	11.77	11.39	10.4	11.03	8.1	6.45
2001	4.55	7.75	10.1	10.8	11.52	11.97	12.55	12.52	10.77	11	7.93	6.94
2002	6.52	8.54	10.06	11.17	11.55	12.87	12.23	12.58	11	10.06	8.93	6.68
2003	6.13	9.71	12	11.77	13.61	12.83	13	13.13	11.53	10.19	8.53	6.61
2004	7.35	8.45	10.48	12.87	12.26	12.4	11.87	12.48	11	9.65	9.37	7.42

Bahir Dar Station

year	Jan	Feb	Mar	Apr	May	Jun	Jul	Aug	Sep	Oct	Nov	Dec
1995	9.45	9.54	11.45	12.43	16.61	16.77	15.42	15.55	14.73	14.26	13.97	12.26
1996	11.97	9.90	12.69	14.48	16.71	15.97	15.00	14.71	14.50	14.19	13.13	12.03
1997	10.77	10.00	11.55	15.17	15.61	15.93	15.00	15.16	14.90	14.23	14.57	13.74
1998	11.03	6.36	6.39	11.40	12.74	14.47	13.87	14.29	14.20	13.06	13.17	8.61
1999	9.32	11.03	10.63	15.68	14.83	13.48	14.00	14.40	13.58	13.80	10.81	10.19
2000	10.19	9.52	10.90	13.53	14.90	15.30	14.61	14.32	13.82	13.55	13.73	11.03
2001	9.10	6.86	10.81	12.53	14.90	14.39	14.04	13.36	12.17	12.65	14.83	11.87
2002	11.13	10.21	12.06	13.47	15.19	15.87	15.32	15.06	14.77	13.94	14.27	12.55
2003	9.65	8.86	12.94	15.30	15.06	17.00	15.65	14.87	15.03	14.26	13.67	11.90
2004	9.19	9.86	10.77	13.23	15.32	15.07	15.35	14.55	14.87	13.94	13.10	12.74
AVG	10.18	9.21	11.02	13.72	15.19	15.43	14.83	14.63	14.26	13.79	13.53	11.69

Dangila Station

year	Jan	Feb	Mar	Apr	May	Jun	Jul	Aug	Sep	Oct	Nov	Dec
1995	9.26	8.89	10.29	12.07	13.65	14.30	12.94	12.29	13.37	11.94	12.70	10.74
1996	9.58	3.62	5.55	7.47	9.94	11.80	11.26	11.84	11.03	9.65	8.73	5.35
1997	5.58	3.75	6.06	8.30	10.00	10.83	10.53	10.61	10.93	9.84	7.53	5.97
1998	4.39	3.71	4.77	8.83	9.63	10.93	10.16	10.74	10.20	9.87	9.30	7.16
1999	4.84	3.79	4.55	11.13	11.68	13.03	12.48	13.06	12.70	11.74	10.77	6.29
2000	3.55	4.59	6.65	5.37	10.81	10.93	10.26	10.94	10.63	9.48	9.30	4.74
2001	3.87	3.46	4.00	5.60	8.61	9.67	9.10	9.35	9.23	8.71	8.57	5.39
2002	5.32	3.57	7.35	8.23	11.74	12.17	12.84	12.94	13.10	11.52	11.43	7.39
2003	6.61	5.96	8.03	10.03	9.84	12.33	13.13	12.90	12.27	11.26	10.30	7.26
2004	4.48	4.28	8.26	10.23	9.94	12.50	13.10	13.42	13.13	11.87	9.73	8.39
AVG	**5.75**	**4.56**	**6.55**	**8.73**	**10.58**	**11.85**	**11.58**	**11.81**	**11.66**	**10.59**	**9.84**	**6.87**

Debre Tabor

year	Jan	Feb	Mar	Apr	May	Jun	Jul	Aug	Sep	Oct	Nov	Dec
1995	9.37	8.59	9.71	10.43	12.06	12.17	11.52	10.77	10.57	9.26	8.4	8.61
1996	8.29	8.45	10.32	10.73	11.65	11.07	10.16	10.55	10.07	9.69	8.23	8.61
1997	7.9	8.18	8.84	10.97	11.03	10.7	10.74	10.61	10.27	9.9	9.27	8.52
1998	8.58	8.86	9.42	11.37	12.97	12	11	10.71	10.53	9.84	9.43	7.39
1999	6.74	8.14	9.68	9.57	11.45	10.9	10.39	10.13	10.27	9.32	9.33	7.03
2000	7.71	7.93	9.03	10.53	10.35	10.63	10.23	9.87	9.9	9.32	9.13	8.32
2001	7.55	7.07	9.58	10.57	11.65	11.57	10.42	10.06	10.47	9.06	9.2	7.55
2002	7.97	7.79	9.39	10.63	11	12	10.58	10.16	9.77	8.81	8.07	7.74
2003	7.32	3.36	9.35	10.43	11.16	12.23	10.68	9.32	9.57	9.06	8.37	8.23
2004	7.97	8.72	9.67	11.23	11.13	10.35	10	10	9.87	9.19	7.73	7.97
AVG	**7.94**	**7.709**	**9.499**	**10.646**	**11.445**	**11.362**	**10.572**	**10.218**	**10.129**	**9.345**	**8.716**	**7.997**

Gondor Station

year	Jan	Feb	Mar	Apr	May	Jun	Jul	Aug	Sep	Oct	Nov	Dec
1995.00	9.35	8.57	9.71	10.43	12.06	12.17	11.52	10.77	10.57	9.26	8.40	8.61
1996.00	8.29	8.45	10.32	10.73	11.65	11.07	10.16	10.55	10.07	9.68	8.23	8.61
1997.00	7.90	8.18	8.84	10.97	11.03	10.70	10.74	10.61	10.27	9.90	9.27	8.52
1998.00	8.58	8.86	9.42	11.37	12.97	12.00	11.00	10.71	10.53	9.84	9.43	7.39
1999.00	6.74	8.14	9.68	9.57	11.45	10.90	10.39	10.13	10.27	9.32	9.33	7.03
2000.00	7.71	7.93	9.03	10.53	10.35	10.63	10.23	9.87	9.90	9.32	9.13	8.32
2001.00	7.55	7.07	9.58	10.57	11.65	11.57	10.42	10.06	10.47	9.06	9.20	7.55
2002.00	7.97	7.79	9.39	10.63	11.00	12.00	10.58	10.16	9.77	8.81	8.07	7.74
2003.00	7.32	7.36	9.35	10.43	11.16	12.23	10.68	9.32	9.57	9.06	8.37	8.23
2004.00	7.97	8.72	8.48	10.90	11.23	11.13	10.35	10.00	9.87	9.19	7.73	7.79
AVG	**7.94**	**8.11**	**9.38**	**10.61**	**11.46**	**11.44**	**10.61**	**10.22**	**10.13**	**9.34**	**8.72**	**7.98**

iv) Annual Average monthly climatic variables for the stations considered for the modeling work

	Station								
	Adet			Bahir Dar			Dangila		
Month	PRCP	TMAX	TMIN	PRCP	TMAX	TMIN	PRCP	TMAX	TMIN
Jan	5.9	26.844	7.35	1.8	26.954	10.18	0.31	25.327	5.748
Feb	2.7	28.657	8.45	2.8	27.228	9.214	2.62	26.229	4.562
Mar	26.3	29.495	10.48	9.9	29.329	11.019	26.06	27.834	6.551
Apr	50.9	29.437	12.87	28.8	30.234	13.722	43.69	28.216	8.726
May	110.8	28.542	12.26	71.4	30.569	15.187	138.04	27.993	10.584
Jun	159.5	25.589	12.4	223.5	29.789	15.425	269.13	26.234	11.849
Jul	316	22.605	11.87	399.9	27.197	14.826	316.15	23.513	11.58
Aug	246.6	22.585	12.48	390.9	24.601	14.627	343.25	21.645	11.809
Sep	175.9	24.169	11	195.7	24.8	14.257	228.06	22.113	11.659
Oct	104.6	24.906	9.65	97.3	26.128	13.788	131.32	23.6	10.588
Nov	30.9	25.547	9.37	11.7	27.05	13.525	35.82	24.192	9.836
Dec	15.7	26.046	7.42	3.9	27.128	11.692	4.43	24.947	6.868

	Station						
	Debre Markos	Debre Tabor			Gondor		
Month	PRCP	PRCP	TMAX	TMIN	PRCP	TMAX	TMIN
Jan	18.21	5.9	22.699	7.94	5.4	22.7	7.938
Feb	7.65	3.4	22.888	7.709	3.6	22.888	8.107
Mar	38.44	36.2	24.378	9.499	16.7	24.378	9.38
Apr	76.97	55	24.675	10.646	37.2	24.675	10.613
May	77.63	115.4	24.299	11.445	91.6	24.299	11.455
Jun	174.15	206.6	23.907	11.362	230.9	23.907	11.44
Jul	266.95	387.3	21.603	10.572	364.3	21.603	10.607
Aug	312.09	346.7	18.524	10.218	339.9	18.524	10.218
Sep	208.2	178.5	18.859	10.129	117.6	18.866	10.129
Oct	107.72	98.1	20.405	9.345	130.5	20.405	9.344
Nov	21.49	15.7	21.307	8.716	17.1	21.314	8.716
Dec	27.17	19.4	22.007	7.997	10.2	22.004	7.979

Appendix 2: Parameter Files for the Climate Projection Obtained from the SDSM

a) Max temperature parameter file

6
1
366
1/1/1990
4383
1/1/1990
2922
#FALSE#
1
1
False
TMAX.dat
ncepmslpaf.dat
ncepp__zaf.dat
ncepp500af.dat
ncepp8_uaf.dat
ncepp8_zaf.dat
nceprhumaf.dat

24.613	-1.523	-0.799	0.778	-0.461	0.323	-0.674	1.767	0.486
24.613	-1.523	-0.799	0.778	-0.461	0.323	-0.674	1.767	0.486
24.613	-1.523	-0.799	0.778	-0.461	0.323	-0.674	1.767	0.486
24.613	-1.523	-0.799	0.778	-0.461	0.323	-0.674	1.767	0.486
24.613	-1.523	-0.799	0.778	-0.461	0.323	-0.674	1.767	0.486
24.613	-1.523	-0.799	0.778	-0.461	0.323	-0.674	1.767	0.486
24.613	-1.523	-0.799	0.778	-0.461	0.323	-0.674	1.767	0.486
24.613	-1.523	-0.799	0.778	-0.461	0.323	-0.674	1.767	0.486
24.613	-1.523	-0.799	0.778	-0.461	0.323	-0.674	1.767	0.486
24.613	-1.523	-0.799	0.778	-0.461	0.323	-0.674	1.767	0.486
24.613	-1.523	-0.799	0.778	-0.461	0.323	-0.674	1.767	0.486
24.613	-1.523	-0.799	0.778	-0.461	0.323	-0.674	1.767	0.486

D:\ClimateTmp_forcast\Observed1990-2001\TMAX.dat

[1] The number of predictors
[2] The season code (12 = months, 4 = seasons, 1 = annual model)
[3] The year length indicator (366, 365, or 360)
[4] Record start date
[5] Record length (days)
[6] Model fitting start date
[7] Number of days used in the model fitting
[8] Whether the model is conditional (true) or unconditional (false)
[9] Transformation (1 = none, 2 = fuorth root, 3 = natural log, 4 = log normal)
[10] Ensemble size
[11] Auto regression indicator (True or false)
[12] Predictand file name
[13-18] predictor files
[19-30] Model Parameters; the first six columns are the parameters (including the intercept), the last two columns are the SE and r^2 statistic
[31] the root directory of the predictand file

b) Parameter file for the Minimum Temperature

5
1
366
1/1/1990
4383
1/1/1990
2922
#FALSE#
1
1
False
TMIN.dat
ncepp__vaf.dat
ncepp_thaf.dat
ncepp_zhaf.dat
ncepp500af.dat
ncepp8_zaf.dat

9.376	-2.036	-0.011	-1.899	0.770	-0.998	2.438	0.467
9.376	-2.036	-0.011	-1.899	0.770	-0.998	2.438	0.467
9.376	-2.036	-0.011	-1.899	0.770	-0.998	2.438	0.467
9.376	-2.036	-0.011	-1.899	0.770	-0.998	2.438	0.467
9.376	-2.036	-0.011	-1.899	0.770	-0.998	2.438	0.467
9.376	-2.036	-0.011	-1.899	0.770	-0.998	2.438	0.467
9.376	-2.036	-0.011	-1.899	0.770	-0.998	2.438	0.467
9.376	-2.036	-0.011	-1.899	0.770	-0.998	2.438	0.467
9.376	-2.036	-0.011	-1.899	0.770	-0.998	2.438	0.467
9.376	-2.036	-0.011	-1.899	0.770	-0.998	2.438	0.467
9.376	-2.036	-0.011	-1.899	0.770	-0.998	2.438	0.467
9.376	-2.036	-0.011	-1.899	0.770	-0.998	2.438	0.467

D:\ClimateTmp_forcast\ObservedTMIN_1990-2001\TMIN.dat

The designation of the data is in-line order as follows:
[1] The number of predictors
[2] The season code (12 = months, 4 = seasons, 1 = annual model)
[3] The year length indicator (366, 365, or 360)
[4] Record start date
[5] Record length (days)
[6] Model fitting start date
[7] Number of days used in the model fitting
[8] Whether the model is conditional (true) or unconditional (false)
[9] Transformation (1 = none, 2 = fuorth root, 3 = natural log, 4 = log normal)
[10] Ensemble size
[11] Auto regression indicator (True or false)
[12] Predictand file name
[13-17] predictor files
[18-29] Model Parameters; the first six columns are the parameters (including the intercept), the last two columns are the SE and r^2 statistic
[30] the root directory of the predictand file

a) Precipitation parameter file

5
1
366
1/1/1990
4383
1/1/1990
2922
#TRUE#
1
1
False
PRCP.dat
ncepp__faf.dat
ncepp500af.dat
ncepp8_uaf.dat
ncepp8_zaf.dat
ncepr500af.dat

0.471	-0.112	0.108	0.107	-0.150	0.071	0.000	0.418	
0.471	-0.112	0.108	0.107	-0.150	0.071	0.000	0.418	
0.471	-0.112	0.108	0.107	-0.150	0.071	0.000	0.418	
0.471	-0.112	0.108	0.107	-0.150	0.071	0.000	0.418	
0.471	-0.112	0.108	0.107	-0.150	0.071	0.000	0.418	
0.471	-0.112	0.108	0.107	-0.150	0.071	0.000	0.418	
0.471	-0.112	0.108	0.107	-0.150	0.071	0.000	0.418	
0.471	-0.112	0.108	0.107	-0.150	0.071	0.000	0.418	
0.471	-0.112	0.108	0.107	-0.150	0.071	0.000	0.418	
0.471	-0.112	0.108	0.107	-0.150	0.071	0.000	0.418	
0.471	-0.112	0.108	0.107	-0.150	0.071	0.000	0.418	
0.471	-0.112	0.108	0.107	-0.150	0.071	0.000	0.418	
7.518	1.000	-1.078	0.200	1.313	-0.055	0.932	9.296	0.047
7.518	1.000	-1.078	0.200	1.313	-0.055	0.932	9.296	0.047
7.518	1.000	-1.078	0.200	1.313	-0.055	0.932	9.296	0.047
7.518	1.000	-1.078	0.200	1.313	-0.055	0.932	9.296	0.047
7.518	1.000	-1.078	0.200	1.313	-0.055	0.932	9.296	0.047
7.518	1.000	-1.078	0.200	1.313	-0.055	0.932	9.296	0.047
7.518	1.000	-1.078	0.200	1.313	-0.055	0.932	9.296	0.047
7.518	1.000	-1.078	0.200	1.313	-0.055	0.932	9.296	0.047
7.518	1.000	-1.078	0.200	1.313	-0.055	0.932	9.296	0.047
7.518	1.000	-1.078	0.200	1.313	-0.055	0.932	9.296	0.047
7.518	1.000	-1.078	0.200	1.313	-0.055	0.932	9.296	0.047
7.518	1.000	-1.078	0.200	1.313	-0.055	0.932	9.296	0.047

D:\Climate_Forcast\Precipitation\PRCP.dat

The assignation of the order of precipitation projection parameter files is the same as the minimum temperature's as both of them have the same number of predictors.

Appendix 3: Land Use Characteristic Values as Presented in the Order Below

CROPID CPNM IDC
BIO_E HVSTI BLAI FRGRW1 LAIMX1 FRGRW2 LAIMX2 DLAI CHTMX RDMX
T_OPT T_BASE CNYLD CPYLD BN1 BN2 BN3 BP1 BP2 BP3
WSYF USLE_C GSI VPDFR FRGMAX WAVP CO2HI BIOEHI RSDCO_PL ALAI_LEAF
BIO_LEAF MAT_YRS BMX_TREES EXT_COEF BM_DIEOFF

1 AGRL 4
33.50 0.45 3.00 0.15 0.05 0.50 0.95 0.64 1.00 2.00
30.00 11.00 0.0199 0.0032 0.0440 0.0164 0.0128 0.0060 0.0022 0.0018
0.250 0.2000 0.0050 4.00 0.750 8.50 660.00 36.00 0.0500 0.000
0.000 0 0.00 0.650 0.100

2 AGRR 4
39.00 0.50 3.00 0.15 0.05 0.50 0.95 0.70 2.50 2.00
25.00 8.00 0.0140 0.0016 0.0470 0.0177 0.0138 0.0048 0.0018 0.0014
0.300 0.2000 0.0070 4.00 0.750 7.20 660.00 45.00 0.0500 0.000
0.000 0 0.00 0.650 0.100

6 FRST 7
15.00 0.76 5.00 0.05 0.05 0.40 0.95 0.99 6.00 3.50
30.00 10.00 0.0015 0.0003 0.0060 0.0020 0.0015 0.0007 0.0004 0.0003
0.010 0.0010 0.0020 4.00 0.750 8.00 660.00 16.00 0.0500 0.750
0.300 50 1000.00 0.650 0.100

7 FRSD 7
15.00 0.76 5.00 0.05 0.05 0.40 0.95 0.99 6.00 3.50
30.00 10.00 0.0015 0.0003 0.0060 0.0020 0.0015 0.0007 0.0004 0.0003
0.010 0.0010 0.0020 4.00 0.750 8.00 660.00 16.00 0.0500 0.750
0.300 10 1000.00 0.650 0.100

8 FRSE 7
15.00 0.76 5.00 0.15 0.70 0.25 0.99 0.99 10.00 3.50
30.00 0.00 0.0015 0.0003 0.0060 0.0020 0.0015 0.0007 0.0004 0.0003
0.600 0.0010 0.0020 4.00 0.750 8.00 660.00 16.00 0.0500 0.750
0.300 30 1000.00 0.650 0.100

11 WETN 6
47.00 0.90 6.00 0.10 0.20 0.20 0.95 0.70 2.50 2.20
25.00 12.00 0.0160 0.0022 0.0350 0.0150 0.0038 0.0014 0.0010 0.0007
0.900 0.0030 0.0050 4.00 0.750 8.50 660.00 54.00 0.0500 0.000
0.000 0 0.00 0.650 0.100

15 RNGE 6
34.00 0.90 2.50 0.05 0.10 0.25 0.70 0.35 1.00 2.00
25.00 12.00 0.0160 0.0022 0.0200 0.0120 0.0050 0.0014 0.0010 0.0007
0.900 0.0030 0.0050 4.00 0.750 10.00 660.00 39.00 0.0500 0.000
0.000 0 0.00 0.330 0.100

```
16  RNGB   6
 34.00   0.90    2.00   0.05   0.10   0.25   0.70   0.35    1.00   2.00
 25.00   12.00   0.0160   0.0022   0.0200   0.0120   0.0050   0.0014   0.0010   0.0007
 0.900   0.0030   0.0050   4.00   0.750   10.00    660.00    39.00   0.0500   0.000
 0.000     0    0.00   0.330   0.100

18  WATR   6
  0.00   0.00    0.00   0.00   0.00   0.00   0.00   0.00    0.00   0.00
  0.00    0.00   0.0000   0.0000   0.0000   0.0000   0.0000   0.0000   0.0000   0.0000
 0.000   0.0000   0.0000   0.00   0.000    0.00      0.00     0.00   0.0000   0.000
 0.000     0    0.00   0.000   0.100

99  TEFF   5
 30.00   0.23    3.00   0.15   0.05   0.50   0.95   0.90    0.90   2.00
 18.00    0.00   0.0234   0.0033   0.0600   0.0231   0.0134   0.0084   0.0032   0.0019
 0.200   0.0300   0.0056   4.00   0.750    8.00    660.00    46.00   0.0500   0.001
 0.001     0    0.00   0.650   0.100
```

Appendix 4: SDSM Climate Change Results

a) A2a scenario

	Precipitation (mm)				Change in precipitation			Percentage change		
Month	base	2020s	2050s	2080s	2020s	2050s	2080s	2020s	2050s	2080s
Jan	2.62	1.86	1.60	1.96	-0.07	-1.02	0.04	-2.63	-0.78	1.94
Feb	2.20	1.80	1.79	3.21	-0.40	-0.41	1.01	-17.98	-12.00	22.00
Mar	5.20	3.69	4.27	6.34	-1.51	-0.93	1.14	-29.00	-6.40	21.90
Apr	6.40	5.77	6.71	8.30	-0.63	0.31	1.90	-9.77	12.40	29.76
May	7.60	7.71	9.28	10.16	0.11	1.68	2.56	1.51	22.16	33.63
Jun	8.20	9.73	10.53	10.97	1.53	2.33	2.77	18.60	28.38	33.74
Jul	8.50	10.14	10.80	11.41	1.64	2.30	2.91	19.32	27.03	34.29
Aug	10.53	10.13	10.71	11.28	-0.40	0.18	0.75	-3.82	15.00	7.17
Sep	10.60	8.00	9.16	10.10	-2.60	-1.43	-0.49	-24.53	-7.50	-4.64
Oct	7.04	5.20	5.74	7.50	-1.84	-1.30	0.46	-26.16	-11.50	6.55
Nov	4.54	3.39	4.05	5.61	-1.15	-0.49	1.08	-25.34	-8.70	23.69
Dec	1.94	1.48	2.12	4.12	-0.46	0.17	2.18	-23.54	-5.80	22.00
Jan	2.62	1.86	1.60	1.96	-0.07	-1.02	0.04	-2.63	-7.80	1.94
Bega	4.03	2.98	3.37	4.80	-0.88	-0.66	0.94	-19.42	-8.45	13.55
Belg	5.35	4.75	5.51	7.00	-0.60	0.16	1.65	-13.81	4.04	26.82
Kiremt	9.46	9.50	10.30	10.94	0.04	0.84	1.49	2.39	15.73	17.64
Annual	6.28	5.74	6.40	7.58	-0.48	0.12	1.36	-10.28	3.77	19.34

b) B2a Scenario

	precipitation (mm)				Change in Precipitation			percent change in precipitation		
month	base	2020s	2050s	2080s	2020s	2050s	2080s	2020s	2050s	2080s
Jan	2.62	1.85	1.89	2.71	-0.77	-0.73	0.09	-3.00	-1.40	3.31
Feb	2.20	1.77	1.94	2.29	-0.43	-0.26	0.09	-19.61	-12.00	4.27
Mar	5.20	3.85	4.59	5.45	-1.35	-0.61	0.25	-25.90	-11.72	4.75
Apr	6.40	5.63	7.13	7.81	-0.77	0.73	1.41	-11.98	11.47	22.03
May	7.60	7.93	8.96	9.61	0.33	1.36	2.01	4.36	17.91	26.39
Jun	8.20	9.56	10.56	10.52	1.36	2.36	2.32	16.59	28.75	28.24
Jul	8.50	10.02	10.86	11.20	1.52	2.36	2.70	17.91	27.77	31.71
Aug	10.53	9.93	10.79	11.24	-0.60	0.27	0.71	-5.66	2.53	6.77
Sep	10.60	7.98	9.59	9.93	-2.62	-1.01	-0.66	-24.71	-9.52	-6.27
Oct	7.04	5.18	6.81	6.76	-1.86	-0.23	-0.28	-26.40	-3.28	-4.03
Nov	4.54	3.20	4.11	5.21	-1.34	-0.43	0.67	-29.48	-9.53	14.73
Dec	1.94	1.45	1.90	2.12	-0.49	-0.04	0.18	-25.11	-2.11	9.36
Bega	4.03	2.92	3.68	4.20	-1.11	-0.36	0.16	-27.75	-7.23	5.84
Belg	5.35	4.80	5.66	6.29	-0.55	0.31	0.94	-13.28	1.41	14.36
Kiremt	9.46	9.37	10.45	10.72	-0.08	0.99	1.26	1.03	12.38	15.11
Annual	6.28	5.70	6.59	7.07	-0.58	0.31	0.79	-13.33	2.19	11.77

c) Maximum Temprature

	A2a Scenario							B2a Scenario						
	Maximum Temprature (^{0}C)			Delta Max temprature				Miniumum Temprature				Delta Min Temprature		
Month	Baseline	2020s	2050s	2080s	2020s	2050s	2080s	Baseline	2020s	2050s	2080s	2020s	2050s	2080s
Jan	24.95	26.03	26.42	28.07	1.07	1.46	3.12	24.95	25.73	26.45	27.26	0.78	1.50	2.30
Feb	25.41	27.17	27.76	29.37	1.76	2.35	3.96	25.41	27.38	27.71	28.91	1.96	2.29	3.50
Mar	26.87	27.13	28.01	29.35	0.25	1.13	2.47	26.87	27.40	27.94	28.97	0.52	1.06	2.10
Apr	27.69	26.21	27.39	28.75	-1.47	-0.30	1.07	27.69	26.43	27.10	28.21	-1.26	-0.59	0.52
May	27.39	24.95	25.87	27.63	-2.45	-1.52	0.23	27.39	24.86	25.96	27.21	-2.53	-1.43	-0.18
Jun	25.47	24.21	25.21	26.89	-1.26	-0.26	1.42	25.47	24.24	25.23	26.39	-1.23	-0.24	0.92
Jul	23.51	23.57	24.69	26.25	0.06	1.18	2.74	23.51	23.54	24.61	25.59	0.03	1.11	2.08
Aug	21.50	23.65	24.44	25.96	2.16	2.94	4.46	21.50	23.77	24.54	25.37	2.27	3.05	3.87
Sep	21.71	24.21	25.09	26.64	2.50	3.39	4.93	21.71	24.44	25.17	25.97	2.73	3.46	4.26
Oct	22.69	24.78	25.77	27.24	2.09	3.08	4.54	22.69	24.88	25.82	26.71	2.19	3.12	4.01
Nov	23.62	24.38	25.17	26.75	0.76	1.55	3.13	23.62	24.32	25.32	26.15	0.70	1.70	2.53
Dec	24.07	24.66	25.34	26.86	0.59	1.27	2.79	24.07	24.43	25.22	26.12	0.36	1.15	2.05
Bega	23.83	24.96	25.67	27.23	1.13	1.84	3.40	23.83	24.84	25.70	26.56	1.01	1.87	2.72
Belg	26.84	26.36	27.26	28.77	-0.48	0.42	1.93	26.84	26.52	27.18	28.32	-0.33	0.33	1.48
Kiremt	23.05	23.91	24.86	26.44	0.86	1.81	3.39	23.05	24.00	24.89	25.83	0.95	1.84	2.78
Annual	24.52	25.08	25.93	27.48	0.55	1.41	2.96	24.52	25.12	25.92	26.90	0.59	1.40	2.38

d) Minimum Temperature

	A2a Scenario							B2a Scenario						
	Minimum Temperature				Delta Min Temperature			Minimum Temperature				Delta Min Temperature		
Month	Baseline	2020s	2050s	2080s	2020s	2050s	2080s	Baseline	2020s	2050s	2080s	2020s	2050s	2080s
Jan	4.70	5.43	5.94	7.13	0.73	1.24	2.42	4.70	5.45	5.95	6.60	0.74	1.25	1.89
Feb	4.17	5.87	6.59	7.95	1.70	2.41	3.78	4.17	5.88	6.36	7.23	1.71	2.18	3.06
Mar	5.09	7.41	8.06	9.31	2.31	2.96	4.22	5.09	7.64	8.33	8.95	2.55	3.24	3.85
Apr	8.02	8.84	9.69	10.81	0.82	1.67	2.79	8.02	8.80	9.75	10.27	0.79	1.73	2.25
May	9.35	9.84	10.55	11.90	0.49	1.19	2.54	9.35	9.81	10.61	11.40	0.46	1.26	2.05
Jun	11.25	10.44	11.36	12.67	-0.81	0.12	1.42	11.25	10.57	11.53	12.20	-0.68	0.28	0.96
Jul	10.86	10.43	11.35	12.50	-0.44	0.49	1.64	10.86	10.44	11.26	12.11	-0.42	0.39	1.25
Aug	11.06	10.29	11.02	12.29	-0.77	-0.04	1.23	11.06	10.54	11.19	11.87	-0.52	0.13	0.81
Sep	10.88	9.71	10.50	11.62	-1.17	-0.38	0.73	10.88	9.86	10.53	11.19	-1.03	-0.35	0.30
Oct	10.20	8.81	9.53	10.74	-1.39	-0.66	0.54	10.20	8.86	9.60	10.41	-1.34	-0.60	0.21
Nov	8.73	7.48	8.19	9.41	-1.24	-0.54	0.68	8.73	7.45	8.35	8.86	-1.28	-0.37	0.13
Dec	6.76	5.89	6.71	7.62	-0.87	-0.05	0.87	6.76	6.00	6.55	7.31	-0.76	-0.21	0.55
Bega	7.60	6.90	7.59	8.73	-0.69	0.00	1.13	7.60	6.94	7.61	8.29	-0.66	0.02	0.69
Belg	6.66	7.99	8.72	9.99	1.33	2.06	3.33	6.66	8.04	8.76	9.46	1.38	2.10	2.80
Kiremt	11.01	10.21	11.06	12.27	-0.80	0.04	1.25	11.01	10.35	11.13	11.84	-0.66	0.11	0.83
Annual	8.39	8.37	9.12	10.33	-0.02	0.74	1.94	8.39	8.44	9.17	9.87	0.05	0.78	1.48

Appendix-5: SWAT Model Results

The results presented were average daily river flows in a month in m^3/s

Baseline

year	Jan	Feb	Mar	Apr	May	Jun	Jul	Aug	Sep	Oct	Nov	Dec
1990.00	0.86	0.11	1.14	3.17	11.02	40.80	102.00	155.10	111.40	61.13	17.13	3.07
1991.00	0.18	0.05	0.62	8.50	14.72	65.57	221.80	223.80	164.10	97.53	28.40	5.89
1992.00	0.41	0.09	0.99	12.85	16.73	3.88	51.44	208.70	153.50	127.60	74.84	26.34
1993.00	5.28	1.70	2.69	2.49	14.81	43.87	107.90	118.70	103.50	90.00	50.37	12.81
1994.00	1.67	0.14	0.32	1.13	29.20	57.11	170.10	172.20	116.40	39.93	11.07	1.39
1995.00	0.12	0.06	0.33	1.14	31.93	21.50	152.00	175.80	153.50	63.99	19.45	21.40
1996.00	5.60	0.60	8.66	23.38	48.10	90.90	136.60	193.90	177.90	88.13	37.25	27.18
1997.00	5.47	0.36	1.63	7.41	29.09	75.78	121.10	149.60	116.20	101.40	71.41	22.96
1998.00	4.17	0.28	0.13	5.23	30.61	32.69	129.70	166.10	145.20	132.00	44.57	11.02
1999.00	2.14	0.33	0.08	2.13	15.79	32.34	115.20	171.60	139.30	107.80	42.86	12.07
2000.00	1.44	0.12	0.06	6.55	11.49	30.09	94.83	161.80	106.50	108.30	54.51	15.31
2001.00	2.35	0.13	0.08	4.09	11.39	72.19	154.50	209.00	147.20	69.25	28.56	6.99
AVG	2.47	0.33	1.39	6.51	22.07	47.23	129.76	175.53	136.23	90.59	40.04	13.87

A2a_2020s period

year	Jan	Feb	Mar	Apr	May	Jun	Jul	Aug	Sep	Oct	Nov	Dec
1.00	0.50	0.09	0.30	0.10	10.77	43.48	141.30	164.20	95.14	46.22	12.04	1.74
2.00	0.10	0.05	0.12	0.19	11.89	92.12	283.90	233.00	142.20	76.17	21.21	3.94
3.00	0.21	0.08	0.26	4.43	9.96	64.59	76.32	214.90	140.40	92.19	55.34	18.19
4.00	2.93	0.72	1.64	0.55	15.09	55.04	142.70	129.30	86.04	65.31	34.77	8.33
5.00	0.85	0.09	0.15	0.07	25.18	72.58	219.00	183.30	105.00	34.38	7.85	0.73
6.00	0.10	0.06	0.07	0.31	31.52	32.66	196.80	186.70	140.80	51.80	13.88	12.47
7.00	3.21	0.26	2.69	11.56	44.82	110.30	173.70	203.70	150.30	71.18	25.94	18.36
8.00	3.14	0.20	0.36	0.15	30.24	91.84	153.40	158.70	98.31	75.35	49.87	14.43
9.00	2.07	0.14	0.08	0.09	32.26	50.18	168.80	177.40	127.20	97.33	34.03	7.89
10.00	1.25	0.21	0.07	0.05	4.72	44.00	152.80	186.30	124.10	79.83	31.09	7.35
11.00	0.79	0.09	0.05	2.60	7.10	39.27	125.60	171.20	97.57	77.86	37.70	9.67
12.00	1.21	0.09	0.05	5.07	1.55	92.04	195.90	218.80	134.10	54.51	19.05	4.08
AVG	1.36	0.17	0.49	2.10	18.76	65.67	169.19	185.63	120.10	68.51	28.56	8.93

A2a: 2050s period

year	Jan	Feb	Mar	Apr	May	Jun	Jul	Aug	Sep	Oct	Nov	Dec
1	0.71	0.11	0.85	0.15	13.53	72.74	160.20	190.50	114.50	57.65	15.76	2.66
2	0.15	0.06	0.45	0.42	12.38	110.10	310.10	270.60	168.60	92.21	26.23	5.24
3	0.33	0.09	0.71	8.87	16.88	89.18	90.03	259.90	166.10	115.40	67.74	23.33
4	4.32	1.03	1.97	1.70	28.48	71.59	160.30	146.60	106.70	82.19	44.31	10.99
5	1.28	0.11	0.22	0.10	39.51	88.11	239.30	210.00	125.10	40.97	10.41	1.24
6	0.12	0.07	0.19	0.80	43.95	51.98	219.00	214.70	166.30	62.81	17.87	18.83
7	4.85	0.46	6.71	24.68	72.77	134.50	192.00	235.80	180.80	85.17	33.91	24.18
8	4.59	0.30	1.11	0.30	50.23	112.70	168.40	183.40	119.50	93.29	62.78	19.35
9	3.21	0.21	0.12	0.19	52.86	67.01	186.50	203.70	151.80	120.30	40.90	9.87
10	1.74	0.26	0.08	0.06	9.50	58.58	170.30	212.90	147.20	98.74	38.48	10.19
11	1.13	0.11	0.06	5.97	11.69	47.76	139.60	201.50	115.20	98.20	47.89	13.03
12	1.81	0.12	0.07	0.10	44.55	116.00	215.70	256.10	155.70	66.11	24.80	5.76
AVG	2.02	0.24	1.05	3.61	33.03	85.02	187.62	215.48	143.13	84.42	35.92	12.05

A2a: 2080s period

year	Jan	Feb	Mar	Apr	May	Jun	Jul	Aug	Sep	Oct	Nov	Dec
1	0.79	0.12	1.98	0.24	62.43	83.86	175.50	184.50	112.40	59.62	16.37	2.77
2	0.16	0.06	1.10	0.74	66.46	119.80	331.30	260.20	166.50	98.01	28.15	5.65
3	0.36	0.09	1.49	14.56	22.84	72.19	104.30	246.50	159.60	133.00	81.80	30.28
4	6.13	3.05	4.10	3.80	38.30	82.20	173.40	143.60	104.50	89.85	54.26	13.41
5	1.68	0.20	0.66	0.17	46.22	97.51	257.20	204.50	121.00	40.06	11.27	1.45
6	0.14	0.07	0.55	1.79	47.30	65.74	236.00	208.60	160.00	62.94	19.99	28.23
7	6.73	0.75	12.54	33.72	90.83	147.20	205.40	227.60	178.80	85.96	43.03	32.21
8	6.38	0.43	2.74	0.58	63.40	123.10	179.20	177.00	117.70	101.10	75.66	25.96
9	4.60	0.31	0.18	0.37	66.29	76.04	199.50	197.50	147.50	135.70	44.57	10.83
10	1.97	0.30	0.08	0.06	13.86	66.85	183.40	207.20	143.10	110.90	44.54	13.14
11	1.54	0.12	0.07	8.36	13.51	54.84	150.80	193.40	111.00	110.50	57.90	16.46
12	2.48	0.14	0.12	0.14	27.43	129.10	229.80	246.70	151.80	69.78	29.38	7.18
AVG	2.75	0.47	2.13	5.38	46.57	93.20	202.15	208.11	139.49	91.45	42.24	15.63

B2a: 2020s Period

year	Jan	Feb	Mar	Apr	May	Jun	Jul	Aug	Sep	Oct	Nov	Dec
1	0.49	0.09	0.35	0.10	9.82	41.40	138.20	161.10	93.86	45.74	11.91	1.71
2	0.10	0.05	0.16	0.20	12.09	89.51	278.50	228.60	140.40	75.48	21.02	3.89
3	0.21	0.08	0.30	4.01	9.22	64.74	74.92	210.20	138.30	91.23	54.00	17.45
4	2.74	0.66	1.57	0.59	16.56	56.04	142.00	127.50	84.86	64.68	33.92	8.09
5	0.82	0.09	0.15	0.07	27.15	71.89	215.40	180.20	103.30	33.89	7.69	0.70
6	0.10	0.06	0.08	0.35	21.66	32.82	193.60	183.40	138.70	51.14	13.63	11.93
7	3.04	0.24	3.13	11.72	45.71	110.00	171.10	200.10	148.40	70.52	25.00	17.08
8	2.82	0.19	0.42	0.16	32.79	91.91	150.80	155.70	96.90	74.69	49.20	13.89
9	1.95	0.14	0.08	0.09	34.90	50.64	166.30	174.40	125.20	96.47	33.76	7.82
10	1.23	0.21	0.07	0.05	14.90	43.62	149.60	182.90	122.20	79.10	30.74	7.10
11	0.76	0.08	0.05	1.80	15.84	38.31	122.50	167.50	95.98	77.15	37.16	9.43
12	1.17	0.09	0.05	0.07	21.86	92.46	193.00	214.70	132.30	53.94	18.72	3.97
AVG	1.28	0.16	0.53	1.60	21.88	65.28	166.33	182.19	118.37	67.84	28.06	8.59

B2a: 2050s period

year	Jan	Feb	Mar	Apr	May	Jun	Jul	Aug	Sep	Oct	Nov	Dec
1	0.75	0.11	0.69	0.13	1.28	38.65	161.60	176.40	108.30	56.74	15.66	2.65
2	0.15	0.05	0.35	0.38	3.77	110.10	312.10	249.30	160.30	92.55	26.68	5.38
3	0.34	0.09	0.58	8.48	16.37	68.75	90.37	234.20	153.50	121.70	69.98	24.10
4	4.54	1.04	1.96	1.53	25.98	69.83	160.50	138.20	99.86	83.58	45.96	11.46
5	1.37	0.12	0.21	0.10	36.42	87.32	240.60	196.80	116.70	38.94	10.39	1.26
6	0.12	0.06	0.14	0.65	43.30	49.69	219.90	200.50	153.90	60.54	17.60	19.90
7	5.10	0.50	5.57	23.10	69.43	132.90	192.90	218.30	171.10	82.76	33.00	23.78
8	4.48	0.29	0.85	0.25	45.63	110.10	168.90	169.90	112.70	94.25	66.40	20.20
9	3.39	0.22	0.11	0.16	48.70	66.07	187.50	189.80	142.00	124.90	42.21	10.28
10	1.82	0.26	0.08	0.06	28.35	57.10	171.20	199.30	137.90	102.30	40.08	10.64
11	1.18	0.11	0.06	5.84	11.50	47.48	140.20	184.80	107.50	101.40	50.31	13.70
12	1.94	0.12	0.07	0.10	13.76	113.70	216.60	235.10	146.90	65.65	25.90	6.12
AVG	2.10	0.25	0.89	3.40	28.71	79.31	188.53	199.38	134.22	85.44	37.01	12.46

B2a: 2080s period

year	Jan	Feb	Mar	Apr	May	Jun	Jul	Aug	Sep	Oct	Nov	Dec
1.00	0.73	0.11	1.24	0.18	1.83	82.86	168.20	182.30	111.40	57.47	15.68	2.61
2.00	0.15	0.06	0.65	0.48	4.74	110.50	321.60	257.70	164.80	93.45	26.63	5.28
3.00	0.33	0.09	0.95	11.48	19.97	80.03	99.43	244.50	159.20	121.30	75.82	27.63
4.00	5.46	1.95	2.88	2.52	32.89	76.27	168.00	142.20	103.30	84.12	49.65	12.30
5.00	1.49	0.15	0.37	0.13	40.44	90.20	249.30	202.60	120.10	39.61	10.37	1.24
6.00	0.13	0.07	0.28	1.07	51.95	57.58	227.90	206.30	159.20	61.68	18.79	23.83
7.00	5.89	0.62	8.85	28.95	80.74	137.20	198.70	225.40	176.90	84.51	39.89	30.07
8.00	5.94	0.39	1.63	0.39	54.97	114.70	173.50	175.20	116.30	95.42	68.94	23.40
9.00	4.06	0.27	0.14	0.26	57.38	69.86	193.00	195.60	146.30	125.30	42.02	10.13
10.00	1.88	0.32	0.08	0.06	11.00	59.78	176.70	205.20	142.00	102.40	41.04	11.85
11.00	1.36	0.12	0.07	6.28	10.78	48.21	144.60	191.40	110.50	102.20	52.86	14.97
12.00	2.20	0.13	0.08	0.12	15.55	118.90	222.70	244.10	150.80	66.50	26.68	6.33
AVG	2.47	0.35	1.43	4.33	31.85	87.17	195.30	206.04	138.40	86.16	39.03	14.14